RESPONSE OF CURVED COMPOSITE PANELS UNDER EXTERNAL BLAST

A Dissertation

Presented to

The Graduate Faculty of The University of Akron

In Partial Fulfillment

of the Requirements for the Degree

Doctor of Philosophy

Yifei Gao

August, 2014

RESPONSE OF CURVED COMPOSITE PANELS

UNDER EXTERNAL BLAST

Yifei Gao

Dissertation

Approved:

_____
Advisor
Dr. Michelle S. Hoo Fatt

_____
Committee Member
Dr. Xiaosheng Gao

_____
Committee Member
Dr. Gregory Morscher

_____
Committee Member
Dr. Ernian Pan

_____
Committee Member
Dr. Kevin Kreider

Accepted:

_____
Department Chair
Dr. Sergio Felicelli

_____
Dean of the College
Dr. George K. Haritos

_____
Dean of the Graduate School
Dr. George R. Newkome

_____
Date

ABSTRACT

The response of single-curvature composite panels under external blast was studied. For the single-curvature composite shells under external pressure pulse loading, Lagrange's equations of motion were established to determine the shell response and the Budiansky-Roth criterion was used to examine the instability. The predicted transient shell response compared very well with FEA results from ABAQUS Implicit, and the predicted buckling loads also agreed with experiments on steel arches. Under various load durations, buckling was impulsive, dynamic and quasi-dynamic. Thicker composite shells were more likely to fail by first-ply failure rather than buckling. It was shown that the composite lay-up could be adjusted to increase the buckling resistance of the shell.

For the single-curvature composite sandwich panels under external pressure pulse loading, a multi-layered approach was used to distinguish facesheets and core deformations. Core compressibility and transverse shear through the thickness were accounted for using linear displacement fields through the thickness. Equations of motion for the facesheet transient deformations were again derived from Lagrange's equations of motion, and predicted solutions using this approach compared very well with FEA results from ABAQUS Implicit. In the case of core undergoing elastic deformations only, both facesheet fracture during stable deformation response and local dynamic pulse buckling of facesheets were considered as possible modes of failure in the curved sandwich panel.

It was found that local facesheets buckling is more likely to occur than facesheet fracture in thin and deeply curved sandwich panels. The facesheet laminate lay-up could also be adjusted to improve the local buckling resistance of the curved sandwich panel. In the case of the core undergoing elastic-plastic deformations, a parametric study showed that blast resistance of the curved sandwich panel can be increased by allowing cores to undergo plastic crushing. Very thick (i.e., radius-to-thickness aspect ratio less than 10) and shallow shells derived much of their resistance to blast from core crushing. Strong, dense foam cores did not increase the blast resistance of the curved sandwich panel but allowed facesheets to fracture while the core remained elastic.

ACKNOWLEDGEMENTS

I would like to take this opportunity to express my sincere gratitude to my advisor Dr. Michelle S. Hoo Fatt for her encouragements, consistent help and, most important, her valuable instructions in the academic area. The accomplishment of this degree would be impossible without her support.

I would like to thank Dr. Yapa Rajapakse at the Office of Naval Research for having financially supported this project under the Grant N00014-07-1-0423.

I would also like to show my thanks to my committee members: Dr. Xiaosheng Gao, Dr. Gregory Morscher from Department of Mechanical Engineering, Dr. Ernian Pan from Department of Civil Engineering, and Dr. Kevin Kreider from Department of Theoretical and Applied Mathematics. Special appreciation is given to them for their time on reading and evaluating my thesis. Their comments and suggestions have improved the quality of my research work.

I would also like to thank the staff and faculty in the Department of Mechanical Engineering for their help during my study at The University of Akron.

I would also like to thank my colleagues, including Min Liu, Dushyanth Sirivolu, Jun Zhou and Shen Shang. During the last six years, discussions on the academic issues with them always enlightened me to approach the research objectives.

I also appreciate the support and love from my dear wife Tingting Zhang. During my study career, she always encouraged me when I encountered difficulties in the research, took care of me when got ill, and sponsored me when lost stipend.

Last but not least, I want to thank my parents for their endless love and support. During the time when I was pursuing my Ph.D. degree, my grandfather passed away. If there were no consolation or encouragement from my parents on the overseas calls, I would be struck down by sorrow and sadness. I love them more and more as time goes by.

TABLE OF CONTENTS

Page

LIST OF TABLES

Table Page

LIST OF FIGURES

Figure Page

CHAPTER I

INTRODUCTION

Curved composite panels are commonly used to construct lightweight aerospace, marine, transportation and civil structures. For example, the Boeing 787 Dreamliner aircraft uses 80% composite materials by volume in the construction of its airframe, as shown in Figure 1.1. Specifically, curved panels made of carbon/epoxy triaxial braided composite material are used to construct its GE GEnx engine cases. The hulls of naval ships can also be made with composite shells. Figure 1.2 shows an operational stealth ship, Swedish Visby-Class corvette, made with carbon/E-glass Vinyl Ester composite materials. A New Generation high-speed train in China is shown in Figure 1.3, where the interior components, such as doors, ceilings, floors and partition walls, are made with Divinycell foam-cored composite sandwich panels. Figure 1.4 shows a road bridge that was approximately 100 years old is being replaced with the first fiber composite sandwich bridge in Switzerland.

When compared to traditional metals, laminated composites offer advantages such as higher strength-to-weight and stiffness-to-weight ratios, improved chemical and environmental resistance and the ability to tailor properties. The increased use of composite materials in many engineering applications has generated much interest in understanding the behavior of curved composite panels. In some cases, these curved composite panels will be exposed to external pressure pulse loadings, like during military

combats, terrorists' attacks or accidental explosions. Therefore, it is necessary to examine the response of curved composite panels under external blast, and this is the objective of the present research.

Figure 1.1 Boeing 787 Dreamliner aircraft. Courtesy of Wikimedia Commons.

Figure 1.2 Swedish Visby-Class corvette. Courtesy of pinterest.com.

Figure 1.3 China Railway High-speed train. Courtesy of Wikimedia Commons.

Figure 1.4 First fiber composite sandwich bridge in Switzerland. Courtesy of 3A Composites, Inc.

Curved panels or shells are structural elements defined by a curved middle surface, and bounded between upper and lower surfaces with a given thickness. The thickness of shell is small compared to the in-plane dimensions and/or the radii of shell curvature. Shell structures can carry much higher lateral loads than flat plates because of the in-plane membrane resistance that it allows from having an initial curvature. An even more

efficient composite shell structure is a composite sandwich shell. A typical sandwich shell is a layered structure consisting of two thin, stiff and high-density facesheets and a thick, soft and low-density core. The facesheets are adhesively bonded to the core. Usually the core is made from honeycomb or foam material while the facesheets could be of metallic or fiber-reinforced composite materials. This type of configuration makes the facesheets carry the in-plane and bending loads, while the core bear the transverse normal and shear loads. The advantages of the sandwich shell over a monolithic shell include higher bending stiffness and strength per unit weight, as well as energy absorption capability of the core.

When exposed to external pressure loadings, shells may fail in one of two ways: buckling or fracture due to large deformation. Which failure mode will occur depends on the shell geometries and materials. To more precisely define the scope of study in this thesis, it is useful to distinguish among several types of buckling. The first distinction is between static buckling and dynamic buckling. The former is due to quasi-static loads and involves the fundamental mode or lowest buckling mode. The latter is from vibratory and/or transient loads. With vibratory loads, the vibration frequency determines the buckling mode when resonance takes place. With transient loads, particularly high amplitude, short-duration pulse loading, the higher-order modes of the structure may become unstable as the buckling modes depend on load amplitude and duration [1].

The above expressions about dynamic buckling can be further described based on the physical phenomena of the buckling processes. The buckling from oscillatory loads is defined as vibration buckling and the buckling from transient loads as pulse buckling. In vibration buckling, the amplitudes of vibration caused by an oscillating load become

unacceptably large at critical combinations of load amplitude, load frequency, and structural damping. A mathematical description of vibration buckling is dynamic stability of vibrations induced by oscillating parametric loading. The resonance (buckling) occurs when the parametric loading frequency coincides with one of the natural frequencies of structure. This type of resonance is so called parametric resonance. In pulse buckling, the structure deforms to unacceptably large amplitude as a result of response to the applied transient load. This transient load consists of a single pulse characterized by its amplitude and duration. A mathematical definition is given to pulse buckling: dynamic response of structural systems induced by time varying parametric loading. If the amplitude of transient load is well below that required to produce pulse buckling, a special form of vibration buckling may occur, which is autoparametric vibration buckling. The specific type of buckling referenced in this thesis is dynamic pulse buckling.

This thesis is organized into six chapters. Chapter II provides a detailed literature review about the development of shell theories and dynamic response of composite shells. In Chapter III, the dynamic pulse buckling of a clamped, single-curvature laminated composite shell under uniformly distributed external pressure pulse loading is investigated. The transient shell response is found using Lagrange's equations of motion. This response is then compared to finite element analysis results using ABAQUS Implicit. Dynamic stability of the composite shell is investigated with the Budiansky and Roth criterion [2]. Failure of the composite shell due to large deformation and not necessarily instability is also addressed. A parametric study is performed to determine the influence of pulse duration, shell aspect ratio, angular extent and laminate lay-up on the failure resistance of the shell.

Chapter IV addresses the problem of local dynamic pulse buckling of a curved composite sandwich panel. In Chapter IV, we expand on previous work in Chapter III, involving the dynamic stability of thin laminated composite shells undergoing pressure pulse loading by considering a curved composite sandwich panel with thin facesheets and an elastic compressible core. Since the sandwich shell consists of two thin facesheets and a compressible core, facesheets may be susceptible to pulse buckling. Equations of motion for the facesheet transient deformations are again derived from Lagrange's equations of motion, and solutions using this approach are then compared to FEA results from ABAQUS Implicit. Both facesheet fracture during stable response and local dynamic pulse buckling of facesheets are considered as possible curved sandwich panel modes of failure. The Budiansky-Roth criterion is also used as the dynamic instability criterion.

Chapter V presents an elastic-plastic analytical model for the blast response of a curved, composite sandwich panel with polymeric foam core. The model will elucidate not only the dynamic response of the sandwich panel but address its ultimate failure and the energy absorption of its core up to the point of failure. The predicted solution from the elastic-plastic model is compared to FEA results from ABAQUS Implicit. Chapter VI concludes the present thesis and gives the suggestions on the future possible research work.

CHAPTER II

LITERATURE REVIEW

2.1 Development of Shell Theories and Sandwich Shell Theories

In this section, the development of classical shell theories, laminated shell theories and sandwich shell theories are discussed respectively.

2.1.1 Development of classical shell theories

In classical linear shell theories, there are two fundamental methods of approach to the problem. The first method was proposed by Cauchy [3] and Poisson [4], which is based on the expansion of displacements and stresses in the shell in power series of the distance z from the middle surface. However, the convergence of these power series was skeptical, which made this method unpopular. The second method was proposed by Kirchhoff [5], and has the advantage of introducing physical meanings into the shell theories.

The first accurate shell theory may be attributed to Love's thin shell theory [6]. When analyzing bending of shells, Love introduced his first approximation to define a linear analysis of thin shells. This approximation assumes (1) strains and displacements to be small such that second and higher-order terms can be neglected, (2) the thickness of the shell to be small compared with other shell parameters, (3) the transverse stress to be

small compared with other stresses in shells, and (4) normals to the undeformed surface to remain straight and normal to the deformed surface. The first of these assumptions defines a linear analysis of shells. This assumption needs to be relaxed if the strains and/or displacements become large. Displacement is considered large if it exceeds the thickness of the shell. It is well known that thin shells may undergo large displacements while the strains at each point remain small.

Following Love's thin shell theory, von Karman [7] extended this approach to study finite deformation of plates by taking nonlinear terms into account. Donnell [8] established the nonlinear theory of circular cylindrical shells under the simplifying shallow shell hypothesis. Because of its relative simplicity and practical accuracy, this theory has been widely used. Mushtari and Galimov [9] presented nonlinear theory for thin shells undergoing moderate and large deformations. A more refined nonlinear theory of shells was developed by Sanders in tensorial form [10] and by Koiter around the same time period [11], leading to Sanders-Koiter theory. Another accurate theory was referred to as the Flugge-Lur'e-Byrne nonlinear shell theory [12, 13], which is very close to the general large deflection theory of thin shells developed by Novozhilov [14]. Additional nonlinear shell theories were formulated by Reissner [15] and by Timoshenko and Woinowsky-Krieger [16]. Vlasov [17] and Sanders [18] tried to resolve some of the inconsistencies which appeared in the shell theories based on Love's approximation, including rigid body motion and asymmetric differential operators.

Actually, in the case of moderately thick shells, the classical shell theories mentioned above can become inaccurate. As early as 1877, Rayleigh [19] noted that rotary inertia terms were important in the analysis of vibrating systems. Decades later,

Timoshenko [20] showed that shear deformation terms are at least as important. Since then, researchers realized that the hypothesis of negligible rotary inertia and shear deformation can be a rough approximation for thick shells. Rotary inertia and shear deformation led to a necessary relaxation of some of the assumptions in Love's first approximation, and shear deformation shell theories were born. The Reissner-Mindlin theory of plates took into account transverse shear strains in order to deal with thicker and laminated composite plates [21, 22]. For moderately thick laminated shells, the nonlinear first-order shear deformation theory of shells was proposed by Reddy and Chandrashekhara [23], which is based on the linear first-order shear deformation theory introduced by Reddy [24]. In these theories, the shear correction factors are required for equilibrium considerations. For this reason, a linear higher-order shear deformation theory of shells proposed by Reddy and Liu [25] and a nonlinear higher-order shear deformation theory of plates proposed by Reddy [26] do not require shear correction factors by satisfying zero transverse shear stresses at the top and bottom surfaces.

2.1.2 Development of laminated shell theories

The use of laminated composite shells in many engineering applications has been expanding rapidly in the past four decades. The shell theories used for isotropic materials need further treatment when laminated composite materials are in consideration. This is because such materials offer stretching-bending coupling effects, and new stiffness coefficients need to be determined. Ambartsumian [27] published probably the first book in the area of composite shells. In his book he presented various laminated composite

shell theories by expanding the stress resultant equation of earlier theories to those for anisotropic shells, and solved for stresses and deformations under static loads. A 1973 monograph by Leissa [28] reviewed shell vibration research up to that time, including both isotropic and laminated composite shells. Librescu covered areas of stability and flutter of laminated composite shells [29] and developed refined nonlinear theories for anisotropic laminated shells [30]. Vinson and Sierakowski [31] presented analysis of composite shells.

Composite materials offer higher shear deformation than typical metallic materials. If the shear strains and shear deformations were neglected, the assumption that normals to the undeformed surface remain straight and normal to the deformed surface leads to an underprediction of the potential strain energy in laminated shells. For this reason, Librescu et al. [32, 33] developed a shear deformation theory for laminated composite shells, which included higher-order terms. This theory failed to consider the trapezoidal shape of the shell cross-section in the stress resultant equations (i.e., the 1+z/R term). Leissa and Chang [34] considered this term but truncated it using a geometric series expansion.

2.1.3 Development of sandwich shell theories

Sandwich constructions are important elements in many fields of lightweight construction like marine vessels, aerospace vehicles, and civil infrastructure [35]. A typical sandwich shell consists of two stiff metallic/composite facesheets and a soft honeycomb/foam core. Within the principle of sandwich construction, the facesheets

carry the membrane and bending loads while the core keeps the facesheets at their desired distance and transmits the transverse normal and shear loads. This layout gives the sandwich shell the integrity of high stiffness and strength with little resultant weight penalty and high energy absorption capability.

In the early studies of the response of a sandwich structure to static loading or dynamic loading with long duration, the compressibility of the core in the transverse direction was neglected [36, 37]. This type of model is the now classical sandwich membrane models which assume membrane theory for the facesheets and pure transverse shear deformation is the only type of deformation considered for the core. However, experimental and numerical results [38-42] have shown that the core undergoes significant transverse deformation when the sandwich structure experiences dynamic loading.

On the other hand, due to the thick core made of relatively soft material, the deformation and instability behaviors of sandwich shells are essentially changed from those behaviors of classical laminated shells and monolayer shells. In addition to the standard overall buckling mode, the transverse compressibility of the core yields a distinctive instability mode, which is buckling of the local facesheets into the core region while the global response of the entire shell remains stable. In the early studies on buckling of sandwich panels, the two instability modes are considered independently [43-45].

To account for the specific deformation and buckling behavior, a number of shell theories and models have been developed for sandwich shells and they can be divided

into two types: effective single layer theories and effective multilayer theories. The former treats the entire sandwich shell as single-layer by using displacement functions related to one reference surface, usually the middle surface of the shell. The latter considers each individual facesheet and core layer separately and the compatibility is ensured by appropriate interface constraint conditions. Skvortsov and Bozhevolnaya [46] studied the linear elastic material behavior of sandwich plates and shells using an effective single layer sandwich model. Ferreira et al. [47] considered geometrical and material nonlinearities when presenting the work on effective single layer sandwich model. Barut et al. [48] presented an advanced effective single layer theory for sandwich plates. This approach accounts for the transverse compressibility of the core by using weighted average displacement functions. The disadvantages of effective single layer models are that they lose accuracy due to the simplified displacement functions, and they cannot predict the instability mode of local facesheets buckling. These disadvantages can be overcome by effective multilayer models which treat each principal layer separately.

Among the first to work on effective multilayer models was Allen [37]. He presented the classical sandwich membrane model which assumes membrane theory for the facesheets and pure transverse shear deformation for the core. Frostig et al. [49] proposed a multilayer model for sandwich beams, which is based on Kirchhoff approximations for the facesheets and includes transverse shear stress of the core. This approach was extended to singly curved sandwich beams by Bozhevolnaya and Frostig [50] and to 2-D sandwich plates by Frostig [51]. Dawe and Yuan [52] proposed a theory for flat sandwich plates accounting for the transverse compressibility of the core, by considering a first and second order displacement expansion for the transverse and

tangential displacements, respectively. Pai and Palazotto [53] developed similar theory by using a second and third order approximation. Librescu and Hause [54] provided surveys on recent developments in the theory and modeling of sandwich panels.

2.2 Dynamic Response of Composite Shells

Dynamic analysis of shells, or curved panels, started at the 19th century. Research on shell dynamics is found to be mainly free vibration analysis at its initial stage. Free vibration is initiated when a curved composite panel is displaced from its equilibrium position due to an energy imparted to the structure through an external source. A restoring force or moment results from its bending stiffness and this pulls it back toward equilibrium. Ganapathi and Haboussi [55] studied the free vibrations of thick laminated anisotropic non-circular cylindrical shells. Korhevskaya and Mikhasev [56] studied the free vibrations of a laminated cylindrical shell subjected to nonuniformly distributed axial forces. Shang [57] presented an exact analytical solution for the free vibration of composite capsule structures. However, when subjected to various kinds of external dynamic loads, shells can present different dynamic behaviors, which lead to several types of dynamic analysis.

Curved panels made of laminated composites under impact loading due to flying foreign objects or other causes have been intensely studied. Such impacts induce a region of high stress concentration in the vicinity of contact area and lead to a localized damage. Krishnamurthy et al. [58, 59] performed a parametric study of the impact response of laminated cylindrical shells. Kim et al. [60] investigated the behavior of laminated

composite shells under transverse impact loading. Hoo Fatt and Sirivolu [61] investigated high velocity impact response of a composite sandwich panel.

Dynamic stability of curved composite panels is a very broad subject that includes not only dynamic buckling from transient and/or vibratory loads, but also interaction of structures with other media, such as in aircraft flutter, and interaction with active control systems that have their own dynamic characteristics [1]. Recent research activities on the dynamic stability behavior of plates and shells were reviewed by Sahu and Datta [62]. Zhou and Wang [63] presented a theory of non-linear dynamic stability for laminated composite cylindrical shells.

Several other studies have addressed the general dynamic behavior of curved composite panels. Von Karman and Tsien [64] performed a seminal study on the stability of axially loaded circular cylindrical shells, based on Donnell's non-linear shallow shell theory. Pinto Correiaa et al. [65] presented a finite element model for the dynamic analysis of laminated axisymmetric shells. Sahu and Datta [66] discussed parametric resonance characteristics of laminated composite shells subjected to nonuniform loading. Ribeiro and Jansen [67] studied the non-linear vibrations of laminated cylindrical shallow shells under thermomechanical loading. Li and Hua [68] studied the transient vibrations of laminated composite cylindrical shells exposed to underwater shock waves. Qatu et al. [69] reviewed most of the research done in recent years on the dynamic behavior of composite shells and that review was conducted with emphasis on the type of dynamic analysis performed.

2.3 Dynamic Pulse Buckling of Composite Shells

The dynamic behavior studied in this research is dynamic pulse buckling from prescribed dynamic loads acting on curved composite panels. This thesis will focus on two types of composite shells: monocoque curved composite panels and curved composite sandwich panels.

2.3.1 Dynamic pulse buckling of monocoque curved composite panels

Composite shells, or curved composite panels, are commonly used to construct lightweight aerospace, military, transportation and civilian structures. When exposed to external pressure pulse loading, such as one caused by a nearby explosion, these shells may undergo dynamic instability instead of stable transient and vibratory response. The specific type of dynamic instability referenced herein is a dynamic pulse buckling [1, 70]. This type of dynamic buckling is characterized by pressure pulse loading and is distinct from vibration buckling, which is characterized by oscillatory or periodic loading.

Dynamic pulse buckling due to lateral pressure pulse has been addressed for isotropic shell structures since the early 1960s [2, 70-73] and only very recently for laminated composite cylindrical shells [74-77]. Hoo Fatt and Pothula [74] developed the equations of motion governing transient motion of a thin composite cylinder under external pressure pulse loading and resulted in a set of Mathieu equations for which the instability conditions are well-known. In particular, parametric resonance occurs when the hoop mode couples with specific bending modes. In addition to this analytical approach, dynamic buckling of composite cylindrical shells under external, step pressure-pulse loading has also been addressed numerically [75-77]. Tanov et al. [75] applied

ABAQUS to determine the stability of the laminated cylindrical shell under suddenly applied pressure loading using both the Budiansky-Roth and Phase-Plane criteria, both of which are explained in the textbook by Simitses [70]. Schokker et al. [76] used an asymptotic procedure in conjunction with p-version finite elements to extract the buckling mode and the associated second-order field of the composite cylindrical shell when they become unstable. Most recently Rahman et al. [77] extended a finite element perturbation method for static buckling to dynamic buckling analysis of composite cylindrical shells subjected to step-pulse radial and axial loading. The dynamic stability of cylindrical shells with finite angular extent and specified boundary conditions cannot be dealt with analytically. The coupled non-linear equations of motion must be dealt with numerically as was the case for isotropic shells [71, 73, 78].

Simitses [70] discusses various approaches for determining the dynamic stability of structures under sudden loading and a more recent review on the topic, including experimental studies, can be found in Singer et al. [79]. In general the dynamic stability of structures can be addressed using direct equations of motion or the Budiansky-Roth approach [2], a total energy-phase plane or the Hsu approach [80], and the total potential energy or Simitses approach [70]. In the last two approaches, lower and upper bounds of critical stability conditions are established. The Budiansky-Roth criterion simply states that instability occurs when there is a large increase in deformation response from little or no increase of load and it involves numerical solution of non-linear coupled equations of motion.

2.3.2 Dynamic pulse buckling of curved composite sandwich panels

Curved composite sandwich panels have widespread applications in aerospace, naval and civil constructions because they offer high bending resistance and strength with little weight penalty. This results in considerably more research and interest in their dynamic behavior. When these structures are exposed to external pressure pulses, the deformation and stability of the curved sandwich panel are affected by the fact that the core is compressible. Transverse or through-thickness deformation of the core allows facesheets to deform as monolithic shells and this may give rise to an additional buckling mode, local facesheet wrinkling, while the global sandwich panel response is in a stable deformation mode.

While many foam core materials exhibit energy absorption through permanent crushing, there are some foams that can be extremely resistant to permanent crushing because of their high compressive strength. The Divinycell HCP foams manufactured by Diab [81], for instance, are designed for lightweight buoyancy, excellent hydraulic compressive properties and high impact resistance. They are typically used in marine and naval applications, and have very high compressive strength.

In recent years, higher-order sandwich shell theories that incorporate compressible cores have been developed to address the dynamic response of composite sandwich shells subjected to external pressure pulses [82-86]. Hohe and Librescu [83] used a multi-layered sandwich model, which distinguished between facesheets and core deformations, and a higher-order displacement field for capturing core compressibility to determine the response of a spherical sandwich cap under uniform pressure. Li et al. [85]

presented a nonlinear compressible core model to capture the transient shock wave response of the individual facesheets and core of a shallow, simply-supported composite sandwich shell. Li and Kardomateas [86] have extended this theory to cylindrical sandwich shells with flexible core, thereby allowing one to differentiate deformations and stresses in individual facesheets and core. The advantage of above-mentioned theories is that they make the facesheets carry the in-plane and bending loads and the core bear the transverse normal and shear loads. However, these theories are restricted to shallow shell assumptions, i.e., small strains and moderately large rotations. The sandwich shell kinematics presented in this thesis is distinguished from the above-mentioned studies. Facesheet strains are derived based on large deflection, thin shell theory [1, 72], while the core strains are obtained using the assumption of small deflection, thick shell theory, in particular first-order shear deformation theory. Modelling the sandwich shell in this way allows one to assess both shallow and deep sandwich shells.

2.4 Curved Composite Sandwich Panels with Crushable Elastic-Plastic Cores

The sandwich core is considered elastic in the analytical formulations of above-mentioned theories. In some instances, however, the core of the sandwich panel can experience plasticity due to permanent foam crushing. An elastic-plastic core may even be more representative of the blast behavior of foams used nowadays in composite sandwich construction. While the current design of a sandwich panel prohibits plastic crushing of the core, plastic core crushing becomes inevitable under very high intensity loading, such as a nearby blast.

Plastic foam core crushing in composite sandwich structures under projectile impact has been addressed extensively in the past and only more recently for blast loading [87, 88]. Hoo Fatt and Surabhi [87] developed analytical models for the blast resistance and energy absorption of cylindrical, composite sandwich shells, while Hoo Fatt and Chapagain [88] presented an elastic-plastic sandwich panel model for simply supported, rectangular flat composite sandwich panels under uniformly distributed pressure pulse. The elastic-plastic behavior of the core is described as crushable foam with isotropic hardening by Deshpande and Fleck [89]. The plastic flow is determined by an associated flow rule. Under plane strain, the elastic-plastic stress-strain relations are generally not ideally plastic (constant stress) for a material that is elastic-perfectly plastic under uniaxial stress [90]. Incremental stress-strain relations can be derived for the foam and the resulting strain hardening plastic stress-strain curve must be integrated from it. Mines and Alias [91] studied the progressive collapse of polymer composite sandwich beams under static loading by using numerical simulations. Rivoz and Mladensky [92] studied the static indentation response of H30 foam experimentally and computationally.

CHAPTER III

CURVED COMPOSITE PANELS UNDER EXTERNAL BLAST

In this chapter, the dynamic pulse buckling of a clamped, curved laminated composite panel under uniformly distributed external pressure pulse loading is investigated. The curved composite panel is also considered as a single curvature composite shell. The transient shell response is found using Lagrange's equations of motion. This response is then compared to finite element analysis results using ABAQUS Implicit. Dynamic instability of the composite shell is investigated with the criterion by Budiansky and Roth, which simply states that instability occurs when there is a large increase in deformation response from little or no increase of load and it involves numerical solution of non-linear coupled equations of motion. Failure of the composite shell due to large deformation and not necessarily instability is also addressed. A parametric study is performed to determine the influence of pulse duration, shell aspect ratio, angular extent and laminate lay-up on the failure resistance of the shell.

3.1 Problem Formulation

Consider a long, laminated composite shell of radius a and thickness h, subjected to uniformly-distributed pressure pulse loading as shown in Figure 3.1. In a previous publication [74], the dynamic stability of a composite cylindrical shell under external blast was analyzed. In this chapter, only a section of the cylindrical shell is

considered so that the shell surface is of a single curvature with a subtended angle θ_0. Points on the mid-surface of the shell have polar coordinates (a,θ). The external pressure pulse loading is defined as

$$p(t) = p_0\left(1-\frac{t}{\Delta T}\right) \tag{3.1}$$

where p_0 is the peak pressure, ΔT is the load duration and t is the time. The shell deforms with mid-surface radial displacement $w(t,\theta)$ and tangential displacement $v(t,\theta)$.

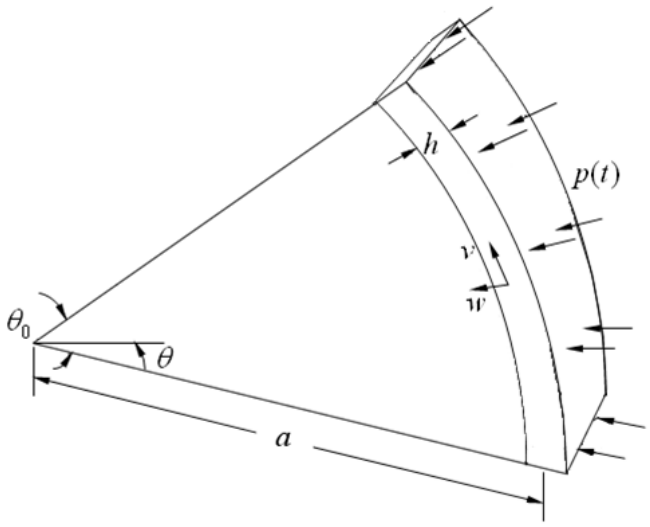

Figure 3.1 Composite shell subjected to external pressure pulse loading.

3.2 Nonlinear Equations of Motion

The equations of motion governing the transient deformations of the shell are defined in normalized radial and tangential displacements $\zeta = w/a$ and $\psi = v/a$,

respectively, and normalized time $\tau = \frac{c\,t}{a}$, where $c = \sqrt{\frac{A_{22}}{\rho h}}$ is the wave speed in the circumferential direction of the shell and A_{22} is the circumferential membrane stiffness. In normalized time, the pressure pulse loading becomes

$$p(\tau) = p_0\left(1 - \frac{\tau}{\tau_0}\right) \tag{3.2}$$

where $\tau_0 = \frac{c\,\Delta T}{a}$ is a normalized load duration.

For fully clamped boundary condition of the shell, $\zeta = 0,\ \partial\zeta/\partial\theta = 0$ and $\psi = 0$ at $\theta = 0, \theta_0$. The boundary conditions of the shell are satisfied by the following Fourier series representations of ζ and ψ:

$$\zeta = \sum_{n=0}^{\infty} b_n(\tau)(1 - \cos\frac{2\pi\theta}{\theta_0})\cos\frac{n\pi\theta}{\theta_0} \tag{3.3}$$

and

$$\psi = \sum_{n=1}^{\infty} c_n(\tau)\sin\frac{n\pi\theta}{\theta_0} \tag{3.4}$$

where $b_n(\tau)$ and $c_n(\tau)$ are mode amplitudes and n is the mode number.

The circumferential membrane and bending strains for the thin shell are taken from References [1, 72] and re-derived in Appendix B. These follow from the deformation of a differential element at the mid-surface of the shell as shown in Figure B.1. Following Appendix B, the hoop strain in the shell is

$$\varepsilon_\theta = \varepsilon_{\theta m} + z\kappa_\theta \tag{3.5}$$

where the mid-surface hoop strain $\varepsilon_{\theta m}$ and the change in hoop curvature κ_θ can be expressed as

$$\varepsilon_{\theta m} = \psi' - \zeta - \zeta\psi' + \frac{1}{2}\zeta'^2 \tag{3.6}$$

$$\kappa_\theta = -\frac{1}{a}(\zeta'' + \zeta) \tag{3.7}$$

The transient shell response is found from Lagrange's equations of motion:

$$\frac{d}{dt}\left(\frac{\partial T}{\partial \dot{q}_n}\right) - \frac{\partial T}{\partial q_n} + \frac{\partial U}{\partial q_n} = Q_n \tag{3.8}$$

where q_n is a generalized coordinate, Q_n is a generalized external force, T is the kinetic energy, U is the strain energy and $\dot{[\ ]} = \partial[\ ]/\partial\tau$. In the following analysis, q_n are the time-varying mode amplitudes b_n and c_n, and Q_n are obtained from virtual work δW as follows:

$$Q_n = \frac{\partial(\delta W)}{\partial(\delta q_n)} \tag{3.9}$$

The kinetic energy T and strain energy U of the shell as well as the virtual work δW are defined respectively as follows:

$$T = \frac{1}{2}A_{22}a\int_0^{\theta_0}(\dot{\zeta}^2 + \dot{\psi}^2)d\theta \tag{3.10}$$

$$U = \frac{1}{2}A_{22}a\int_0^{\theta_0}[(\psi' - \zeta)^2 + (\psi' - \zeta)(\zeta'^2 - 2\zeta\psi') + \left(\zeta\psi' - \frac{1}{2}\zeta'^2\right)^2 + \alpha^2(\zeta'' + \zeta)^2]d\theta \tag{3.11}$$

and

$$\delta W = \int_0^{\theta_0} p(\tau)\delta\zeta\, a^2 d\theta \tag{3.12}$$

where $\delta\zeta$ is the virtual normalized radial displacement, $[\ ]' = \partial[\ ]/\partial\theta$, $\alpha^2 = \dfrac{D_{22}}{a^2 A_{22}}$ is the circumferential bending-to-membrane stiffness ratio and D_{22} is the circumferential bending stiffness. The derivation of strain energy U of the shell is given in Appendix C.

Substitution of Equations (3.3) and (3.4) into Equation (3.10) gives

$$T = \frac{1}{2} A_{22} a \int_0^{\theta_0} I_T \, d\theta \tag{3.13}$$

where

$$I_T = \sum_{n=0}^{\infty}\sum_{m=0}^{\infty}\left\{ \dot{b}_n \dot{b}_m (1-\cos\frac{2\pi\theta}{\theta_0})^2 \cos\frac{n\pi\theta}{\theta_0}\cos\frac{m\pi\theta}{\theta_0} \right\} + \sum_{n=1}^{\infty}\sum_{m=1}^{\infty}\left\{ \dot{c}_n \dot{c}_m \sin\frac{n\pi\theta}{\theta_0}\sin\frac{m\pi\theta}{\theta_0} \right\}$$

On neglecting fourth-order terms, Equation (3.11) becomes

$$U = \frac{1}{2} A_{22} a \int_0^{\theta_0} [\psi'^2 - 2\psi'\zeta + (1+\alpha^2)\zeta^2 + \psi'\zeta'^2 - 2\zeta\psi'^2 - \zeta\zeta'^2 + 2\zeta^2\psi' + \alpha^2\zeta''^2 + 2\alpha^2\zeta''\zeta] d\theta \tag{3.14}$$

Substitution of Equations (3.3) and (3.4) into Equation (3.14) gives

$$U = \frac{1}{2} A_{22} a \int_0^{\theta_0} I_U \, d\theta \tag{3.15}$$

where

$$I_U = \sum_{n=1}^{\infty}\sum_{m=1}^{\infty}\left\{ c_n c_m nm (\frac{\pi}{\theta_0})^2 \cos\frac{n\pi\theta}{\theta_0}\cos\frac{m\pi\theta}{\theta_0} \right\} - 2\sum_{n=0}^{\infty}\sum_{m=1}^{\infty}\left\{ b_n c_m m \frac{\pi}{\theta_0}(1-\cos\frac{2\pi\theta}{\theta_0})\cos\frac{n\pi\theta}{\theta_0}\cos\frac{m\pi\theta}{\theta_0} \right\}$$
$$+ (1+\alpha^2)\sum_{n=0}^{\infty}\sum_{m=0}^{\infty}\left\{ b_n b_m (1-\cos\frac{2\pi\theta}{\theta_0})^2 \cos\frac{n\pi\theta}{\theta_0}\cos\frac{m\pi\theta}{\theta_0} \right\}$$

$$+\sum_{n=0}^{\infty}\sum_{m=0}^{\infty}\sum_{p=1}^{\infty}\{\ b_n b_m c_p p\frac{\pi}{\theta_0}[-n\frac{\pi}{\theta_0}\sin\frac{n\pi\theta}{\theta_0}+\frac{1}{2}(n+2)\frac{\pi}{\theta_0}\sin\frac{(n+2)\pi\theta}{\theta_0}+\frac{1}{2}(n-2)\frac{\pi}{\theta_0}\sin\frac{(n-2)\pi\theta}{\theta_0}]$$
$$\times[-m\frac{\pi}{\theta_0}\sin\frac{m\pi\theta}{\theta_0}+\frac{1}{2}(m+2)\frac{\pi}{\theta_0}\sin\frac{(m+2)\pi\theta}{\theta_0}+\frac{1}{2}(m-2)\frac{\pi}{\theta_0}\sin\frac{(m-2)\pi\theta}{\theta_0}]\cos\frac{p\pi\theta}{\theta_0}\ \}$$
$$-2\sum_{n=0}^{\infty}\sum_{m=1}^{\infty}\sum_{p=1}^{\infty}\{\ b_n c_m c_p mp(\frac{\pi}{\theta_0})^2(1-\cos\frac{2\pi\theta}{\theta_0})\cos\frac{n\pi\theta}{\theta_0}\cos\frac{m\pi\theta}{\theta_0}\cos\frac{p\pi\theta}{\theta_0}\ \}$$
$$-\sum_{n=0}^{\infty}\sum_{m=0}^{\infty}\sum_{p=0}^{\infty}\{\ b_n b_m b_p(1-\cos\frac{2\pi\theta}{\theta_0})[-n\frac{\pi}{\theta_0}\sin\frac{n\pi\theta}{\theta_0}+\frac{1}{2}(n+2)\frac{\pi}{\theta_0}\sin\frac{(n+2)\pi\theta}{\theta_0}+\frac{1}{2}(n-2)\frac{\pi}{\theta_0}\sin\frac{(n-2)\pi\theta}{\theta_0}]$$
$$\times[-m\frac{\pi}{\theta_0}\sin\frac{m\pi\theta}{\theta_0}+\frac{1}{2}(m+2)\frac{\pi}{\theta_0}\sin\frac{(m+2)\pi\theta}{\theta_0}+\frac{1}{2}(m-2)\frac{\pi}{\theta_0}\sin\frac{(m-2)\pi\theta}{\theta_0}]\cos\frac{p\pi\theta}{\theta_0}\ \}$$
$$+2\sum_{n=0}^{\infty}\sum_{m=0}^{\infty}\sum_{p=1}^{\infty}\{\ b_n b_m c_p p\frac{\pi}{\theta_0}(1-\cos\frac{2\pi\theta}{\theta_0})^2\cos\frac{n\pi\theta}{\theta_0}\cos\frac{m\pi\theta}{\theta_0}\cos\frac{p\pi\theta}{\theta_0}\ \}$$
$$+\alpha^2\sum_{n=0}^{\infty}\sum_{m=0}^{\infty}\{\ b_n b_m[-(\frac{n\pi}{\theta_0})^2\cos\frac{n\pi\theta}{\theta_0}+\frac{1}{2}(n+2)^2(\frac{\pi}{\theta_0})^2\cos\frac{(n+2)\pi\theta}{\theta_0}+\frac{1}{2}(n-2)^2(\frac{\pi}{\theta_0})^2\cos\frac{(n-2)\pi\theta}{\theta_0}]$$
$$\times[-(\frac{m\pi}{\theta_0})^2\cos\frac{m\pi\theta}{\theta_0}+\frac{1}{2}(m+2)^2(\frac{\pi}{\theta_0})^2\cos\frac{(m+2)\pi\theta}{\theta_0}+\frac{1}{2}(m-2)^2(\frac{\pi}{\theta_0})^2\cos\frac{(m-2)\pi\theta}{\theta_0}]\ \}$$
$$+2\alpha^2\sum_{n=0}^{\infty}\sum_{m=0}^{\infty}\{\ b_n b_m[-(\frac{n\pi}{\theta_0})^2\cos\frac{n\pi\theta}{\theta_0}+\frac{1}{2}(n+2)^2(\frac{\pi}{\theta_0})^2\cos\frac{(n+2)\pi\theta}{\theta_0}+\frac{1}{2}(n-2)^2(\frac{\pi}{\theta_0})^2\cos\frac{(n-2)\pi\theta}{\theta_0}]$$
$$\times(1-\cos\frac{2\pi\theta}{\theta_0})\cos\frac{m\pi\theta}{\theta_0}\ \}$$

Finally, substituting Equation (3.3) into Equation (3.12) gives

$$\delta W = a^2 p_0\theta_0(1-\frac{\tau}{\tau_0})(\delta b_0-\frac{\delta b_2}{2}) \tag{3.16}$$

The equations of motion for the shell are developed by substituting the above energy expressions into Equation (3.8). For example, a one-term approximation is given when $n=m=p=0$:

$$3\ddot{b}_0+\frac{1}{\theta_0^{\,4}}[3\theta_0^{\,4}b_0-6\theta_0^{\,2}\pi^2 b_0^{\,2}+\alpha^2(16\pi^4 b_0+3\theta_0^{\,4}b_0-8\theta_0^{\,2}\pi^2 b_0)]=2\bar{p}_0(1-\frac{\tau}{\tau_0}) \tag{3.17}$$

where $\bar{p}_0=\frac{ap_0}{A_{22}}$ is the normalized peak pressure. A three-term approximation is given when $n=m=p=0,2$:

$$3\ddot{b}_0 - 2\ddot{b}_2 + \frac{1}{\theta_0^4}[(3\theta_0^4 b_0 - 2\theta_0^4 b_2 + 2\theta_0^3 \pi c_2) + (-6\theta_0^2 \pi^2 b_0^2 - 9\theta_0^2 \pi^2 b_2^2$$
$$- 4\theta_0^2 \pi^2 c_2^2 + 13\theta_0^2 \pi^2 b_0 b_2 - 8\theta_0^3 \pi b_0 c_2 + 4\theta_0 \pi^3 b_2 c_2 + 7\theta_0^3 \pi b_2 c_2) \tag{3.18}$$
$$+ \alpha^2(16\pi^4 b_0 + 3\theta_0^4 b_0 - 8\theta_0^2 \pi^2 b_0 - 16\pi^4 b_2 - 2\theta_0^4 b_2 + 8\theta_0^2 \pi^2 b_2)] = 2\bar{p}_0(1 - \frac{\tau}{\tau_0})$$

$$-2\ddot{b}_0 + \frac{7}{4}\ddot{b}_2 + \frac{1}{\theta_0^4}[(-2\theta_0^4 b_0 + \frac{7}{4}\theta_0^4 b_2 - 2\theta_0^3 \pi c_2) + (\frac{13}{2}\theta_0^2 \pi^2 b_0^2 + \frac{21}{2}\theta_0^2 \pi^2 b_2^2$$
$$+ 3\theta_0^2 \pi^2 c_2^2 - 18\theta_0^2 \pi^2 b_0 b_2 + 4\theta_0 \pi^3 b_0 c_2 + 7\theta_0^3 \pi b_0 c_2 - 8\theta_0 \pi^3 b_2 c_2 - 6\theta_0^3 \pi b_2 c_2) \tag{3.19}$$
$$+ \alpha^2(-16\pi^4 b_0 - 2\theta_0^4 b_0 + 8\theta_0^2 \pi^2 b_0 + 80\pi^4 b_2 + \frac{7}{4}\theta_0^4 b_2 - 16\theta_0^2 \pi^2 b_2)] = -\bar{p}_0(1 - \frac{\tau}{\tau_0})$$

and

$$\ddot{c}_2 + \frac{1}{\theta_0^4}[(2\theta_0^3 \pi b_0 - 2\theta_0^3 \pi b_2 + 4\theta_0^2 \pi^2 c_2) + (-4\theta_0^3 \pi b_0^2 - 4\theta_0 \pi^3 b_2^2$$
$$- 3\theta_0^3 \pi b_2^2 + 4\theta_0 \pi^3 b_0 b_2 + 7\theta_0^3 \pi b_0 b_2 - 8\theta_0^2 \pi^2 b_0 c_2 + 6\theta_0^2 \pi^2 b_2 c_2)] = 0 \tag{3.20}$$

Note that the equations of motion are coupled second-order ordinary differential equations in which only the symmetric mode amplitudes exist for ζ, i.e., $b_0, b_2, b_4, \ldots$, while only the anti-symmetric exist for ψ, i.e., $c_2, c_4, c_6, \ldots$. However, both symmetric and anti-symmetric mode amplitudes could exist if shell imperfections were taken into account.

3.3 An Example

Consider an orthotropic shell made of 0/90 Woven Roving E-Glass/Vinyl Ester with thickness $h = 2$ mm, radius $a = 80$ mm (aspect ratio $a/h = 40$) and subtended angle $\theta_0 = \pi$. Material properties for the 0/90 Woven Roving E-Glass/Vinyl Ester were taken from Boh et al. [93] and are shown in Table 3.1.

Table 3.1 Material properties of 0/90 Woven Roving E-glass/Vinyl Ester and Uni-Directional E-Glass/Epoxy.

Material	0/90 Woven Roving E-Glass/Vinyl Ester	Uni-Directional E-Glass/Epoxy
Density (kg/m^3)	1,391	2,050
E_{11} (+) (GPa)	17	48
E_{22} (+) (GPa)	17	12
E_{33} (+) (GPa)	7.48	12
E_{11} (-) (GPa)	19	--
E_{22} (-) (GPa)	19	--
E_{33} (-) (GPa)	--	--
ν_{12}	0.13	0.19
ν_{23}	0.28	0.26
ν_{13}	0.28	0.19
ν_{31}	0.12	0.05
$G_{12}=G_{21}$ (GPa)	4.0	6
$G_{23}=G_{32}$ (GPa)	1.73	5
$G_{13}=G_{31}$ (GPa)	1.73	6
X_T, σ_{10} (+) (MPa)	270	1,020
X_C, σ_{10} (-) (MPa)	200	490
Y_T, σ_{20} (+) (MPa)	270	8
Y_C, σ_{20} (-) (MPa)	200	78
Z_T, σ_{30} (+) (MPa)	23.2	8
Z_C, σ_{30} (-) (MPa)	343.5	78
S_L, $\tau_{120}=\tau_{210}$ (MPa)	40	23
S_T, $\tau_{130}=\tau_{310}$ (MPa)	31.6	23
S_T, $\tau_{230}=\tau_{320}$ (MPa)	31.6	66

The external pressure pulse loading has peak pressure $p_0 = 0.6\,\text{MPa}$ and load duration $\Delta T = 1\,\text{ms}$. The normalized radial displacement ζ of the center point of the

shell, which has coordinate $(a, \frac{\pi}{2})$, is shown in Figure 3.2. This solutions was produced in MATLAB using ode15s, which was found to be the most efficient solver. The total step time $t = 3.6$ ms, corresponds to a normalized step time $\tau = 160$ on the abscissa axis. The results are shown when the total number of terms are succesively increased to approach the converged solution. It can be seen that the analytical results converged with 15 terms, i.e., up to and including $n = m = p = 14$.

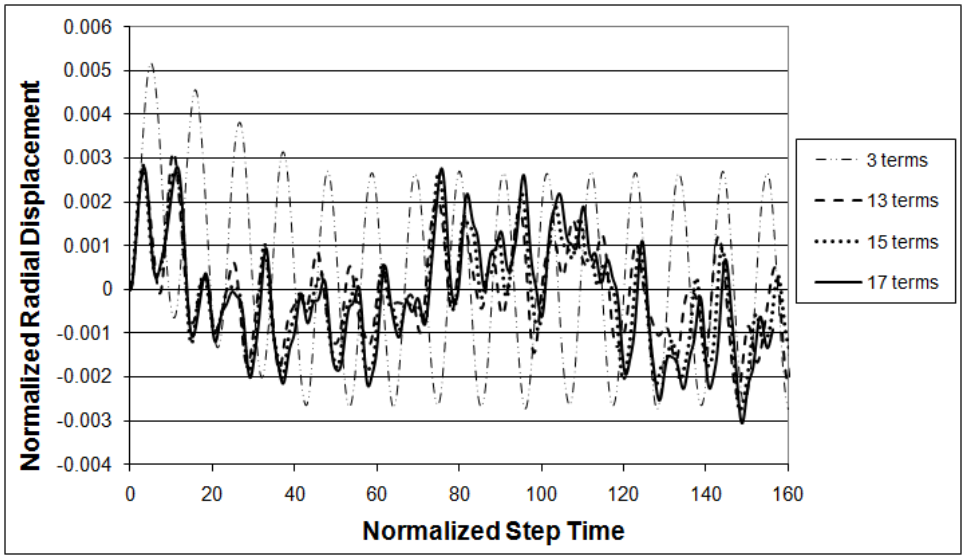

Figure 3.2 Convergence of normalized radial displacement at shell center.

3.4 Finite Element Analysis

The example problem above was numerically solved using ABAQUS Implicit [94]. The FEA model is shown in Figures 3.3(a) and (b). Four-node bilinear plane strain quadrilateral elements (CPE4) were used to model the shell segment in a plane strain condition. There were 2000 elements in the meshed shell. To show the mesh clearly, only one half section is presented in Figure 3.3(b). The material properties of the shell were

assigned using Elastic Engineering Constants with data for the 0/90 Woven Roving E-Glass/Vinyl Ester from Table 3.1. Implicit dynamic analysis was performed with automatic time increment and a specified half-step residual. The size of the half-step residual was small enough to yield accurate results. No damping was specified in the problem. Non-linear geometry was also used in the analysis.

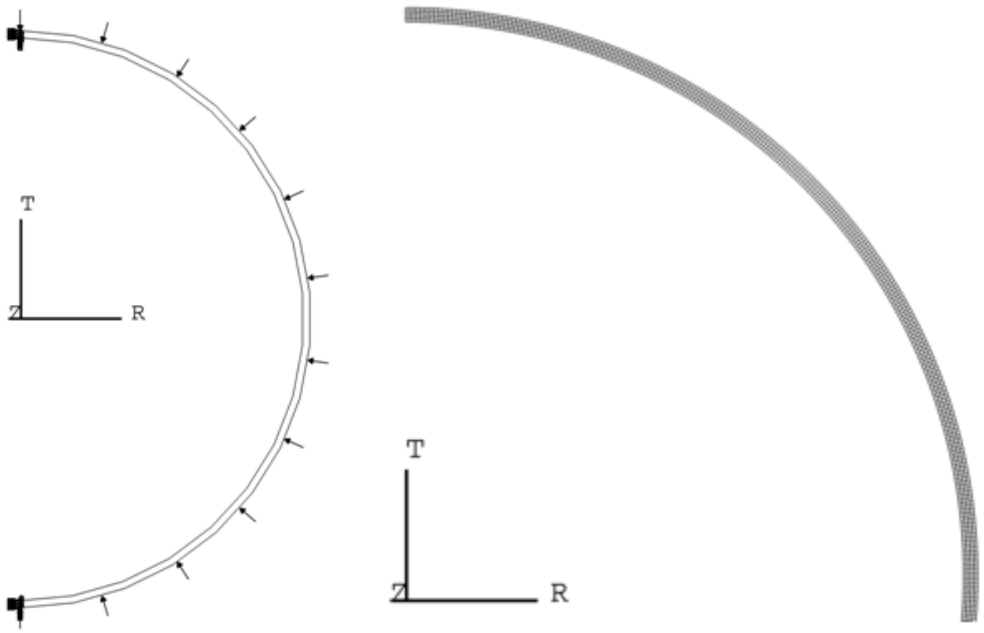

(a) geometry (b) mesh

Figure 3.3 Finite element model of composite shell for (a) geometry and (b) mesh.

The numerical results for ζ of the center point of the shell is shown in Figure 3.4, in comparison with the converged analytical results in Section 3.3. The analytical and finite element analysis (FEA) results are in very good agreement. During the first cycle they are almost the same. After the first cycle, the analytical and FEA results begin to deviate and the deviation gets worse as time progresses, although the low frequency response of the two still compare very well. There are two reasons for the deviation.

Firstly, the FEA model used two-dimensional continuum elements so that radial stress waves were generated in addition to circumferential waves, while the analytical shell model neglected radial stress waves through the thickness of the shell. Secondly, the FEA solution used implicit time integration to determine the transient shell response, while the MATLAB program used explicit time integration to solve the equations of motion. Both numerical schemes had errors which accumulated differently over time.

Two other shells with the same radius and thickness but subtended angle $\theta_0 = \pi/2$ and $\theta_0 = \pi/3$ were simulated in ABAQUS Implicit. Predictions of the normalized radial displacement ζ at the center point of the shell were compared to the FEA in Figures 3.5 and 3.6. Again 15 terms of the Fourier series expression for ζ were taken to assure convergence in the analysis. There is even better agreement between the FEA and predicted results for small angular extents than was the case for a semi-circular shell ($\theta_0 = \pi$). The best agreement between FEA and the predicted transient response was for the smallest angular extent, $\theta_0 = \pi/3$. This suggests that the model is better for shallow shells, when the geometric nonlinearities are not as severe.

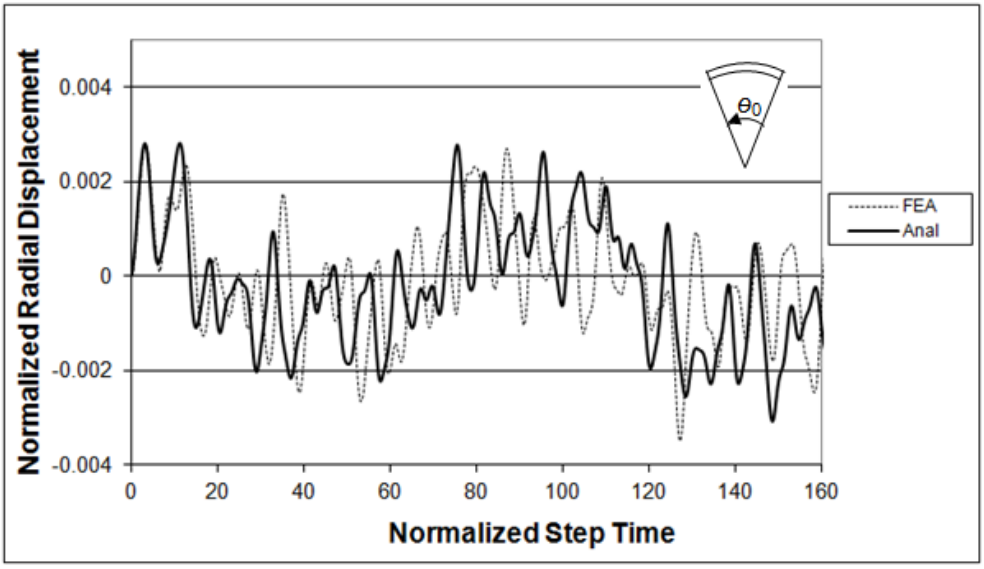

Figure 3.4 Comparison of FEA and analytical solutions for ζ at shell center, $\theta_0 = \pi$.

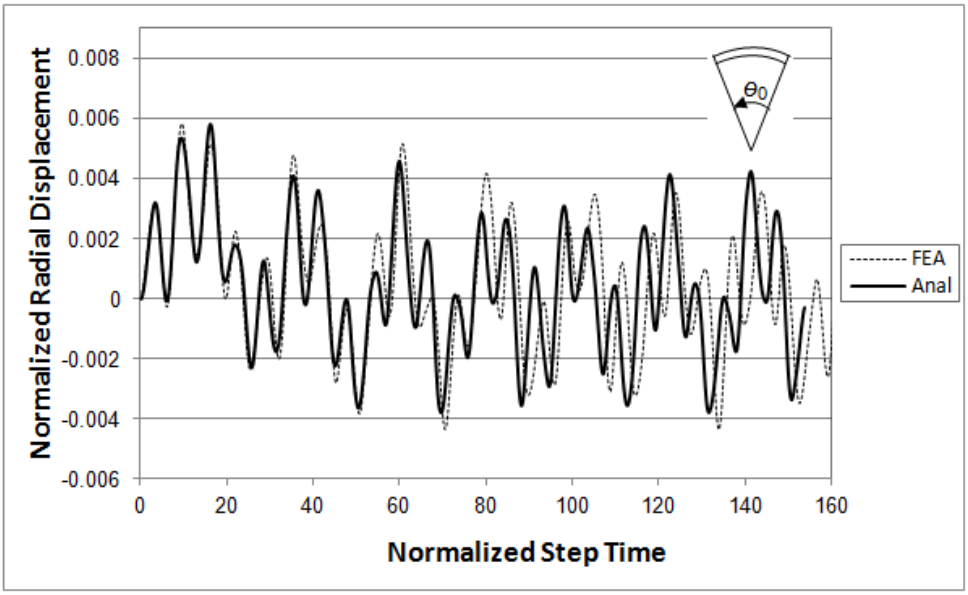

Figure 3.5 Comparison of FEA and analytical solutions for ζ at shell center, $\theta_0 = \pi / 2$.

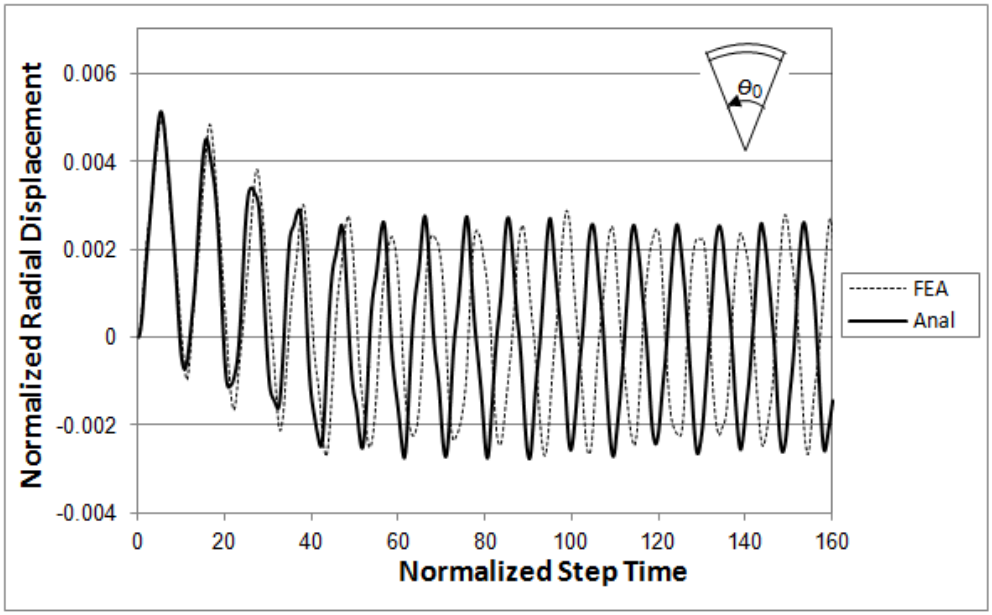

Figure 3.6 Comparison of FEA and analytical solutions for ζ at shell center, $\theta_0 = \pi/3$.

3.5 Dynamic Instability

When assessing the dynamic instability of the shell, the Budiansky-Roth buckling criterion [2] was used: the equations of motion were solved for various values of the loading and the value at which there was a significant jump in the response signified the onset of dynamic instability or buckling. The application of this criterion requires solving the equations of motion for different values of peak pressure p_0, monitoring the significant change in shell responses and determining the critical peak pressure p_{0cr}. Characterized by pressure pulse loading, this specific type of dynamic instability is defined as dynamic pulse buckling [1, 70]. The example in Section 3.3 was performed again to assess shell dynamic buckling. The normalized radial displacement ζ of the

center point of the shell was obtained for various values of peak pressure p_0, as shown in Figure 3.7.

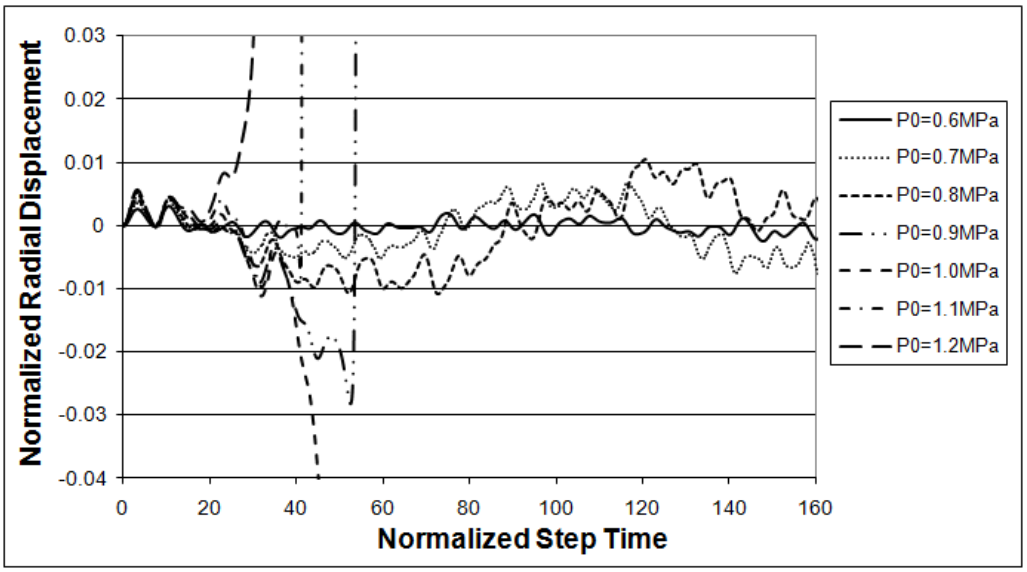

Figure 3.7 Occurrence of dynamic buckling in response of ζ at shell center.

It can be observed that for small values of peak pressure, there are small oscillations for ζ, and the oscillation amplitudes gradually increase with increasing magnitude of the peak pressure. When the peak pressure reaches a critical value $0.9MPa$, ζ goes to infinity, which means nothing else but the occurrence of shell buckling. A peak pressure larger than the critical value only makes the buckling occur sooner.

3.6 Comparison with Dynamic Pulse Bucking Tests

Experiments concerning dynamic pulse buckling of laminated composite shells are lacking, even though they are needed to compare the analytical model and FEA.

However, test data on the dynamic stability of clamped steel arches subjected to impulsive loading were presented by Humphreys in Reference [71]. His test data was given in dimensionless form for the impulse and arch geometry and is shown in Figure 3.8. The solid circles indicate buckled and failed shells, while the open circles indicate unbuckled or undamaged shells. Marginal cases are shown with partially filled circles. Dynamic buckling of the steel arch is a special case of the solution for the composite arch. The circumferential membrane and bending stiffness reduce to $A_{22} = Eh/\left(1-\nu^2\right)$ and $D_{22} = Eh^3/12\left[\left(1-\nu^2\right)\right]$, respectively, where E and ν are the Young's modulus and Poisson's ratio of steel, respectively. Hence, $\alpha^2 = h^2/\left(12a^2\right)$. Predicted buckling loads, expressed in terms of the impulse parameter, is shown for several shell geometries, expressed in terms of shape parameter, in Figure 3.8. The impulse was taken as the area under the pressure pulse. There is very good agreement between the predicted and test results. Therefore, the criterion for dynamic buckling has been validated, at least on isotropic shells. It is assumed that similar conclusions could be made for a laminated composite shell.

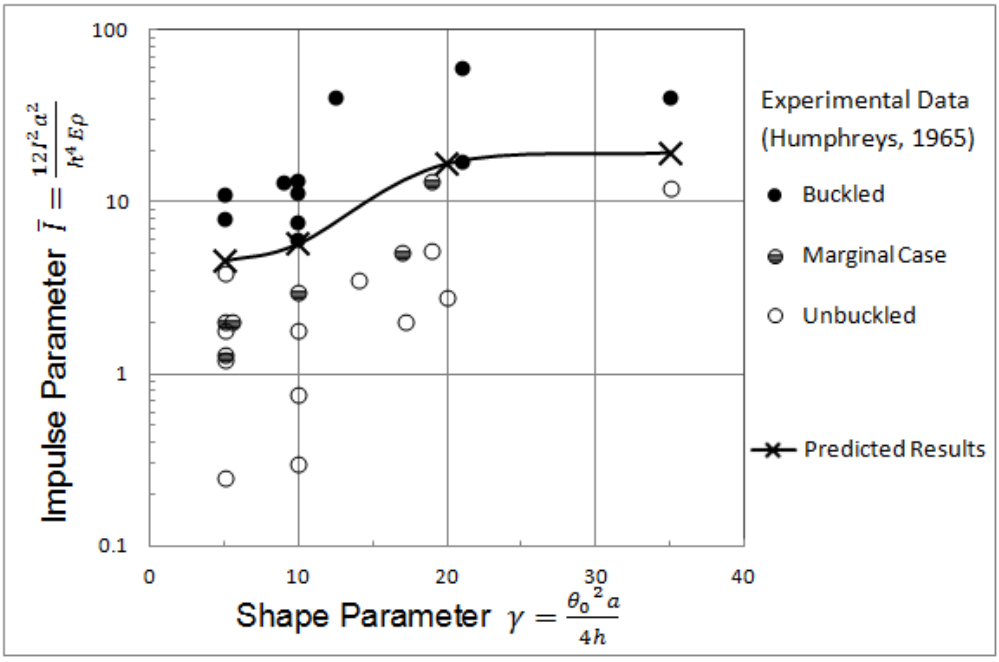

Figure 3.8 Comparison of predicted buckling load with experimental results on steel arches (Humphreys, 1965).

3.7 Parametric Study

Parametric studies on load duration, shell aspect ratio, shell subtended angle and laminate lay-up are performed in this section.

3.7.1 Load duration

Load duration ΔT determines whether the pressure pulse loading is impulsive, dynamic or quasi-dynamic. Consider the 0/90 Woven Roving E-Glass/Vinyl Ester shell with radius $a = 80mm$, aspect ratio $a/h = 40$ and subtended angle $\theta_0 = \pi$. The critical peak pressures for different load durations are shown in Figure 3.9, where the abscissa axis is on logarithmic scale.

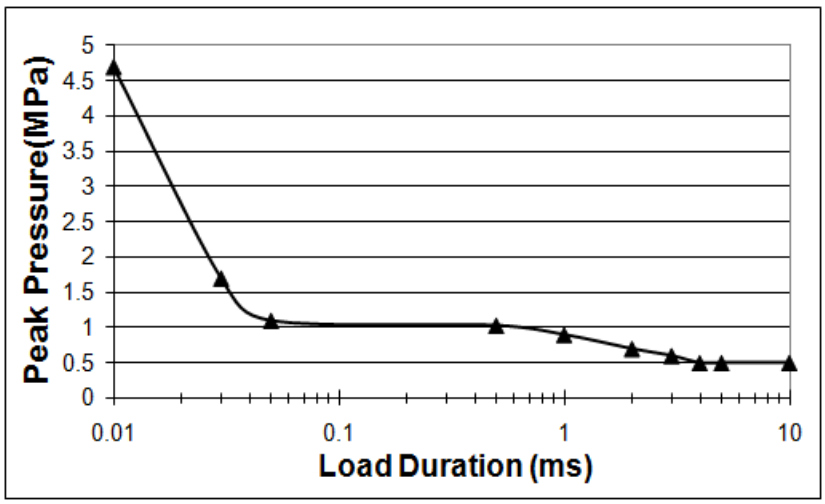

Figure 3.9 Influence of load duration on critical peak pressure for 0/90 E-Glass/Vinyl Ester shell.

The shell fails due to buckling for all the load durations. From the plot it can be seen that in the load duration range 0.01-0.05 ms there is a sharp decrease in critical peak pressure with pulse duration and the pressure pulse loading is considered as impulsive. In the range 0.05-4 ms the critical peak pressure decreases gently with pusle duration and the pressure pulse loading is dynamic. In the range 4-10 ms the critical peak pressure is relatively constant and the pressure pulse loading is said to be quasi-dynamic.

3.7.2 Aspect ratio

A brittle orthotropic composite shell may actually fail due to local tensile or compressive failure of individual plies instead of buckling of whole shell. Ply failure criteria for an orthotropic shell is given in Appendix D. Consider the orthotropic shell made of 0/90 Woven Roving E-Glass/Vinyl Ester with radius $a = 80$ mm and

subtended angle $\theta_0 = \pi$. The load duration is $\Delta T = 1$ ms. Both ply failure and buckling are carried out for different aspect ratios (a/h) and the critical peak pressures are shown in Figure 3.10. It can be seen that thicker shells are more likely to fail by ply failure, while thinner ones by buckling.

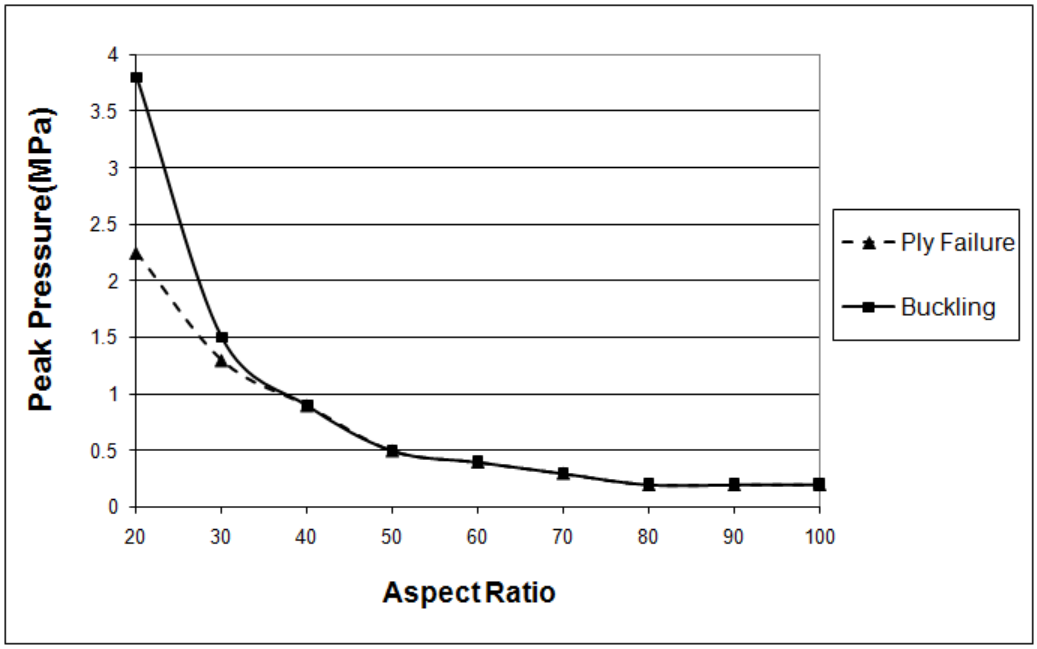

Figure 3.10 Influence of aspect ratio on the type of failure for 0/90 E-Glass/Vinyl Ester shell.

3.7.3 Subtended angle

The subtended angle θ_0 is an important parameter because it determines whether the shell is a shallow or deep shell. In this parametric study, consider the orthotropic shell of radius $a = 80$ mm made of 0/90 Woven Roving E-Glass/Vinyl Ester. The load duration is $\Delta T = 1$ ms. For different subtended angles, ply failure and buckling are carried with two different aspect ratios, as shown in Figure 3.11.

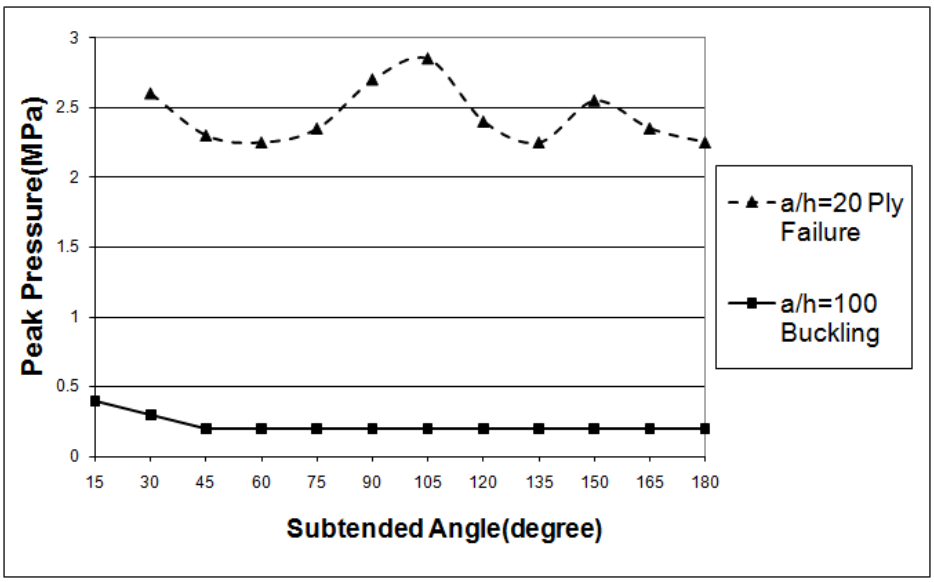

Figure 3.11 Influence of subtended angle on critical peak pressure for 0/90 E-Glass/Vinyl Ester shell.

For the shells with aspect ratio $a/h = 20$, ply failure is the dominant mode of shell failure, and 30^0, 105^0, 150^0 give higher failure resistances. For those shells with aspect ratio $a/h = 100$, buckling dominates the mode of shell failure and subtended angle has little effect on critical peak pressure. The curve of aspect ratio $a/h = 20$ is truncated at $\theta_0 = 30^\circ$ because the curved shell assumption breaks down when $\frac{a \cdot \theta_0}{h} < 10$.

3.7.4 Laminate lay-up

The dynamic instability of laminated composite shell will be influenced by shell lay-up. Three different lay-ups are chosen for laminated shells made of unidirectional E-Glass/Epoxy: symmetric ($[90^0/0^0]_s$), anti-symmetric ($[90^0/45^0/-45^0/90^0]$) and quasi-isotropic ($[90^0/45^0/0^0/-45^0]$). Material properties for the unidirectional E-Glass/Epoxy

were taken from Peters [95] and are also shown in Table 3.1. Each of the shells has a radius $a = 80\,\text{mm}$, aspect ratio $a/h = 60$, and subtended angle $\theta_0 = \pi$. The shells all weigh the same. The load duration is $\Delta T = 1$ ms.

With an aspect ratio $a/h = 60$, failure is due to buckling for all the lay-ups considered. The critical peak pressures for these shells are listed in Table 3.2. It can be seen that even though all the shells have the same geometry and weight, their lay-ups affect c and α^2 and play an important role in determining the shell resistance to dynamic instability. According to Table 3.2, the quasi-isotropic lay-up gives the lowest buckling resistance, while the symmetric lay-up gives the highest buckling resistance of all three lay-ups.

Table 3.2 Critical peak pressure for laminated composite shells with different lay-ups.

Uni-Directional E-Glass/Epoxy Lay-up	$c(m/s)$	α^2	$P_{0cr}(MPa)$
Symmetric $[90^0/0^0]_s$	3,843.9	3.36e-5	0.71
Anti-symmetric $[90^0/45^0/-45^0/90^0]$	4,154	2.96e-5	0.7
Quasi-isotropic $[90^0/45^0/0^0/-45^0]$	3,581.1	2.92e-5	0.53

3.8 Concluding remarks

Dynamic pulse buckling of a single curvature laminated composite shell under uniformly distributed external pressure pulse loading was examined in this chapter. The transient shell response was found using Lagrange's equation of motion. The analytical

solution governing the transient shell response compared very well with finite element analysis results using ABAQUS Implicit.

Buckling pressures were determined using the Budiansky and Roth criterion. The predicted buckling was shown to agree with experimental results on impulsively loaded steel arches from Humphreys in 1965. A parametric study was then performed on the composite shell. Load duration determined whether the buckling response was impulsive, dynamic or quasi-dynamic. It was found that thicker shells were more likely to fail by first-ply failure rather than buckling, while thinner shells were more susceptible to fail by buckling than first-ply failure. The angular extent of the thicker shell also appeared to influence the critical peak pressure at which first-ply failure occurs, although shell angular extent of the thinner had no influence on the buckling pressure. Finally, lay-up of the composite shell affects the critical pressure at the onset of dynamic instability and may be adjusted to increase the buckling resistance of the shell.

CHAPTER IV

CURVED COMPOSITE SANDWICH PANELS UNDER EXTERNAL BLAST

When the curved composite sandwich panels are exposed to external pressure pulses, their deformation and stability are affected by the fact that the core is compressible. In Chapter III, it was found that thicker shells were more likely to fail by fracture during stable response rather than buckling, while the opposite was true for thinner shells. This conclusion also indicates that it is unlikely that a composite sandwich shell, which behaves globally like a thick shell, would undergo global buckling before stable deformation and fracture of its facesheet and/or core. However, the sandwich shell consists of two thin facesheets and a compressible core, and transverse or through-thickness deformation of the core allows facesheets to deform as monolithic shells. This may give rise to an additional buckling mode, local facesheet wrinkling, while the global sandwich shell response is in a stable deformation mode.

This chapter addresses the problem of local dynamic pulse buckling of a curved composite sandwich panel. The facesheets of the sandwich panel are considered to be made from fiber-reinforced polymeric materials, while the core is considered to be made of elastically deformable polymeric foam. While many foam core materials exhibit energy absorption through permanent crushing, there are some foams that can be extremely resistant to permanent crushing because of their high compressive strength.

The Divinycell HCP foams manufactured by Diab [81], for instance, are designed for lightweight buoyancy, excellent hydraulic compressive properties and high impact resistance. They are typically used in marine and naval applications, and have very high compressive strength. Composite sandwich panels made with this type of core material will exhibit purely elastic response before facesheet fracture. Equations of motion for the facesheet transient deformations are derived from Lagrange's equations of motion, and solutions using this approach are compared to FEA results from ABAQUS Implicit. Both facesheet fracture during stable response and local dynamic pulse buckling of facesheets are considered as possible curved sandwich panel modes of failure. The Budiansky-Roth criterion is also used as the dynamic instability criterion.

4.1 Problem Formulation

Consider the two-sided clamped, curved sandwich panel shown in Figure 4.1. The single curvature, composite sandwich shell has facesheet thickness h and core thickness H. The mid-surfaces of the composite facesheets are defined with radius a_1 and a_2, and the shell subtends an angle θ_0. The panel is fixed or clamped at the edges $\theta = 0, \theta_0$. The facesheets consist of orthotropic, linear elastic material, while the foam core is idealized as isotropic, elastic material. The mass densities of facesheets and core are ρ_f and ρ_c, respectively. There is perfect bonding between facesheets and core. The length of the shell is very long and it is subjected to uniformly distributed pressure pulse:

$$p(t) = p_0\left(1 - \frac{t}{\Delta T}\right) \tag{4.1}$$

where p_0 is the peak pressure, ΔT is the load duration and t is the time. The sandwich shell therefore deforms in a state of plane strain.

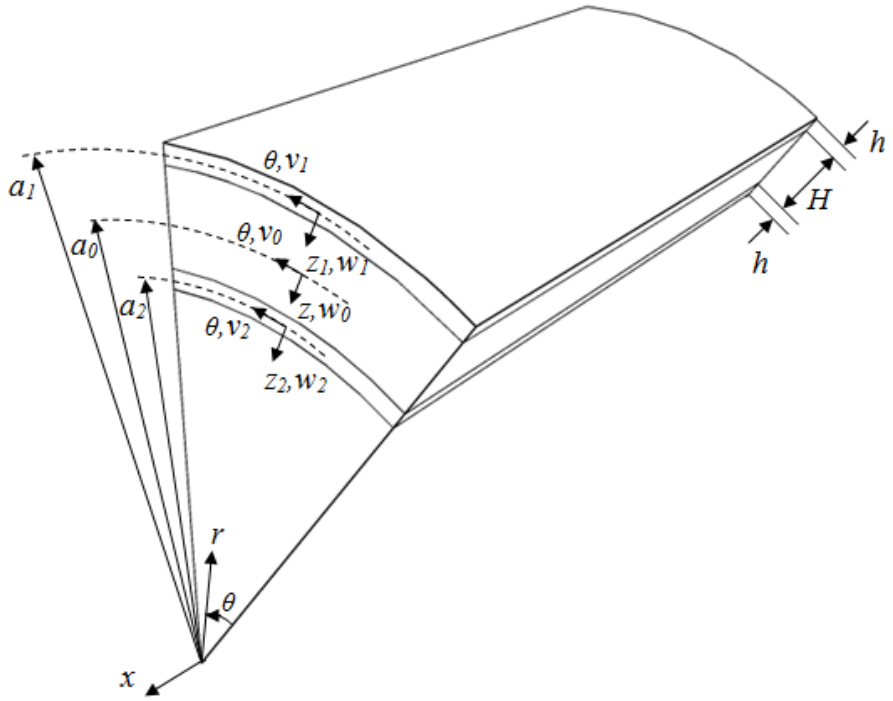

Figure 4.1 Geometry of composite sandwich shell.

The facesheets are thin shells with radial deflections w_1 and w_2 and tangential deformations v_1 and v_2, as shown in Figure 4.1. These deformations are related to local coordinate systems θ, z_1 and θ, z_2, where z_1 and z_2 are defined at the mid-surface of the facesheets. The deformations at the mid-surface of the core are denoted w_0 and v_0 and likewise, these are defined with respect to θ, z. Geometric imperfection, which may trigger buckling modes, could be introduced in the above expressions for radial and tangential deformations. However, they are not necessary for type of pulse buckling that is the subject of this chapter and are omitted.

Facesheet strains are derived based on large deflection, thin shell theory, while the core strains are obtained using the assumption of small deflection, thick shell theory, in particular first order shear deformation theory. Modeling the sandwich shell in this way allows one to assess both shallow and deep sandwich shells. Specialized strain-displacement relations for the facesheets and core are derived in the following sections.

4.1.1 Facesheet kinematics

We introduce normalized facesheet deflections as follows: $\zeta_1 = w_1/a_1$, $\psi_1 = v_1/a_1$, $\zeta_2 = w_2/a_2$, $\psi_2 = v_2/a_2$. For fully clamped boundary condition of the sandwich shell, the facesheet deflections are subject to $\zeta_1 = \zeta_2 = 0$, $\partial\zeta_1/\partial\theta = \partial\zeta_2/\partial\theta = 0$ and $\psi_1 = \psi_2 = 0$ at $\theta = 0, \theta_0$. The boundary conditions of the facesheets are satisfied by the following Fourier series representations:

$$\zeta_1 = \sum_{n=0}^{\infty} e_n \left(1 - \cos\frac{2\pi\theta}{\theta_0}\right)\cos\frac{n\pi\theta}{\theta_0} \tag{4.2}$$

$$\psi_1 = \sum_{n=1}^{\infty} f_n \sin\frac{n\pi\theta}{\theta_0} \tag{4.3}$$

$$\zeta_2 = \sum_{n=0}^{\infty} g_n \left(1 - \cos\frac{2\pi\theta}{\theta_0}\right)\cos\frac{n\pi\theta}{\theta_0} \tag{4.4}$$

$$\psi_2 = \sum_{n=1}^{\infty} h_n \sin\frac{n\pi\theta}{\theta_0} \tag{4.5}$$

where e_n, f_n, g_n and h_n are time-varying amplitudes.

Following Appendix B, the hoop strain in the outer and inner facesheets can be expressed as

$$\varepsilon_{\theta 1} = \varepsilon_{\theta m1} + z_1 \kappa_{\theta 1} \tag{4.6}$$

and

$$\varepsilon_{\theta 2} = \varepsilon_{\theta m2} + z_2 \kappa_{\theta 2} \tag{4.7}$$

where the mid-surface strain and the change in curvature in the outer (inner) facesheets are

$$\varepsilon_{\theta m1} = \psi_1' - \zeta_1 - \underline{\zeta_1 \psi_1'} + \frac{1}{2}\zeta_1'^2 \tag{4.8}$$

$$\kappa_{\theta 1} = -\frac{1}{a_1}(\zeta_1'' + \underline{\zeta_1}) \tag{4.9}$$

$$\varepsilon_{\theta m2} = \psi_2' - \zeta_2 - \underline{\zeta_2 \psi_2'} + \frac{1}{2}\zeta_2'^2 \tag{4.10}$$

$$\kappa_{\theta 2} = -\frac{1}{a_2}(\zeta_2'' + \underline{\zeta_2}) \tag{4.11}$$

and $[\ ]'$ denotes derivative with respect to θ. The above expressions are based on large deflections of the shell and include geometric nonlinearities. The terms underlined in Equations (4.8)-(4.11) do not appear in shallow shell theory, but they are necessary for a deep shell.

4.1.2 Core kinematics

The following assumptions are made to enable core strains to be fully determined by the facesheet deformations:

1. Since the facesheets are perfectly bonded to the core, the radial and tangential deformations of the core at the bond interface can be determined from facesheet deformations. The radial deformations of the core at the bond interface are equal to the mid-surface radial deformation of the facesheets because the through-thickness deformation of the thin facesheet was ignored. A similar assumption is made for the core tangential deformations at the bond interface since variations in the tangential deformation from the mid-surface to the outer surfaces of the facesheets would be small because of the thinness of the facesheet to the core.

2. The radial and tangential deformations at the core mid-surface are given by

$$w_0 = \frac{w_1 + w_2}{2} \tag{4.12}$$

and

$$v_0 = \frac{v_1 + v_2}{2} \tag{4.13}$$

The above assumption may be verified by FEA, as will be discussed later.

3. To account for transverse shear deformation of the core, it is assumed that plane sections of the core (transverse normal to the mid-surface) rotate uniformly with angle

$$\phi_0 = \frac{v_2 - v_1}{H} \tag{4.14}$$

Equation (4.14) is consistent with first-order shear deformation theory, although the rotation is treated as an independent of tangential deformation in first-order shear deformation theory.

4. To account for transverse compressibility of the core, an average radial strain is as calculated as

$$\varepsilon_r = \frac{w_2 - w_1}{H} \tag{4.15}$$

Following Assumptions 3 and 4 are linear through-thickness variation of tangential and radial deformations

$$v(r,\theta,t) = v_0(\theta,t) + z\phi_0 \tag{4.16}$$

and

$$w(r,\theta,t) = w_0(\theta,t) + z\varepsilon_r \tag{4.17}$$

The boundary conditions for the core $v = 0,\ w = 0$ and $\phi_0 = 0$ at $\theta = 0, \theta_0$ then follow naturally from Equations (4.14)-(4.17), based on the Fourier series chosen for facesheet deformations.

The tangential and radial displacement fields for the core are first order approximations. They allow resistance from core transverse shear and radial compressive stresses on the facesheets to be evaluated in an average sense. Higher-order sandwich shell theory involving nonlinear variations of the tangential and radial displacement fields with respect to through-thickness coordinate have been proposed to account for core transverse shear and compressibility [82-86]. Such theories are limited to shallow shells and do not involve higher order terms in the membrane strains of the facesheet, which are important for determining its dynamic stability. It will be shown later that Equations (4.16) and (4.17) yield sufficient accuracy for predicting local facesheet buckling.

The above core mid-surface deformations are normalized as follows: $\zeta_0 = w_0/a_0$, $\psi_0 = v_0/a_0$, where $a_0 = (a_1 + a_2)/2$. Since the core is thick compared to its mean radius, small deflection, first-order shear deformation theory is used to evaluate hoop strain and transverse shear strain in the core:

$$\varepsilon_\theta = \psi_0' - \zeta_0 + \frac{z}{a_0}\phi_0' \tag{4.18}$$

$$\gamma_{r\theta} = -\zeta_0' - \phi_0 + \psi_0 \tag{4.19}$$

The transverse shear strains are constant through the thickness in first-order shear deformation theory. These core strains can be expressed further in facesheet dimensionless variables as

$$\varepsilon_r = \frac{a_1}{H}(\mu\zeta_2 - \zeta_1) \tag{4.20}$$

$$\varepsilon_\theta = \frac{(\psi_1' + \mu\psi_2')}{(1+\mu)} - \frac{(\zeta_1 + \mu\zeta_2)}{(1+\mu)} + \frac{z}{a_0}\frac{a_1}{H}(\mu\psi_2' - \psi_1') \tag{4.21}$$

$$\gamma_{r\theta} = -\frac{(\zeta_1' + \mu\zeta_2')}{(1+\mu)} - a_1\frac{(\mu\psi_2 - \psi_1)}{H} + \frac{(\psi_1 + \mu\psi_2)}{(1+\mu)} \tag{4.22}$$

where $\mu = a_2/a_1$ is the inner-to-outer radius ratio.

4.2 Lagrange's Equations of Motion

The equations of motion governing the transient deformations of the shell are defined in normalized radial and tangential displacements and normalized time $\tau = \frac{c\,t}{a_1}$,

where $c = \sqrt{\frac{A_{22}}{\rho_f h}}$ is the wave speed and A_{22} is the membrane stiffness in the circumferential direction of the facesheet. In normalized time, the pressure pulse loading becomes

$$p(\tau) = p_0\left(1 - \frac{\tau}{\tau_0}\right) \tag{4.23}$$

where $\tau_0 = \frac{c\,\Delta T}{a_1}$ is a normalized load duration.

The transient shell response is found from Lagrange's equations of motion:

$$\frac{d}{d\tau}\left(\frac{\partial T}{\partial \dot{q}_n}\right) - \frac{\partial T}{\partial q_n} + \frac{\partial U}{\partial q_n} = Q_n \tag{4.24}$$

where q_n is a generalized coordinate, Q_n is a generalized force, T is the kinetic energy, U is the strain energy and $\dot{[\ ]} = \partial[\ ]/\partial\tau$. Generalized forces Q_n are obtained from virtual work δW:

$$Q_n = \frac{\partial(\delta W)}{\partial(\delta q_n)} \tag{4.25}$$

For uniformly distributed external pressure pulse,

$$\delta W = \int_0^{\theta_0} p(\tau)\,\delta\zeta_1\, a_1^2\, d\theta = \sum_{n=0}^{\infty} Q_n \delta e_n \tag{4.26}$$

where

$$Q_n = p(\tau) a_1^2 \int_0^{\theta_0} \left(1 - \cos\frac{2\pi\theta}{\theta_0}\right)\cos\frac{n\pi\theta}{\theta_0}\, d\theta \tag{4.27}$$

The kinetic energy of the facesheets and core are as follows:

$$T_f = \frac{A_{22}a_1}{2}\int_0^{\theta_0}\left[\dot{\zeta}_1^2 + \dot{\psi}_1^2 + \mu^3\left(\dot{\zeta}_2^2 + \dot{\psi}_2^2\right)\right]d\theta \tag{4.28}$$

and

$$T_c = \bar{\rho}\frac{A_{22}a_1}{2}\int_0^{\theta_0}\left[\dot{\zeta}_1^2 + \mu^2\dot{\zeta}_2^2 + 2\mu\dot{\zeta}_1\dot{\zeta}_2 + \frac{4}{3}\left(\dot{\psi}_1^2 + \mu^2\dot{\psi}_2^2 + \mu\dot{\psi}_1\dot{\psi}_2\right)\right]d\theta \tag{4.29}$$

where $\bar{\rho} = (1+\mu)\rho_c H/(8\rho_f h)$.

The elastic strain energy of the facesheets is from Appendix C

$$U_i = \frac{1}{2}\int (A_{22}\varepsilon_{\theta mi}^2 + D_{22}\kappa_{\theta i}^2)a d\theta,\ i = 1,2 \tag{4.30}$$

where A_{22} and D_{22} are the facesheet circumferential membrane and bending resistance, respectively. Substituting the facesheet strains given in Equations (4.8)-(4.11) into Equation (4.30) gives the strain energy of the outer and inner facesheets as

$$\begin{aligned} U_f &= \frac{A_{22}a_1}{2}\int_0^{\theta_0}\left[\left(\psi_1' - \zeta_1 - \zeta_1\psi_1' + \frac{1}{2}\zeta_1'^2\right)^2 + \alpha_1^2(\zeta_1'' + \zeta_1)^2\right]d\theta \\ &+ \mu\frac{A_{22}a_1}{2}\int_0^{\theta_0}\left[\left(\psi_2' - \zeta_2 - \zeta_2\psi_2' + \frac{1}{2}\zeta_2'^2\right)^2 + \alpha_2^2(\zeta_2'' + \zeta_2)^2\right]d\theta \end{aligned} \tag{4.31}$$

where $\alpha_1^2 = D_{22}/(a_1^2 A_{22})$ and $\alpha_2^2 = D_{22}/(a_2^2 A_{22})$. The core elastic strain energy is derived in Appendix E for the special case of plane strain as

$$\begin{aligned} U_{ce} = \eta\frac{A_{22}a_1}{2}\int_0^{\theta_0}\Big\{&(\mu\zeta_2 - \zeta_1)^2 + \omega^2(\psi_1' + \mu\psi_2' - \zeta_1 - \mu\zeta_2)^2 \\ &+ \frac{\omega^2}{3\Lambda}(\mu\psi_2' - \psi_1')\left[(-\psi_1' - \mu\psi_2' + \zeta_1 + \mu\zeta_2) + \Lambda(\mu\psi_2' - \psi_1')\right] \\ &+ \frac{\beta^2}{6\Lambda}(\mu\zeta_2 - \zeta_1)\left[6\Lambda(\psi_1' + \mu\psi_2' - \zeta_1 - \mu\zeta_2) - (\mu\psi_2' - \psi_1')\right] \\ &+ \gamma^2\left[-\zeta_1' - \mu\zeta_2' - 2\Lambda(\mu\psi_2 - \psi_1) + \psi_1 + \mu\psi_2\right]^2\Big\}d\theta \end{aligned} \tag{4.32}$$

where $\Lambda = (1+\mu)/(2(1-\mu))$, and $\eta, \omega^2, \beta^2, \gamma^2$ are elastic constants of the foam defined in Appendix E.

Coupled elastic equations of motion result from satisfying Lagrange's equation of motion as follows:

$$\sum_{m=0}^{N}\left[2(1+\bar{\rho})\ddot{e}_m + 2\mu\bar{\rho}\ddot{g}_m\right]\hat{f}_0(m,n) + P_e = \bar{Q}_n \tag{4.33}$$

$$\sum_{m=0}^{N}\left[2\mu(\bar{\rho}+\mu)\ddot{g}_m + 2\mu\ddot{e}_m\right]\hat{f}_0(m,n) + P_g = 0 \tag{4.34}$$

$$\left[\frac{2}{3}(3+4\bar{\rho})\ddot{f}_n + \frac{4}{3}\mu\ddot{h}_n\right]\frac{\theta_0}{2} + P_f = 0 \tag{4.35}$$

$$\left[\frac{2}{3}\mu(3\mu^2+4\bar{\rho})\ddot{h}_n + \frac{4}{3}\mu\ddot{f}_n\right]\frac{\theta_0}{2} + P_h = 0 \tag{4.36}$$

where n is the particular mode of the Fourier series, N is the chosen number of terms in the Fourier series, $\bar{Q}_n$ is a normalized load, P_e, P_g, P_f, P_h are elastic spring forces and $\hat{f}_0$ is given by

$$\hat{f}_0(m,n) = \int_0^{\theta_0}\left(1-\cos\frac{2\pi\theta}{\theta_0}\right)^2 \cos\frac{m\pi\theta}{\theta_0}\cos\frac{n\pi\theta}{\theta_0}\,d\theta \tag{4.37}$$

In Equations (4.33) and (4.34) there is coupling not only between each deformation mode but also between mode numbers of the same deformation mode. The normalized external load is

$$\bar{Q}_n = 2\bar{p}(\tau)\int_R\left(1-\cos\frac{2\pi\theta}{\theta_0}\right)\cos\frac{n\pi\theta}{\theta_0}\,d\theta \tag{4.38}$$

where $\bar{p}(\tau) = \frac{a_1 p_0}{A_{22}}\left(1 - \frac{\tau}{\tau_0}\right)$ is the normalized pressure pulse loading. The elastic spring forces P_e, P_g, P_f, P_h result from taking derivatives of the strain energy in terms of the generalized coordinates.

4.3 An Example

The composite sandwich shell considered has dimensions $h = 5.08\,\text{mm}$, $H = 25.4$ mm, $a_1 = 396.24$ mm, $a_2 = 365.76$ mm and $\theta_0 = 90^o$. The mean radius-to-thickness ratio of this sandwich shell is 10.71, which implies a rather thick shell. It is made with 0/90 woven E-Glass/Vinyl Ester facesheets and a Divinycell PVC HCP100 foam core, with properties of the facesheet and core listed in Table 4.1. The shell is subjected to the uniformly distributed pressure pulse described in Equation (4.1) where $p_0 = 2$ MPa and $\Delta T = 1\,\text{ms}$.

Table 4.1 Material properties of 0/90 Woven Roving E-glass/Vinyl Ester, Uni-Directional E-glass/Epoxy and foam Divinycell HCP100.

Material	0/90 Woven Roving E-Glass/Vinyl Ester	Uni-Directional E-Glass/Epoxy	Divinycell HCP100
Density (kg/m^3)	1,391	2,050	400
E_{11} (+) (GPa)	17	48	--
E_{22} (+) (GPa)	17	12	--
E_{33} (+) (GPa)	7.48	12	--
E_{11} (-) (GPa)	19	--	0.34
E_{22} (-) (GPa)	19	--	0.34
E_{33} (-) (GPa)	--	--	0.34
ν_{12}	0.13	0.19	0.3
ν_{23}	0.28	0.26	0.3
ν_{13}	0.28	0.19	0.3
ν_{31}	0.12	0.05	0.3
$G_{12}=G_{21}$ (GPa)	4.0	6	0.131
$G_{23}=G_{32}$ (GPa)	1.73	5	0.131
$G_{13}=G_{31}$ (GPa)	1.73	6	0.131
q (MPa)	--	--	10.3
γ_f	--	--	0.35
X_T, σ_{10} (+) (MPa)	270	1,020	--
X_C, σ_{10} (-) (MPa)	200	490	--
Y_T, σ_{20} (+) (MPa)	270	8	--
Y_C, σ_{20} (-) (MPa)	200	78	--
Z_T, σ_{30} (+) (MPa)	23.2	8	--
Z_C, σ_{30} (-) (MPa)	343.5	78	--
S_L, $\tau_{120}=\tau_{210}$ (MPa)	40	23	7.44
S_T, $\tau_{130}=\tau_{310}$ (MPa)	31.6	23	7.44
S_T, $\tau_{230}=\tau_{320}$ (MPa)	31.6	66	7.44

A MATLAB program was written to solve coupled equations of motion for time-varying amplitudes of the Fourier series in Equations (4.2)-(4.5), i.e., coefficients e_n, f_n, g_n and h_n. The radial or transverse deflections of the outer and inner facesheets at 0.297 ms for various numbers of terms of the Fourier series are shown in Figures 4.2 (a) and (b), respectively. The outer facesheet deflections were found to converge with 17 terms or n=16 in the Fourier series expansion (n=0 exists for the radial deflection). Curiously the inner facesheet deflections converged more rapidly with only 15 terms. Predictions from finite element analysis, which will be discussed later, are shown for comparison.

The tangential deformations of the outer and inner facesheets at 0.297 ms are also shown in Figures 4.3 (a) and (b), respectively, with various numbers of terms in the Fourier series. The Fourier series for tangential deformations start at n=2. The tangential deformations converged more rapidly than the radial deflections; it only took 6 terms for the tangential deformations to converge. From the convergence study, it was concluded that 17 terms would give sufficient accuracy.

Hoop stresses in the inner and outer facesheets were calculated at 0.297 ms and are shown in Figures 4.4 (a) and (b) with 17 terms of the Fourier series. Because the bending stresses vary through the facesheet thickness, maximum and minimum hoop stresses are shown at positions S_1 and S_2 for the outer facesheet and S_3 and S_4 for the inner facesheet. It can be seen that S_4 surface, i.e., the back of the inner facesheet, is more critical with respect to failure than other three surfaces due to hoop direction compressive fracture near the clamped boundaries. A condition for facesheet failure will be discussed later in Section 4.5.

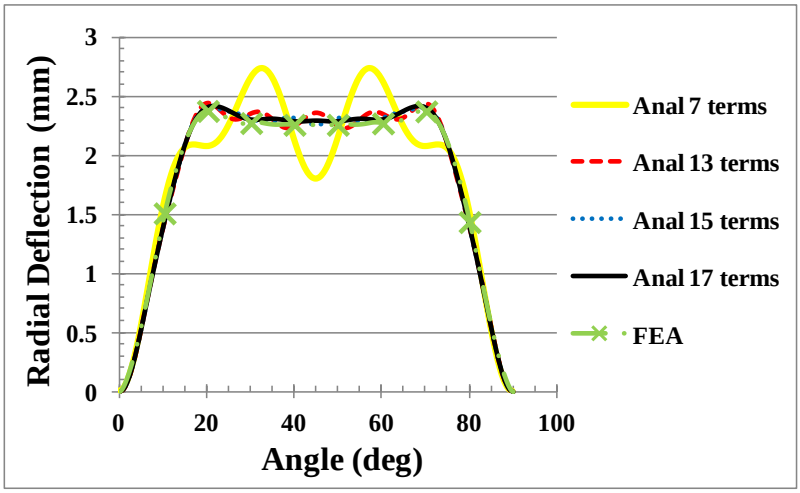

(a)

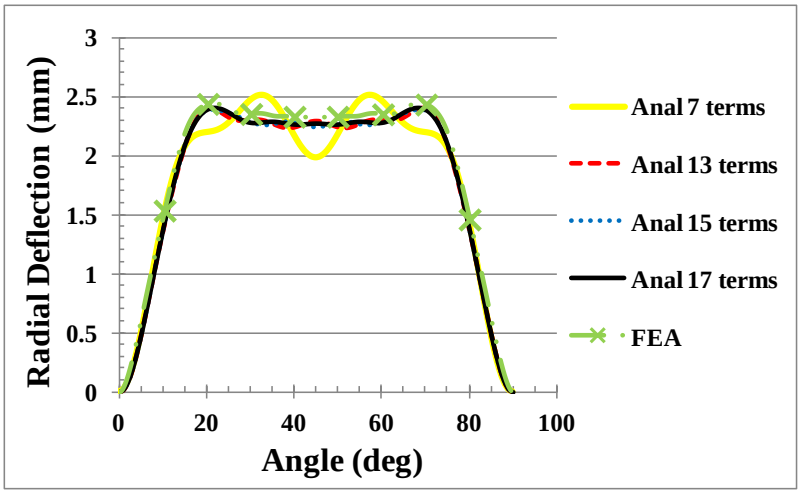

(b)

Figure 4.2 Facesheet radial deflections at 0.297 ms with increasing number of terms in Fourier series and as predicted by FEA: (a) outer facesheet and (b) inner facesheet.

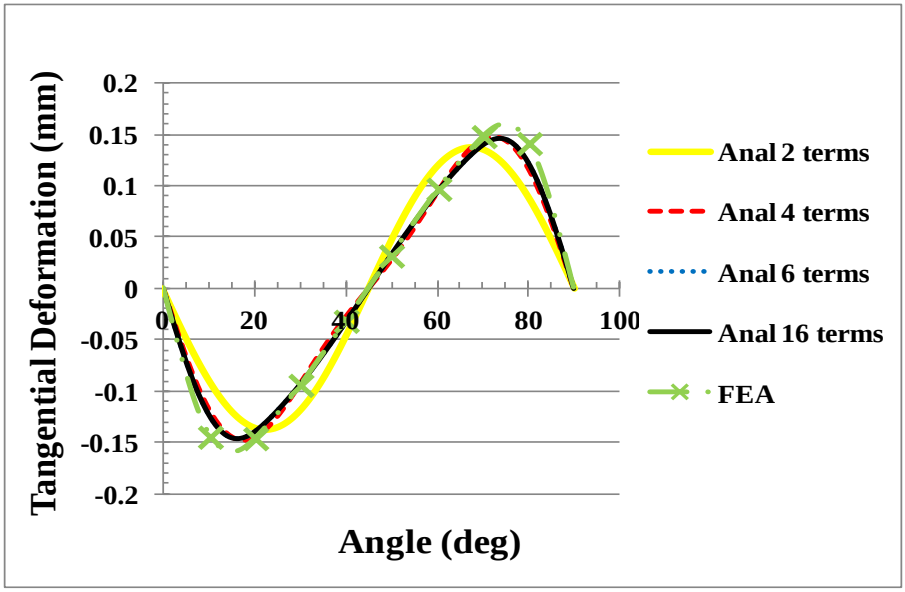

(a)

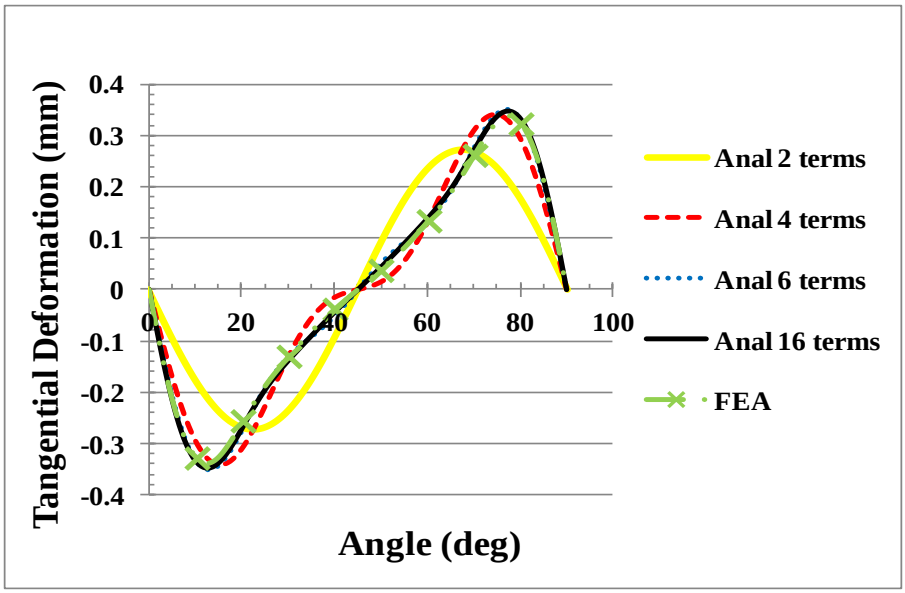

(b)

Figure 4.3 Facesheet tangential deformations at 0.297 ms with increasing number of terms in Fourier series and as predicted by FEA: (a) outer facesheet and (b) inner facesheet.

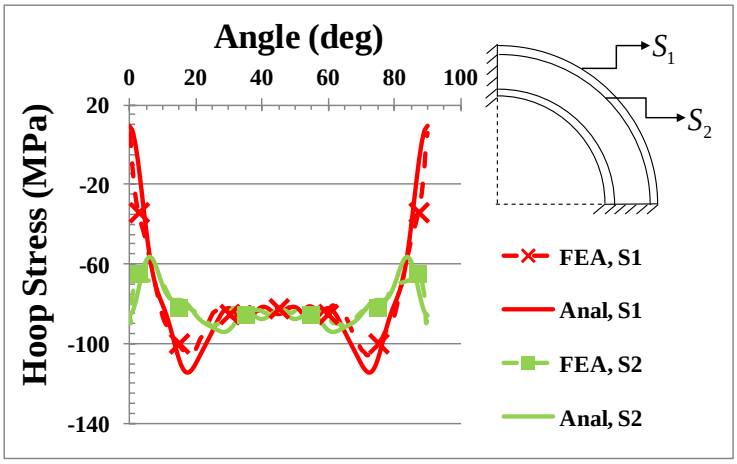

(a)

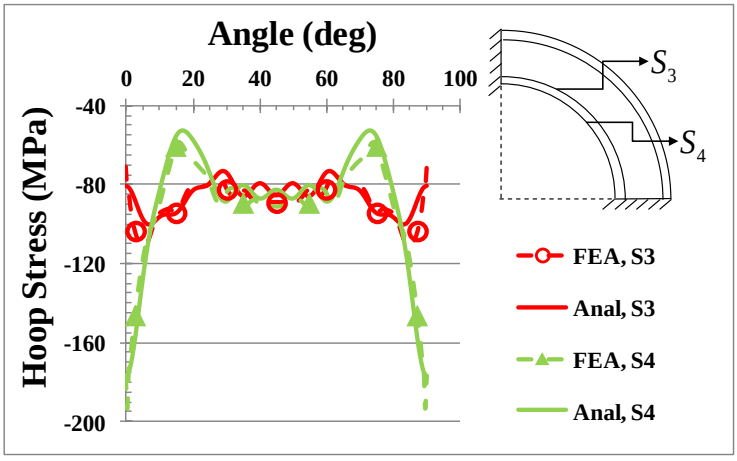

(b)

Figure 4.4 Variation of hoop stress with angle: (a) outer facesheet and (b) inner facesheet at t=0.297ms.

In order to assess the behaviour of the core, the radial and tangential deformations of the sandwich mid-plane are shown at various times in Figures 4.5 and 4.6, respectively. These are again after the 17 terms Fourier series expansion. Stresses at the sandwich mid-plane were calculated at 0.22 ms from the solutions and are shown in Figure 4.7. It is very apparent that for this rather thick shell, all stress components in the foam are at their greatest near the clamped boundaries. Also note that the magnitudes of

the peak radial, hoop and axial stresses are of the same order of magnitude as the peak transverse shear stress. A sandwich theory that ignores radial stress in the core would therefore be inaccurate in predicting the behavior of a thick curved sandwich panel. Finite element analysis predictions of the corresponding variables in the composite sandwich shell are also shown in Figures 4.2-4.7, and discussed below.

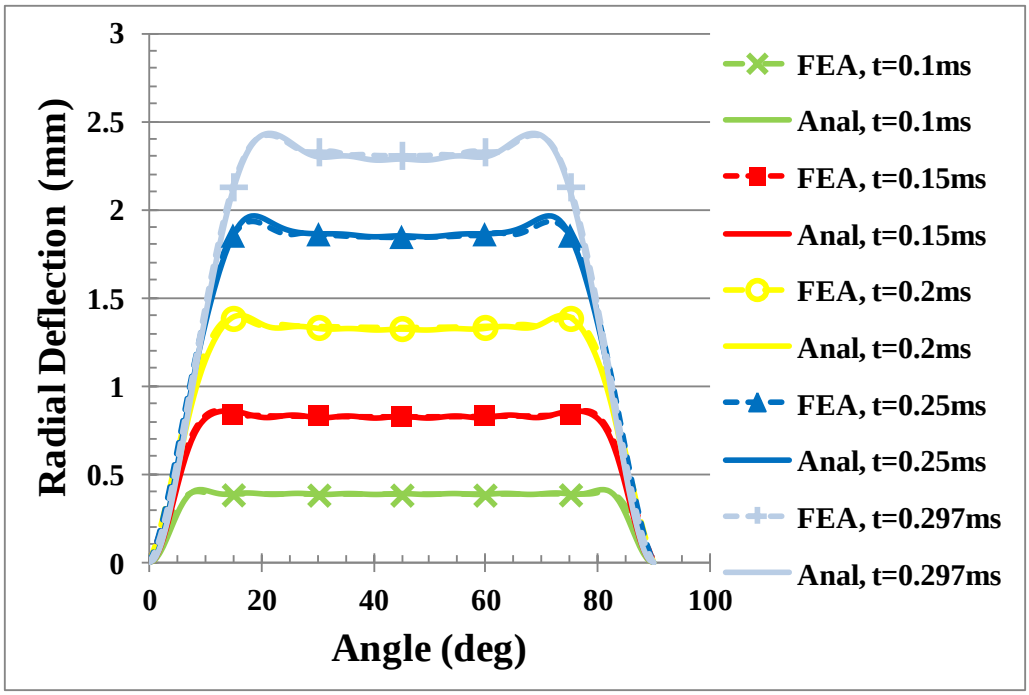

Figure 4.5 Radial deflections taken at mid-surface of sandwich shell.

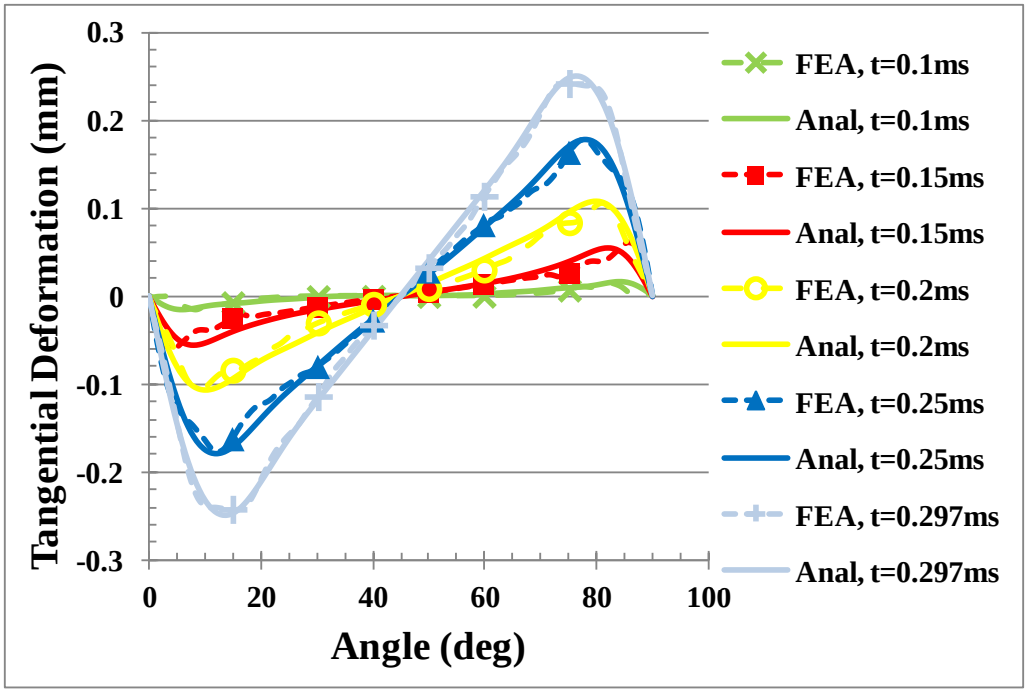

Figure 4.6 Tangential deformations taken at mid-surface of sandwich shell.

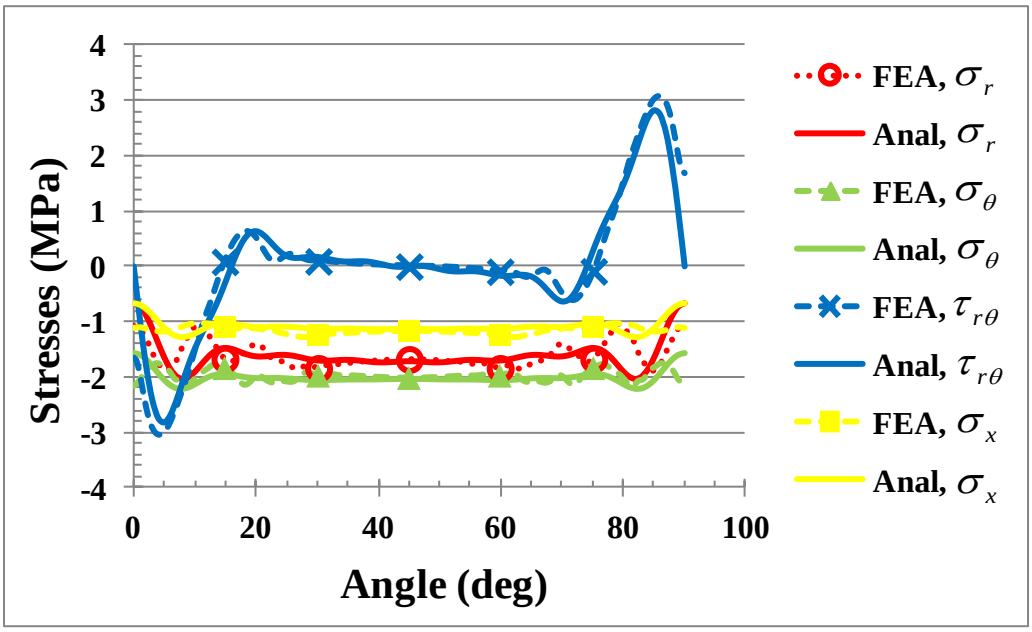

Figure 4.7 Stress variations along the mid-surface of core at t=0.22ms.

4.4 Finite Element Analysis

Finite element analysis with ABAQUS Implicit Version 6.9 [94] was done in order to corroborate solutions with the analytical model. The FEA model is shown in Figure 4.8. The sandwich panel dimensions and pulse loading are the same in the example problem of Section 4.3. The facesheets were rigidly tied using surface-to-surface tie constraint. The core was meshed with 1200 elements, while each facesheet had 400 elements. Continuum plane strain four node elements (CPE4) were chosen for both facesheets and core. The CPE4 element is a linear quadrilateral element. The facesheet material was modeled as linear elastic, orthotropic material and the core was modeled using crushable foam with isotropic hardening [94]. Plasticity properties for HCP100 were taken from Rizov [96]. However, this foam is so stiff and strong that it will not undergo crushing or plasticity for the pressure loading considered in this study.

The numerical implementation in ABAQUS Implicit involved Dynamic, Implicit analysis. The direct-integration method provided for Dynamic, Implicit analysis in ABAQUS Implicit is the Hilber-Hughes Taylor operator, which is an extension of the trapezoidal rule. Automatic time increment with specified half-step residual was used. A parametric study was done to determine that a half-step residual tolerance of 2,794 N would yield accurate results. No numerical damping was specified in the problem.

Results from the ABAQUS Implicit are compared to the results from MATLAB in Figures 4.2-4.7. Good agreement was found between the MATLAB and FEA solutions in all cases. Stresses near the clamped edges (Figures 4.4 and 4.7) were not evaluated as well as at other locations even with 17-term Fourier series in the model. The solution

from the analytical model is within 5% of the FEA radial deformations and about 15% of the FEA stresses. Fourier series solutions for deflections converge more rapidly than for stresses because the stresses are expressed in terms of derivatives of the deflections. The above result is typical of the Fourier series approach, and was deemed sufficient for this study.

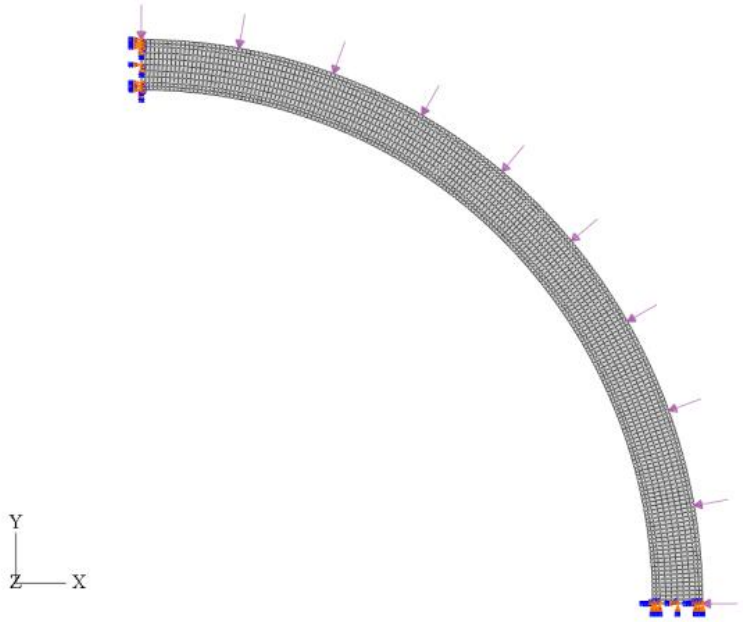

Figure 4.8 Finite element model of composite sandwich shell.

4.5 Sandwich Panel Failure

Sandwich panel failure may occur in the modes shown in Figures 4.9 (a) and (b). Facesheet failure is primarily due to compressive hoop stresses because of the initial shell curvature. As indicated in Figure 4.9 (a), it is the distal or inner facesheet, with a smaller radius of curvature and higher circumferential strain than the loaded or outer facesheet, that first experiences compressive facesheet fracture near the clamped boundaries. On the other hand, a very strong core and facesheet may prevent the failure mode shown in

Figure 4.9 (a) but the curved sandwich panel may still fail due to local facesheets dynamic pulse buckling as described in Figure 4.9 (b).

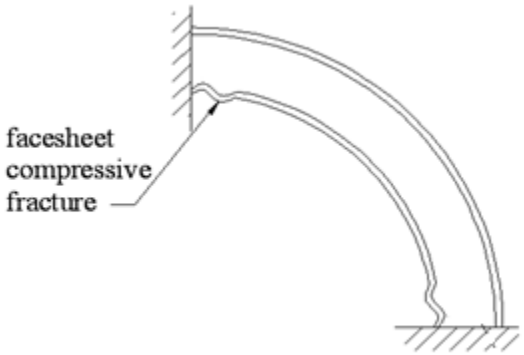

(a)

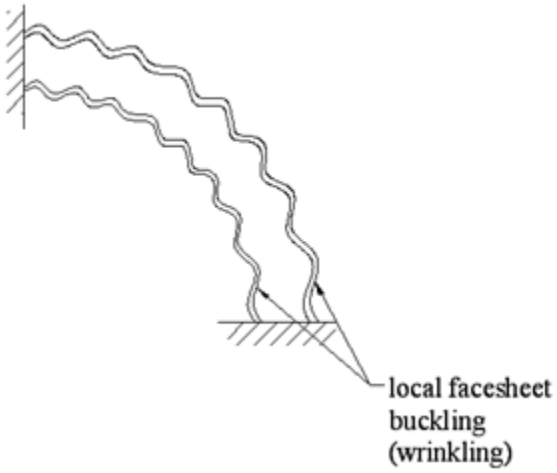

(b)

Figure 4.9 Failure modes of sandwich shell: (a) facesheet fracture during stable response and (b) dynamic instability of facesheets.

4.5.1 Facesheet failure

The modified Hashin-Rotem criteria are used to examine lamina failure of the woven roving E-Glass/Vinyl Ester [97]. According to Appendix D, the modified Hashin-

Rotem failure criteria can be used by substituting Equation (D.6) into Equation (D.2),

$$\frac{\left|\overline{Q}_{22}\varepsilon_\theta\right|}{Y_T}=1 \text{ if } \sigma_\theta > 0 \tag{4.39}$$

and

$$\frac{\left|\overline{Q}_{22}\varepsilon_\theta\right|}{Y_C}=1 \text{ if } \sigma_\theta < 0 \tag{4.40}$$

Thus the value of the hoop strain at which failure occurs is given by

$$\varepsilon_f = \frac{\min\left(Y_T, Y_c\right)}{\overline{Q}_{22}} \tag{4.41}$$

The above expression describes the maximum allowable strain based on a Hashin-Rotem composite failure criterion.

4.5.2 Facesheet dynamic instability

In order to examining dynamic instability of the facesheets, the Budiansky-Roth buckling criterion [2] was used again: the equations of motion were solved for various values of the loading and the value at which there was a significant jump in the response signified the onset of dynamic instability or buckling. The application of this criterion requires solving the equations of motion for different values of peak pressure p_0, monitoring the significant changes in facesheets radial deflections and determining the critical peak pressure p_{0cr}. Because the instability occurs under pressure pulse loading, this specific type of dynamic instability is defined as dynamic pulse buckling [1].

To illustrate dynamic pulse buckling of the facesheet, consider the composite sandwich shell made of 0/90 woven E-Glass/Vinyl Ester facesheets and Divinycell HCP100 foam core with dimensions $h = 6.4$ mm, $H = 25.4$ mm, $a_1 = 1158.9$ mm, $a_2 = 1127.1$mm and $\theta_0 = 90^o$. The mean radius-to-thickness ratio of this sandwich shell is $a_0 / h_{tot} = 29.92$, which implies it is a thin shell. The load duration is fixed at $\Delta T = 1$ ms. The normalized radial displacement of the center point of the outer facesheet ζ_{10} was obtained for various values of peak pressure p_0, as shown in Figure 4.10. A normalized step time of 100 on the abscissa corresponds to the total step time $t = 32.9$ ms.

It can be observed that for small peak pressures, there are small oscillations in ζ_{10}, and the oscillation amplitudes gradually increase with increasing magnitude of the peak pressure. When the peak pressure reaches a critical value 1.1MPa, ζ_{10} goes to infinity, which means the occurrence of facesheets dynamic pulse buckling. Also note that a peak pressure larger than the critical value only makes buckling occur sooner.

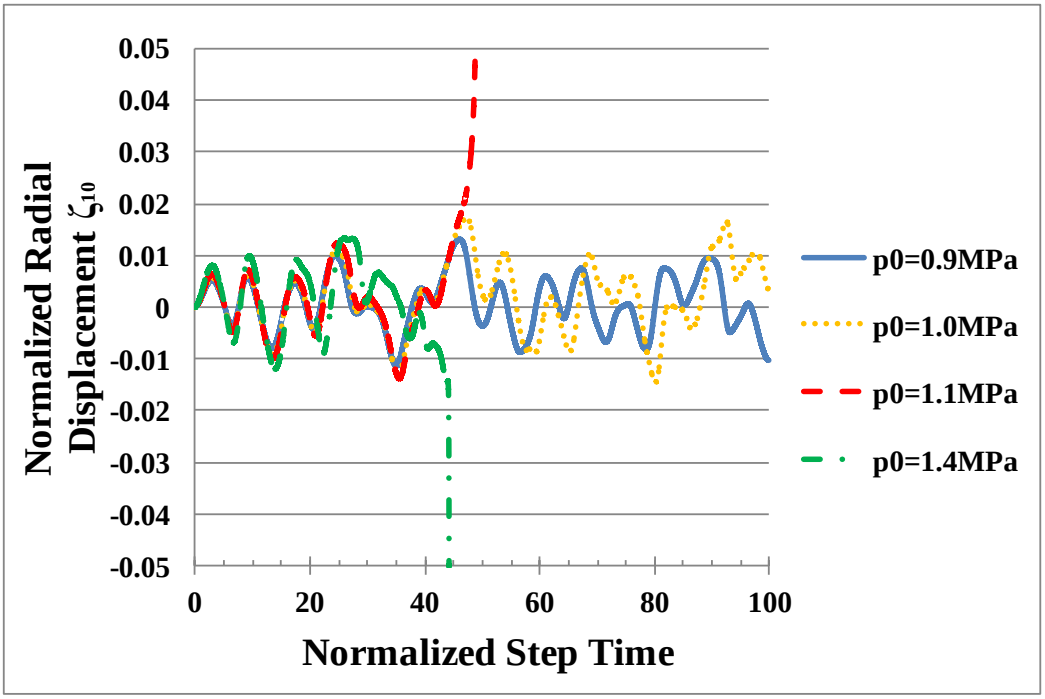

Figure 4.10 Radial deflections during stable and unstable response (ζ_{10} is the normalized radial displacement at center point of outer facesheet).

4.6 Parametric Study

A parametric study was used to determine the failure modes of curved sandwich panels. The effects of sandwich radius-to-thickness ratio, angular extent, load duration as well as composite lay-up are discussed below.

4.6.1 Radius-to-thickness ratio

The mean radius-to-thickness ratio of the sandwich shell will determine its global stiffness and strength. This parametric study was done on a curved composite sandwich panel made of 0/90 woven E-Glass/Vinyl Ester facesheets and Divinycell HCP100 foam core. The core thickness and angular extent of sandwich shell are both fixed as $H = 25.4$

mm (1 inch) and $\theta_0 = 90^o$, while the mid-surface radius of foam core a_0 and facesheet thickness h vary. The load duration is $\Delta T = 1$ ms. Facesheets failure (fracture) and dynamic pulse buckling are carried out for different mean radius-to-thickness ratios (a_0 / h_{tot}) and the critical peak pressures p_0 are shown in Figure 4.11. In the plot, a_0 / H is the sandwich core radius-to-thickness ratio and a_1 / h is the outer facesheet radius-to-thickness ratio. Higher ratio means a relatively thinner shell. It can be seen that facesheets buckling is more likely than facesheets fracture when $a_0 / H > 28$, regardless of facesheet thickness. Also note that the three facesheet fracture curves coincide to form a master curve.

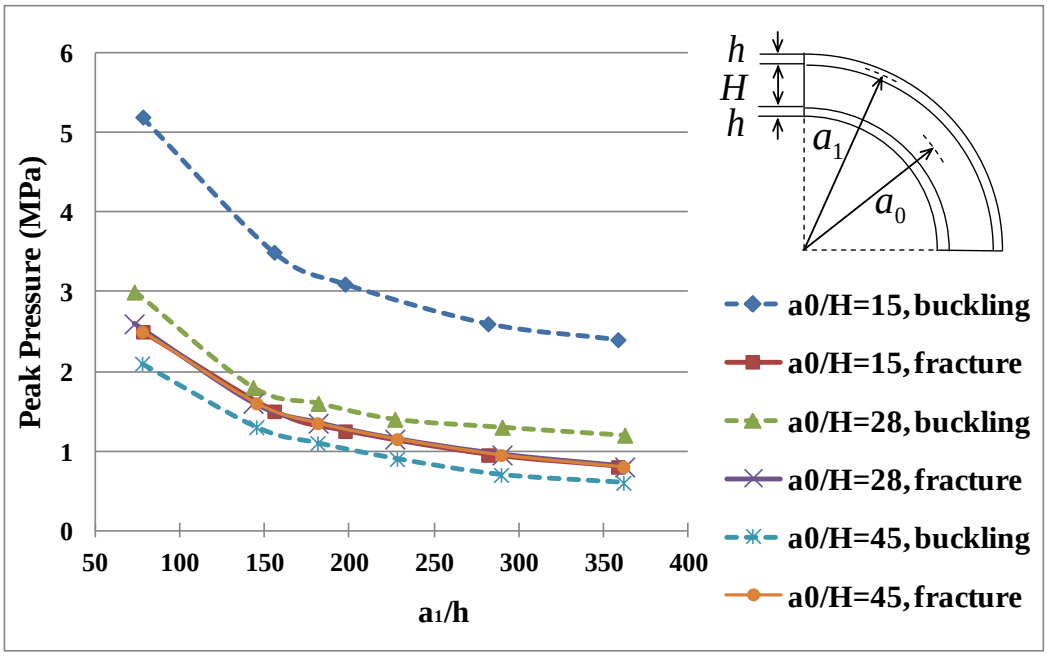

Figure 4.11 Influence of mean radius-to-thickness ratio on the failure modes of composite sandwich shell.

4.6.2 Angular extent/shallowness

Many analytical models for double curvature sandwich shells are based on shallow shell theory in order to simplify shell kinematics. The mid-surface of a shallow shell has a small rise compared to its span on a projected plane. This allows infinitesimal line elements of the mid-surface to be approximated in the rectangular coordinates of the projected plane. Vlasov [17] suggested that shallow shell theory gives sufficient accuracy for shells with a rise-to-span ratio of less than 1/5, although the delineation of shallow shell theory might vary slightly by other researchers [98-100]. A rise-to-span ratio of less than 1/5 corresponds to approximately 25 degrees of angular extent in the single curvature shell geometry.

A parametric study was done to examine how the analysis changes with angular extent. The angular extent and shallowness of the shell are related. Thus a sandwich shell with small angular extent would be categorized as shallow, while a sandwich shell with a large angular extent would correspond to a deep shell. Consider a composite sandwich shell with 0/90 woven E-Glass/Vinyl Ester facesheets and Divinycell HCP100 foam core. The thicknesses of sandwich shell are fixed as $H = 25.4\,\text{mm}$ (1 inch) and $h = 5.08\,\text{mm}$ (1/5 inch), while two different mid-surface radii of foam core a_0, 381mm (15 inch) and 1143mm (45 inch), are selected. Again the load duration is $\Delta T = 1\,\text{ms}$. For various angular extent θ_0, facesheets failure (fracture) and dynamic pulse buckling analyses are carried with mean radius-to-thickness ratios $a_0 / h_{tot} = 10.71$ and $a_0 / h_{tot} = 32.14$, as shown in Figure 4.12.

For thick curved sandwich panels ($a_0 / h_{tot} = 10.71$), failure is always in the form of facesheet fracture, i.e., the buckling loads are much higher than the facesheet fracture load. The angular extent has little effect on peak pressure to cause facesheet fracture. The curve in the plot is truncated at $\theta_0 = 45^\circ$ because the shell assumption breaks down when $\frac{a_0 \cdot \theta_0}{h_{tot}} < 10$. For thin curved sandwich panels ($a_0 / h_{tot} = 32.14$), the failure mode depends on angular extent. Thin, shallow shells undergo facesheet fracture, while thin, deep shells are more likely to fail by facesheet buckling. It also can be observed that for deep shells, the pressure amplitude at failure does not vary substantially, but it increases as θ_0 decreases in the case of shallow shells.

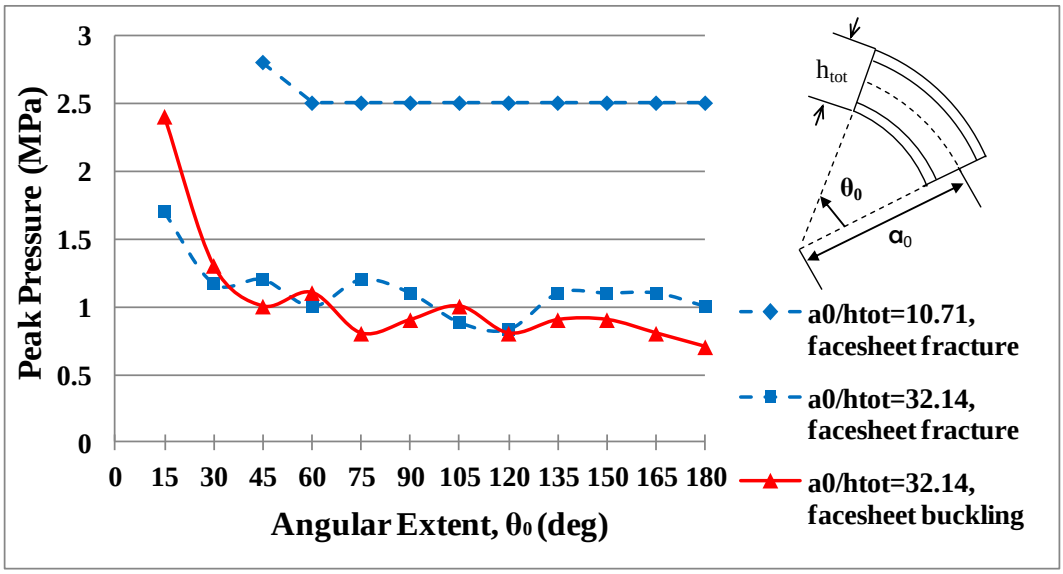

Figure 4.12 Influence of angular extent on critical peak pressure and mode of failure for composite sandwich shell.

4.6.3 Load duration

Load duration ΔT determines whether the pressure pulse loading is impulsive, dynamic or quasi-dynamic. Consider a curved composite sandwich panel made of 0/90 woven E-Glass/Vinyl Ester facesheets and Divinycell HCP100 foam core with dimensions $H = 25.4\text{mm}$, $h = 5.08\text{mm}$, $a_0 = 1143\text{mm}$ and $\theta_0 = 90^0$. The critical peak pressures for different load durations are shown in Figure 4.13, whose abscissa is on logarithmic scale.

From the plot it can be seen that the curved sandwich panel fails due to facesheet buckling for all the load durations. In the load duration range 0.1-1ms, critical peak pressure decreases sharply as ΔT increases and the pressure pulse loading is considered as impulsive. In the range 1-10ms, the critical peak pressure decreases gently as ΔT increases and the pressure pulse loading is dynamic. In the range 10-30ms, the critical peak pressure is relatively constant and the pressure pulse loading is said to be quasi-dynamic, approaching the solution for a step loading condition.

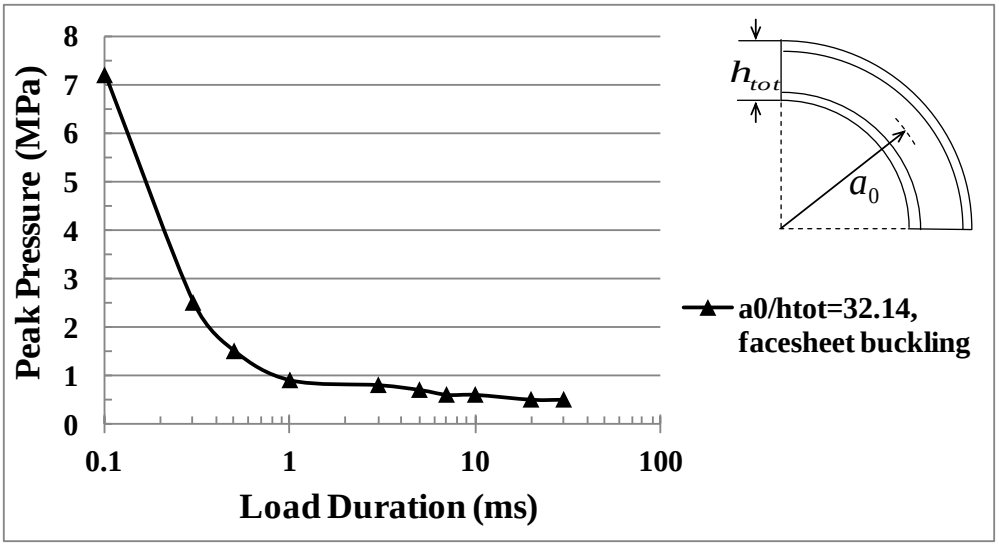

Figure 4.13 Influence of load duration on critical peak pressure for composite sandwich shell.

4.6.4 Laminate lay-up

Facesheets dynamic instability of laminated composite sandwich shell will be influenced by facesheet lay-up. Consider a curved composite sandwich panel made of laminated uni-directional E-Glass/Epoxy facesheets and Divinycell HCP100 foam core with dimensions $H = 25.4$ mm, $h = 5.08$ mm, $a_0 = 1143$ mm and $\theta_0 = 90^0$. Three different lay-ups are chosen for laminated facesheets: symmetric $[90^0/0^0]_s$, anti-symmetric $[90^0/45^0/-45^0/90^0]$ and quasi-isotropic $[90^0/45^0/0^0/-45^0]$. Material properties of uni-directional E-Glass/Epoxy were taken from Peters [95] and are also shown in Table 4.1. The three sandwich panels all weigh the same. The load duration is kept the same at $\Delta T = 1$ms.

The curved sandwich panels fail due to facesheet buckling for all the lay-ups considered and the critical peak pressures are listed in Table 4.2. It can be seen that even

though all the sandwich panels have the same geometry and weight, their lay-ups affect c, α_1^2 and α_2^2, and play an important role in determining the resistance to dynamic instability. According to Table 4.2, the symmetric lay-up gives the lowest buckling resistance of all three lay-ups. This means that the curved composite sandwich panel can be tailored for high buckling resistance.

Table 4.2 Critical peak pressure for laminated curved composite sandwich panels with different lay-ups.

Uni-Directional E-Glass/Epoxy Lay-up	$c\ (m/s)$	α_1^2	α_2^2	$p_{0cr}\ (MPa)$
Symmetric $[90^0/0^0]_s$	3,843.9	2.32e-6	2.45e-6	1.1
Anti-symmetric $[90^0/45^0/-45^0/90^0]$	4,154	2.05e-6	2.16e-6	1.3
Quasi-isotropic $[90^0/45^0/0^0/-45^0]$	3,581.1	2.02e-6	2.13e-6	1.3

4.7 Concluding Remarks

In this chapter, the author expanded on previous work in Chapter III involving the dynamic instability of thin laminated composite shells undergoing pressure pulse loading by considering a curved composite sandwich panel with thin facesheets and an elastic compressible core. Equations of motion for the facesheet transient deformations were derived from Lagrange's equations of motion, and solutions using this approach compared well with FEA results from ABAQUS Implicit. Both facesheet fracture during stable response and local dynamic pulse buckling of facesheets were considered as

possible curved sandwich panel modes of failure. The Budiansky-Roth criterion was used as the dynamic instability criterion. Parametric studies indicated the following:

1. Local facesheets buckling is more likely to occur than facesheets fracture in thin curved sandwich panels with mean radius-to-thickness ratios above a critical value, regardless of facesheet thickness.
2. Thin, shallow shells undergo facesheet fracture, while thin, deep shells are more likely to fail by local facesheet buckling.
3. For the curved sandwich panels which fail by local facesheet buckling, the buckling load decreases with increasing load duration and approaches the quasi-static buckling load at long load durations.
4. Facesheet laminate lay-up can be adjusted to improve the local buckling resistance of the curved panel.

CHAPTER V

CURVED COMPOSITE SANDWICH PANELS WITH CRUSHABLE FOAM CORE UNDER EXTERNAL BLAST

When exposed to the high intensity loading of a blast, curved composite sandwich panels with polymeric foam core could undergo dynamic instability or fracture under stable response if not properly designed. In some instances, however, the core of the sandwich panel can experience plasticity due to permanent foam crushing. An elastic-plastic core may even be more representative of the blast behaviour of foams used nowadays in composite sandwich construction. While the current design of a sandwich panel prohibits plastic crushing of the core, plastic core crushing becomes inevitable under very high intensity loading, such as a nearby blast.

In this chapter, an elastic-plastic model is developed for predicting the blast response of a foam-core, curved composite sandwich panel. The model will elucidate not only the dynamic response of the sandwich panel but address its ultimate failure and the energy absorption of its core up to the point of failure. The curved sandwich panel is described with a single radius of curvature, being clamped along the axis of zero curvature. It is also long enough along the clamped edge to be in a state of plane strain. A multi-layered approach is used to distinguish facesheets and core deformations. Core compressibility and transverse shear through the thickness are accounted for using linear

displacement fields through the thickness. The predicted solutions from the elastic-plastic model are compared to FEA results from ABAQUS Implicit. A parametric study is performed to determine the blast resistance of the sandwich shell by allowing cores to undergo plastic crushing.

5.1 Problem Formulation

Consider a single curvature, composite sandwich shell with facesheet thickness h and core thickness H, as shown in Figure 4.1. The mid-surfaces of the composite facesheets are defined with radius a_1 and a_2, and the shell subtends an angle θ_0. It is fixed at the edges $\theta = 0, \theta_0$.

The mass density of facesheets and core are ρ_f and ρ_c, respectively. The following assumptions concerning material behaviors are made:

1. Foam cores do not experience appreciable crushing (core compression) before facesheet fracture so that they can be described as an elastic, perfectly-plastic material. This assumption is generally applicable to composite sandwich panels with fiber-reinforced polymeric facesheets, which are brittle (fracture strains less than 5%).
2. There is perfect bonding between facesheets and core. The low strain deformation limits of the core will also ensure no interfacial cracking between facesheets and core.

3. Although many of the foams used in composite sandwich panels are transversely isotropic, the foam is assumed to be isotropic in this analysis. While transversely isotropic elastic properties of foam are readily available, transversely isotropic plastic flow properties are not. The model is therefore limited to the current state-of-the-art in crushable foam constitutive modeling.
4. Strain rate effects in both facesheet and core material behaviour are neglected. Under blast loading, facesheet and core materials may experience high strain rates, and both facesheet and core material behaviour are best described by dynamic constitutive relations.

In summary, the facesheets are therefore considered to be orthotropic, linear elastic-brittle material, while the foam core is idealized as isotropic, elastic, perfectly-plastic material.

The length of the shell is very long and it is subjected to uniformly distributed pressure pulse:

$$p(t) = p_0\left(1 - \frac{t}{\Delta T}\right) \tag{5.1}$$

where p_0 is the peak pressure, ΔT is the load duration and t is the time. The sandwich shell therefore deforms in a state of plane strain.

The facesheet and core kinematics used in this Chapter are identical to those derived in Chapter IV, and they are derived here again for reading convenience.

The facesheets are thin shells with radial deflections w_1 and w_2 and tangential deformations v_1 and v_2, as shown in Figure 4.1. These deformations are related to local

coordinate systems θ, z_1 and θ, z_2, where z_1 and z_2 are defined at the mid-surface of the facesheets. The deformations at the mid-surface of the core are denoted w_0 and v_0 and likewise, these are defined with respect to θ, z. Specialized strain-displacement relations are derived in the following sections.

5.1.1 Facesheet kinematics

We introduce normalized facesheet deflections as follows: $\zeta_1 = w_1/a_1$, $\psi_1 = v_1/a_1$, $\zeta_2 = w_2/a_2$, $\psi_2 = v_2/a_2$. For fully clamped boundary condition of the sandwich shell, the facesheet deflections are subjected to $\zeta_1 = \zeta_2 = 0$, $\partial\zeta_1/\partial\theta = \partial\zeta_2/\partial\theta = 0$ and $\psi_1 = \psi_2 = 0$ at $\theta = 0, \theta_0$. The boundary conditions of the facesheets are satisfied by the following Fourier series representations:

$$\zeta_1 = \sum_{n=0}^{\infty} e_n \left(1 - \cos\frac{2\pi\theta}{\theta_0}\right)\cos\frac{n\pi\theta}{\theta_0} \tag{5.2}$$

$$\psi_1 = \sum_{n=1}^{\infty} f_n \sin\frac{n\pi\theta}{\theta_0} \tag{5.3}$$

$$\zeta_2 = \sum_{n=0}^{\infty} g_n \left(1 - \cos\frac{2\pi\theta}{\theta_0}\right)\cos\frac{n\pi\theta}{\theta_0} \tag{5.4}$$

$$\psi_2 = \sum_{n=1}^{\infty} h_n \sin\frac{n\pi\theta}{\theta_0} \tag{5.5}$$

where e_n, f_n, g_n and h_n are time-varying amplitudes. Other boundary conditions, such as pinned, will give rise to different Fourier series.

One of the reasons for considering the clamped boundary conditions is because these boundary conditions are easy to model in finite element analysis, which will be

discussed later. Pinned boundary conditions on foam-core sandwich structure are very difficult to apply because failure will always take place at the pinned boundary of the soft core. Using roller boundary conditions for the curved sandwich panel is also not feasible if it is a deeply curved sandwich panel since membrane forces force the panel to slip out of the rollers.

Strains in the facesheet are based on large deflection, thin shell theory. The circumferential membrane and bending strains for a thin shell are taken from Appendix B as

$$\varepsilon_{\theta 1} = \varepsilon_{\theta m1} + z_1 \kappa_{\theta 1} \tag{5.6}$$

and

$$\varepsilon_{\theta 2} = \varepsilon_{\theta m2} + z_2 \kappa_{\theta 2} \tag{5.7}$$

where the mid-surface strain and curvature in the outer (inner) facesheets are

$$\varepsilon_{\theta m1} = \psi_1' - \zeta_1 - \zeta_1 \psi_1' + \frac{1}{2}\zeta_1'^2 \tag{5.8}$$

$$\kappa_{\theta 1} = -\frac{1}{a_1}(\zeta_1'' + \zeta_1) \tag{5.9}$$

$$\varepsilon_{\theta m2} = \psi_2' - \zeta_2 - \zeta_2 \psi_2' + \frac{1}{2}\zeta_2'^2 \tag{5.10}$$

$$\kappa_{\theta 2} = -\frac{1}{a_2}(\zeta_2'' + \zeta_2) \tag{5.11}$$

and $[\ ]'$ denotes derivative with respect to θ.

5.1.2 Simplified core kinematics

Facesheets are assumed to be perfectly bonded to the core. The radial and tangential deformations of the core at the bond interface are thus continuous with the facesheet deformations. Radial deformations do not vary through the thickness of the facesheet so that radial deformations of the core at the bond interface are equal to the mid-surface radial deformation of the facesheets. A similar assumption is made for the core tangential deformations at the bond interface since variations in the tangential deformation from the mid-surface to the outer surfaces of the facesheets would be small because of the thinness of the facesheet to the core.

The radial and tangential deformations are assumed to vary linearly through the core. Following this assumption, the radial and tangential deformation at the core mid-surface are

$$w_0 = \frac{w_1 + w_2}{2} \tag{5.12}$$

$$v_0 = \frac{v_1 + v_2}{2} \tag{5.13}$$

In addition to this, the core compresses with uniform radial strains

$$\varepsilon_r = \frac{w_2 - w_1}{H} \tag{5.14}$$

and plane sections (transverse normals to the mid-surface) of the core rotate uniformly with angle

$$\phi_0 = \frac{v_2 - v_1}{H} \tag{5.15}$$

The tangential and radial deformations in the core are

$$v(r,\theta,t) = v_0(\theta,t) + z\phi_0 \tag{5.16}$$

$$w(r,\theta,t) = w_0(\theta,t) + z\varepsilon_r \tag{5.17}$$

The above core mid-surface deflections are normalized as follows: $\zeta_0 = w_0/a_0$, $\psi_0 = v_0/a_0$, where $a_0 = (a_1 + a_2)/2$.

Following small deflection, thick core shell theory, the strain-displacement relations are

$$\varepsilon_\theta = \psi_0' - \zeta_0 + \frac{z}{a_0}\phi_0' \tag{5.18}$$

and the transverse shear strains are

$$\gamma_{r\theta} = -\zeta_0' - \phi_0 + \psi_0 \tag{5.19}$$

Note that transverse shear strains are constant through the thickness, as in first-order shear deformation theory. These core strains can be expressed further in facesheet dimensionless variables as

$$\varepsilon_r = \frac{a_1}{H}(\mu\zeta_2 - \zeta_1) \tag{5.20}$$

$$\varepsilon_\theta = \frac{(\psi_1' + \mu\psi_2')}{(1+\mu)} - \frac{(\zeta_1 + \mu\zeta_2)}{(1+\mu)} + \frac{z}{a_0}\frac{a_1}{H}(\mu\psi_2' - \psi_1') \tag{5.21}$$

$$\gamma_{r\theta} = -\frac{(\zeta_1' + \mu\zeta_2')}{(1+\mu)} - a_1\frac{(\mu\psi_2 - \psi_1)}{H} + \frac{(\psi_1 + \mu\psi_2)}{(1+\mu)} \tag{5.22}$$

where $\mu = a_2/a_1$ is the inner-to-outer radius ratio.

5.2 Lagrange's Equations of Motion

The elastic equations of motion used in this Chapter are identical to those derived in Chapter IV, and they are derived here again for reading convenience.

The equations of motion governing the transient deformations of the shell are defined in normalized radial and tangential displacements and normalized time $\tau = ct/a_1$, where $c = \sqrt{A_{22}/(\rho_f h)}$ is the wave speed and A_{22} is the membrane stiffness in the circumferential direction of the facesheet. In normalized time, the pressure pulse loading becomes

$$p(\tau) = p_0\left(1 - \frac{\tau}{\tau_0}\right) \tag{5.23}$$

where $\tau_0 = \dfrac{c\Delta T}{a_1}$ is a normalized load duration.

The transient shell response is found from Lagrange's equations of motion:

$$\frac{d}{d\tau}\left(\frac{\partial T}{\partial \dot{q}_n}\right) - \frac{\partial T}{\partial q_n} + \frac{\partial U}{\partial q_n} = Q_n \tag{5.24}$$

where q_n is a generalized coordinate, Q_n is a generalized force, T is the kinetic energy, U is the strain energy and $\dot{[\ ]} = \partial[\ ]/\partial\tau$. Generalized forces Q_n are obtained from virtual work δW:

$$Q_n = \frac{\partial(\delta W)}{\partial(\delta q_n)} \tag{5.25}$$

For uniformly distributed external pressure pulse,

$$\delta W = \int_0^{\theta_0} p(\tau)\,\delta\zeta_1\, a_1^2 d\theta = \sum_{n=0}^{\infty} Q_n \delta e_n \tag{5.26}$$

where

$$Q_n = p(\tau) a_1^2 \int_0^{\theta_0} \left(1 - \cos\frac{2\pi\theta}{\theta_0}\right)\cos\frac{n\pi\theta}{\theta_0} d\theta \tag{5.27}$$

The kinetic energy of the facesheets and core are as follows:

$$T_f = \frac{A_{22} a_1}{2} \int_0^{\theta_0} \left[\dot{\zeta}_1^2 + \dot{\psi}_1^2 + \mu^3\left(\dot{\zeta}_2^2 + \dot{\psi}_2^2\right)\right] d\theta \tag{5.28}$$

and

$$T_c = \bar{\rho}\frac{A_{22} a_1}{2} \int_0^{\theta_0} \left[\dot{\zeta}_1^2 + \mu^2\dot{\zeta}_2^2 + 2\mu\dot{\zeta}_1\dot{\zeta}_2 + \frac{4}{3}\left(\dot{\psi}_1^2 + \mu^2\dot{\psi}_2^2 + \mu\dot{\psi}_1\dot{\psi}_2\right)\right] d\theta \tag{5.29}$$

where $\bar{\rho} = (1+\mu)\rho_c H/(8\rho_f h)$.

5.2.1 Elastic equations of motion

The elastic strain energy of the facesheets is from Appendix C,

$$U_i = \frac{1}{2}\int (A_{22}\varepsilon_{\theta mi}^2 + D_{22}\kappa_{\theta i}^2) a d\theta,\ i = 1,2 \tag{5.30}$$

where A_{22} and D_{22} are the facesheet circumferential membrane and bending resistance, respectively. Substituting the facesheet strains given in Equations (5.8)-(5.11) into Equation (5.30) gives the strain energy of the outer and inner facesheets as

$$\begin{aligned} U_f = {} & \frac{A_{22} a_1}{2} \int_0^{\theta_0} \left[\left(\psi_1' - \zeta_1 - \zeta_1\psi_1' + \frac{1}{2}\zeta_1'^2\right)^2 + \alpha_1^2\left(\zeta_1'' + \zeta_1\right)^2\right] d\theta \\ & + \mu\frac{A_{22} a_1}{2} \int_0^{\theta_0} \left[\left(\psi_2' - \zeta_2 - \zeta_2\psi_2' + \frac{1}{2}\zeta_2'^2\right)^2 + \alpha_2^2\left(\zeta_2'' + \zeta_2\right)^2\right] d\theta \end{aligned} \tag{5.31}$$

where $\alpha_1^2 = D_{22}/\left(a_1^2 A_{22}\right)$ and $\alpha_2^2 = D_{22}/\left(a_2^2 A_{22}\right)$. The core elastic strain energy is derived in Appendix E for the special case of plane strain as

$$
\begin{aligned}
U_{ce} = \eta \frac{A_{22} a_1}{2} \int_0^{\theta_0} \{ & (\mu\zeta_2 - \zeta_1)^2 + \omega^2 (\psi_1' + \mu\psi_2' - \zeta_1 - \mu\zeta_2)^2 \\
& + \frac{\omega^2}{3\Lambda} (\mu\psi_2' - \psi_1')[(-\psi_1' - \mu\psi_2' + \zeta_1 + \mu\zeta_2) + \Lambda(\mu\psi_2' - \psi_1')] \\
& + \frac{\beta^2}{6\Lambda} (\mu\zeta_2 - \zeta_1)[6\Lambda(\psi_1' + \mu\psi_2' - \zeta_1 - \mu\zeta_2) - (\mu\psi_2' - \psi_1')] \\
& + \gamma^2 [-\zeta_1' - \mu\zeta_2' - 2\Lambda(\mu\psi_2 - \psi_1) + \psi_1 + \mu\psi_2]^2 \} d\theta
\end{aligned}
\tag{5.32}
$$

where $\Lambda = (1+\mu)/(2(1-\mu))$, and η, ω^2, β^2, and γ^2 are elastic constants of the foam defined in Appendix E.

Coupled elastic equations of motion result from satisfying Lagrange's equation of motion as follows:

$$
\sum_{m=0}^{N} [2(1+\bar{\rho})\ddot{e}_m + 2\mu\lambda\ddot{g}_m] \hat{f}_0(m,n) + P_e = \bar{Q}_n \tag{5.33}
$$

$$
\sum_{m=0}^{N} [2\mu(\bar{\rho}+\mu)\ddot{g}_m + 2\mu\ddot{e}_m] \hat{f}_0(m,n) + P_g = 0 \tag{5.34}
$$

$$
\left[\frac{2}{3}(3+4\bar{\rho})\ddot{f}_n + \frac{4}{3}\mu\ddot{h}_n \right] \frac{\theta_0}{2} + P_f = 0 \tag{5.35}
$$

$$
\left[\frac{2}{3}\mu(3\mu^2 + 4\bar{\rho})\ddot{h}_n + \frac{4}{3}\mu\ddot{f}_n \right] \frac{\theta_0}{2} + P_h = 0 \tag{5.36}
$$

where n is the particular mode of the Fourier series, N is the chosen number of terms in the Fourier series, $\bar{Q}_n$ is a normalized load, P_e, P_g, P_f, P_h are elastic spring forces and $\hat{f}_0$ is given by

$$\hat{f}_0(m,n)=\int_0^{\theta_0}\left(1-\cos\frac{2\pi\theta}{\theta_0}\right)^2\cos\frac{m\pi\theta}{\theta_0}\cos\frac{n\pi\theta}{\theta_0}\,d\theta \tag{5.37}$$

The normalized external load is

$$\overline{Q}_n=2\bar{p}(\tau)\int_R\left(1-\cos\frac{2\pi\theta}{\theta_0}\right)\cos\frac{n\pi\theta}{\theta_0}\,d\theta \tag{5.38}$$

where $\bar{p}(\tau)=\frac{a_1 p_0}{A_{22}}\left(1-\frac{\tau}{\tau_0}\right)$ is the normalized pressure pulse loading. The elastic spring forces P_e, P_g, P_f, P_h result from taking derivatives of the strain energy in terms of the generalized coordinates. Explicit equations for them are not given here because they are very lengthy.

5.2.2 Elastic-plastic equations of motion

For high enough pressure pulse amplitude, the core may yield and undergo plasticity. The elastic-plastic behaviour of the core is described as crushable foam with isotropic hardening [89]. The condition for initial core yielding under plane strain conditions is given by the yield condition

$$f=\hat{\sigma}-\sigma_0=0 \tag{5.39}$$

where σ_0 is the flow stress and the effective stress $\hat{\sigma}$ is given by

$$\hat{\sigma}^2=\frac{1}{\left[1+\left(\frac{\alpha_p}{3}\right)^2\right]}\left(\sigma_e^2+\alpha_p^2\sigma_m^2\right) \tag{5.40}$$

where $\alpha_p = 3/\sqrt{2}$, assuming the foam plastic Poisson's ratio is approximately zero, and the mean stress σ_m and von Mises stress σ_e. Under plane strain conditions and elastic conditions,

$$\sigma_m = \frac{(1+\nu)}{3}(\sigma_r + \sigma_\theta) \tag{5.41}$$

$$\sigma_e = \frac{1}{\sqrt{2}}\left\{(\sigma_r - \sigma_\theta)^2 + [(1-\nu)\sigma_r - \sigma_\theta]^2 + [(1-\nu)\sigma_\theta - \sigma_r]^2 + 6\tau_{r\theta}^2\right\}^{\frac{1}{2}} \tag{5.42}$$

where ν is the elastic Poisson's ratio. Substituting Equations (5.41) and (5.42) in Equation (5.39) gives the effective stress of the foam at initial yield as

$$\hat{\sigma} = \left[\sigma_r^2 + \sigma_\theta^2 + \nu^2(\sigma_r + \sigma_\theta)^2 + 2\tau_{r\theta}^2\right]^{\frac{1}{2}} \tag{5.43}$$

Subsequent plastic flow is determined by an associated flow rule. Under plane strain, the elastic-plastic stress-strain relations are generally not ideally plastic (constant stress) for a material that is elastic-perfectly plastic under uniaxial stress [90]. Incremental stress-strain relations can be derived for the foam and the resulting strain hardening plastic stress-strain curve must be integrated from it. This approach will not be used here. Instead we neglect strain hardening of the foam due to plane strain constraint and assume that continued plastic flow is at a constant stress. A material point in the foam that has yielded will exhibit the stress-strain curve described by the solid line in Figure 5.1. Equations (5.39) and (5.43) are used to determine plastic regions in the foam. These plastic regions are more likely to develop near the clamp edges where transverse shear stresses are high, as indicated in Figure 5.2. Although the hoop strains in Equation (5.21) contain a bending strain that is linear in z- or the through-thickness coordinate, this term is negligible compared with the hoop membrane strain, as well as the radial and

transverse shear strains. As such, foam stresses do not vary through the thickness and are primarily a function of θ.

Foam plasticity is accounted for by assuming non-linear elasticity. The strain energy density for the foam that is undergoing yielding is calculated from the areas under the stress-strain curve shown in Figure 5.1:

$$U_{OACD} = U_{OBD} - U_{ABC} \tag{5.44}$$

The hatched region in Figure 5.1 is represented as negative area or strain energy density in Equation (5.44). In terms of total strain energy, the foam

$$\begin{aligned} U_{cep} = {} & \frac{1}{2}\int_{V_e}\left(C_{11}\varepsilon_r^2 + 2C_{12}\varepsilon_\theta\varepsilon_r + C_{11}\varepsilon_\theta^2 + C_{66}\gamma_{r\theta}^2\right)dV + \frac{1}{2}\int_{V_p}\Big[C_{11}\varepsilon_r^2 + 2C_{12}\varepsilon_\theta\varepsilon_r + C_{11}\varepsilon_\theta^2 + C_{66}\gamma_{r\theta}^2 \\ & - C_{11}\left(\varepsilon_r - \varepsilon_{r0}\right)^2 - 2C_{12}\left(\varepsilon_\theta - \varepsilon_{\theta 0}\right)\left(\varepsilon_r - \varepsilon_{r0}\right) - C_{11}\left(\varepsilon_\theta - \varepsilon_{\theta 0}\right)^2 - C_{66}\left(\gamma_{r\theta} - \gamma_{r\theta 0}\right)^2\Big]dV \end{aligned} \tag{5.45}$$

where V_e and V_p are the volumes of the elastic and plastic regions (see Figure 5.2). The above expression is expanded in terms of foam strains defined in Equations (5.20) – (5.22) as

$$\begin{aligned} U_{cep} = {} & \eta\frac{A_{22}a_1}{2}\int_{R_e}\Big\{\left(\mu\zeta_2 - \zeta_1\right)^2 + \omega^2\left(\psi_1' + \mu\psi_2' - \zeta_1 - \mu\zeta_2\right)^2 \\ & + \frac{\omega^2}{3\Lambda}\left(\mu\psi_2' - \psi_1'\right)\left[\left(-\psi_1' - \mu\psi_2' + \zeta_1 + \mu\zeta_2\right) + \Lambda\left(\mu\psi_2' - \psi_1'\right)\right] \\ & + \frac{\beta^2}{6\Lambda}\left(\mu\zeta_2 - \zeta_1\right)\left[6\Lambda\left(\psi_1' + \mu\psi_2' - \zeta_1 - \mu\zeta_2\right) - \left(\mu\psi_2' - \psi_1'\right)\right] \\ & + \gamma^2\left[-\zeta_1' - \mu\zeta_2' - 2\Lambda\left(\mu\psi_2 - \psi_1\right) + \psi_1 + \mu\psi_2\right]^2\Big\}d\theta \\ & + \eta_0\frac{A_{22}a_1}{2}\int_{R_p}\Big\{\mu\zeta_2 - \zeta_1 + \omega_0^2\left(\psi_1' + \mu\psi_2' - \zeta_1 - \mu\zeta_2\right) + \frac{\omega_0^2}{6\Lambda}\left(\psi_1' - \mu\psi_2'\right) \\ & + \gamma_0^2\left[-\zeta_1' - \mu\zeta_2' - 2\Lambda\left(\mu\psi_2 - \psi_1\right) + \psi_1 + \mu\psi_2\right]\Big\}d\theta \end{aligned} \tag{5.46}$$

where R_e and R_p are angular elastic and plastic regions and $\eta_0, \omega_0^2, \gamma_0^2$ are plastic constants of the foam defined in Appendix F.

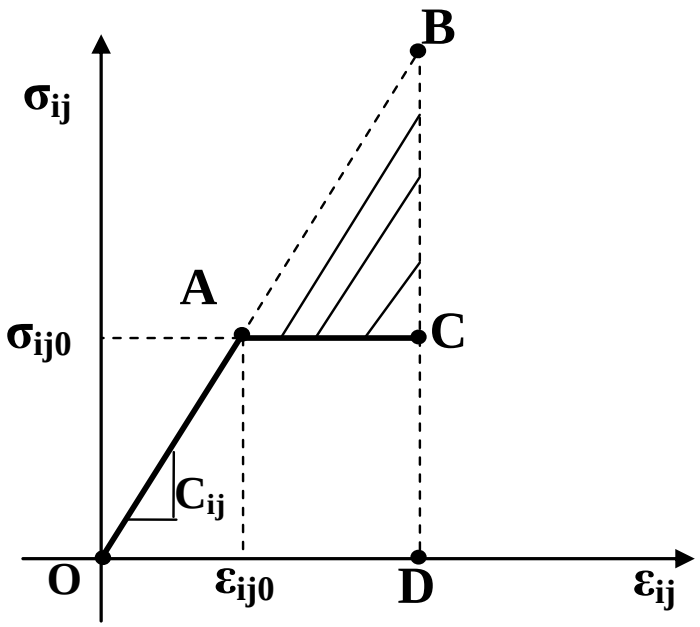

Figure 5.1 Representation of nonlinear elastic strain energy density in an elastic perfectly plastic material (solid line).

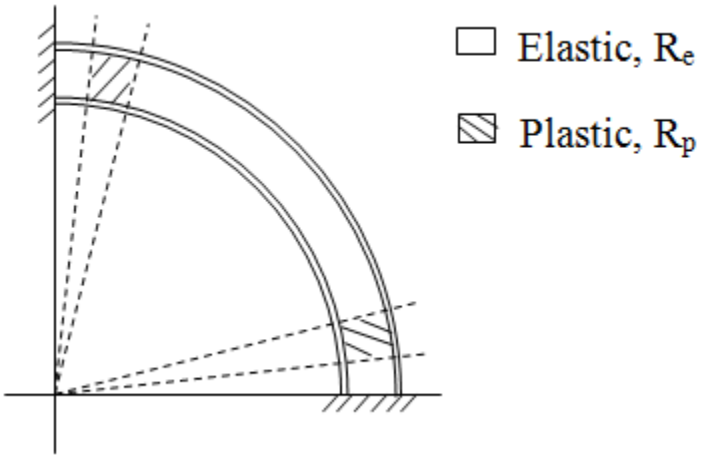

Figure 5.2 Elastic and plastic regions in the foam.

Coupled elastic-plastic equations of motion result from satisfying Lagrange's equation of motion:

$$\sum_{m=0}^{N}\left[2(1+\bar{\rho})\ddot{e}_m + 2\mu\lambda\ddot{g}_m\right]\hat{f}_0(m) + P_{ep} = \bar{Q}_n - Q_{de} \tag{5.47}$$

$$\sum_{m=0}^{N}\left[2\mu(\bar{\rho}+\mu)\ddot{g}_m + 2\mu\ddot{e}_m\right]\hat{f}_0(m) + P_{gp} = -Q_{dg} \tag{5.48}$$

$$\left[\frac{2}{3}(3+4\bar{\rho})\ddot{f}_n + \frac{4}{3}\mu\ddot{h}_n\right]\frac{\theta_0}{2} + P_{fp} = -Q_{df} \tag{5.49}$$

$$\left[\frac{2}{3}\mu(3\mu^2+4\bar{\rho})\ddot{h}_n + \frac{4}{3}\mu\ddot{f}_n\right]\frac{\theta_0}{2} + P_{hp} = -Q_{dh} \tag{5.50}$$

where elastic spring forces are $P_{ep}, P_{gp}, P_{fp}, P_{hp}$ and plastic damping forces are $Q_{de}, Q_{dg}, Q_{df}, Q_{dh}$. The elastic spring forces and damping forces result from the first and last integrals of Equation (5.46), respectively. They are described by very lengthy equations and are not shown for brevity. Since the elastic strain energy is integrated only over the elastic core regions, $P_{ep}, P_{gp}, P_{fp}, P_{hp}$ are smaller than P_e, P_g, P_f, P_h. The plastic damping forces $Q_{de}, Q_{dg}, Q_{df}, Q_{dh}$ are introduced on the right-hand side of the equations of motion to indicate that they retard deformation.

5.3 An Example

The composite sandwich shell considered has dimensions $h = 5$ mm, $H = 25$ mm, $a_1 = 396$ mm, $a_2 = 365$ mm and $\theta_0 = 90^o$. The mean radius-to-thickness ratio of this curved sandwich shell is 10.71, which implies a rather thick shell. It is made with 0/90 woven E-Glass/Vinyl Ester facesheets and a Divinycell PVC H200 foam core, with properties of the facesheet and core listed in Table 5.1. The shell is subjected to the

uniformly distributed pressure pulse described in Equation (1) where $p_0 = 2.2$ MPa and $\Delta T = 1$ ms.

Table 5.1 Material properties of 0/90 woven roving E-glass/Vinyl Ester and different foams.

	E-Glass/ Vinyl Ester	Divinycell H30	Divinycell H100	Divinycell H200	Klegecell R300	Divinycell HCP100
Density(kg/m^3)	1391.3	36	100	200	300	400
E_{11} (+) (GPa)	17	0.044	0.149	0.277	--	--
E_{22} (+) (GPa)	17	0.044	0.149	0.277	--	--
E_{33} (+) (GPa)	7.48	0.044	0.149	0.277	--	--
E_{11} (-) (GPa)	19	0.027	0.105	0.293	0.338	0.340
E_{22} (-) (GPa)	19	0.027	0.105	0.293	0.338	0.340
E_{33} (-) (GPa)	--	0.027	0.105	0.293	0.338	0.340
$\nu_{12} = \nu_{21}$	0.13	0.25	0.31	0.3	0.23	0.3
$\nu_{13} = \nu_{23}$	0.28	0.25	0.31	0.3	0.23	0.3
$\nu_{31} = \nu_{32}$	0.12	0.25	0.31	0.3	0.23	0.3
$G_{12}=G_{21}$ (GPa)	4.0	0.013	0.0438	0.110	0.123	0.131
$G_{23}=G_{32}$ (GPa)	1.73	0.013	0.0438	0.110	0.123	0.131
$G_{13}=G_{31}$ (GPa)	1.73	0.013	0.0438	0.110	0.123	0.131
q (MPa)	--	0.3	1.66	4.35	7.8	10.3
γ_f	--	0.09	0.4	0.45	0.27	0.35
X_T, σ_{10} (+) (MPa)	270	0.57	3.2	6.4	--	--
X_C, σ_{10} (-) (MPa)	200	0.29	1.53	4.36	--	--
Y_T, σ_{20} (+) (MPa)	270	0.57	3.5	6.4	--	--
Y_C, σ_{20} (-) (MPa)	200	0.29	1.53	4.36	--	--
S_L, $\tau_{120}=\tau_{210}$ (MPa)	40	0.35	1.47	3.86	--	7.44
S_T,$\tau_{13f} = \tau_{310}$ (MPa)	31.6	0.35	1.47	3.86	--	7.44
S_T,$\tau_{230}=\tau_{320}$ (MPa)	31.6	0.35	1.47	3.86	--	7.44

A MATLAB program was written to solve coupled equations of motion for time-varying amplitudes of the Fourier series in Equations (5.2)-(5.5), i.e., coefficients e_n, f_n, g_n and h_n . It was found that converged solutions for the deformations could be obtained by setting n=16 in the Fourier series. The radial deformation of the sandwich mid-plane is shown at various times in Figure 5.3. Stresses at the sandwich mid-plane were calculated at 0.13ms, which is the time just before the onset of plastic flow, and are shown in Figure 5.4. It is very apparent that for this rather thick shell, foam plasticity will begin near the clamped boundaries where all stress components in the foam are at their greatest. Also note that the magnitudes of the peak radial, hoop and axial stresses are of the same order of magnitude as the peak transverse shear stress. A sandwich theory that ignores radial stress in the core would therefore be inaccurate in predicting the behavior of a thick curved sandwich panel. The effective stress $\hat{\sigma}$, as expressed by Equation (5.43), was calculated for the corresponding times given in Figure 5.3, and the distribution of the effective stress in the mid-plane of the core is plotted in Figure 5.5 to indicate that plasticity begins near the clamped ends at about 0.13ms. This plastic region grows until about 0.35ms when the facesheet ruptures. A condition for facesheet rupture will be given later. Finite element analysis predictions of the corresponding variables in the composite sandwich shell are also shown in Figures 5.3-5.5, and discussed below.

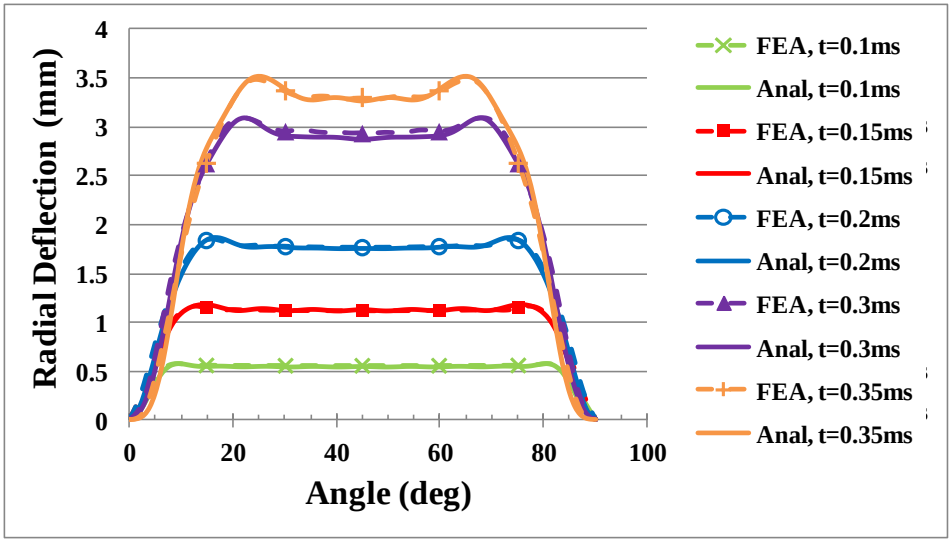

Figure 5.3 Radial displacements taken at mid-surface of sandwich shell.

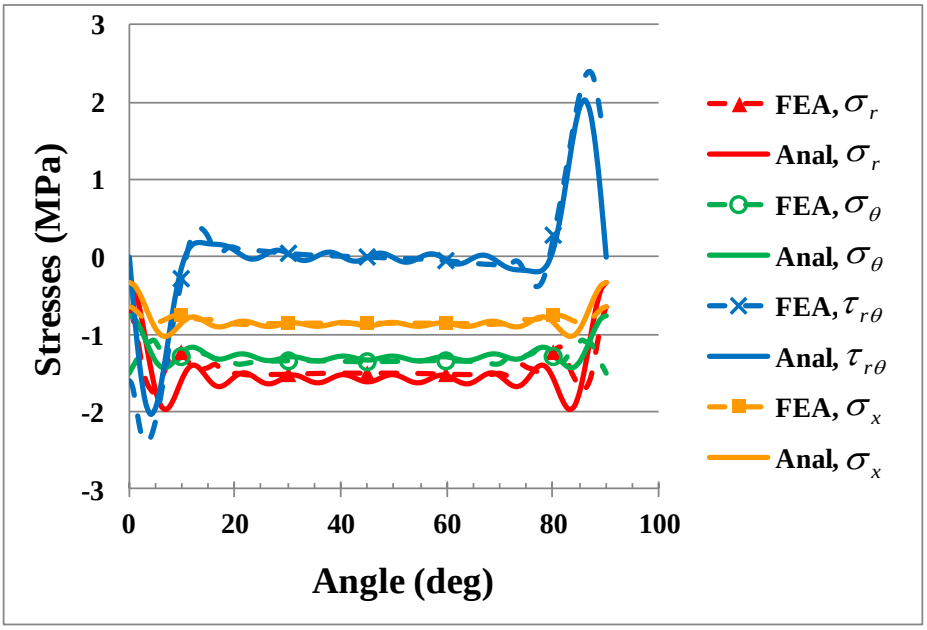

Figure 5.4 Stress variations along the mid-surface of core at t= 0.13ms, right before core yielding.

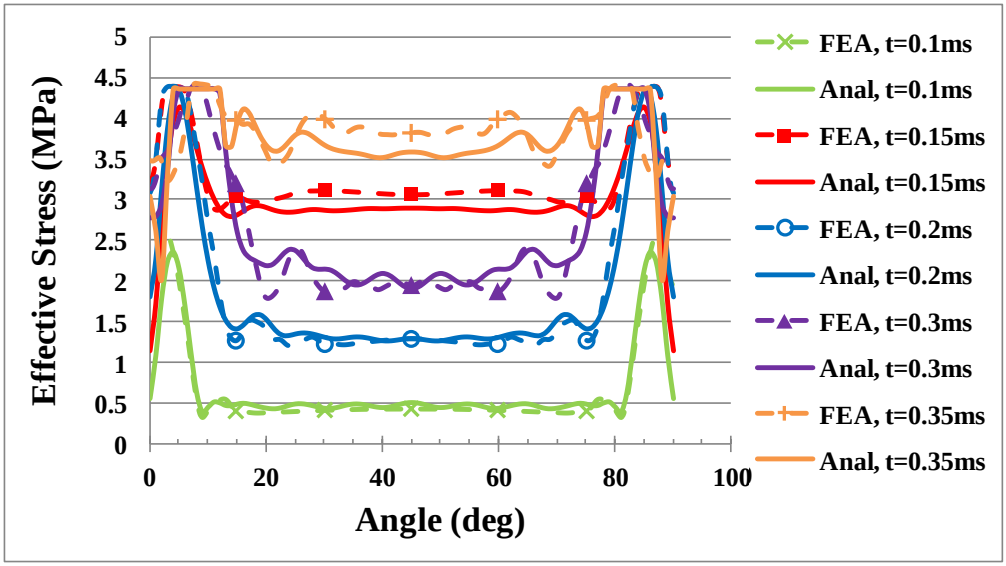

Figure 5.5 Effective stress at mid-surface of sandwich shell (core becomes plastic right after t= 0.13ms).

5.4 Finite Element Analysis

Finite element analysis with ABAQUS Standard Version 6.9 [94] was done in order to corroborate solutions with the analytical model. The FEA model is shown in Figure 5.6. Continuum plane strain four node elements (CPE4) were chosen for both facesheets and core. The facesheet was modeled as linear elastic, orthotropic material and the core was modeled by using crushable foam with isotropic hardening [89, 94]. Plasticity properties for the Divinycell H200 foam were taken from Mines and Alias [91].

Results from the ABAQUS Standard are compared to the results from MATLAB in Figures 5.3-5.5. The numerical implementation in ABAQUS Standard involved Dynamic, Implicit analysis. The direct-integration method provided for Dynamic, Implicit analysis in ABAQUS Standard is the Hilber-Hughes Taylor operator, which is an extension of the trapezoidal rule. Automatic time increment with specified half-step

residual was used. A parametric study was done to determine the appropriate size of the half-step residual that would yield accurate results. No numerical damping was specified in the problem.

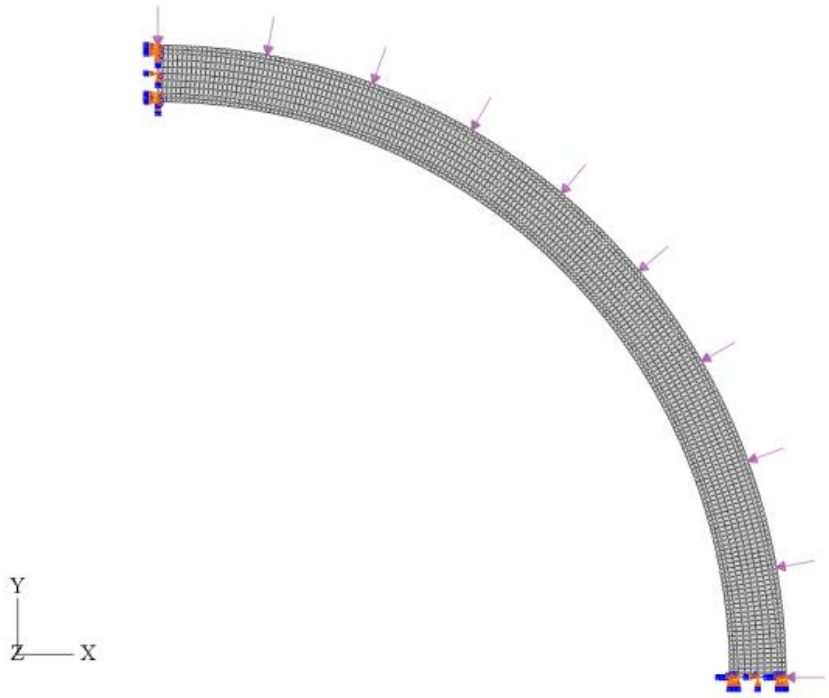

Figure 5.6 Finite element model of composite sandwich shell.

Good agreement was found between the MATLAB and FEA solutions in all cases. There is better agreement in mid-surface radial deformation of the foam (Figure 5.3) and effective stress (Figure 5.5) when the core is elastic than when it is elastic-plastic. This is because of the approximate nature of the calculated elastic-plastic strain energy in core. Also, stresses near the clamped edge (Figure 5.4) are not evaluated as well as at other locations even with a 16-term Fourier series in the model. The solution from the elastic-plastic model is within 5% of the FEA radial deformations and 15% of the FEA stresses. Fourier series solutions converge more rapidly for deflections than stresses because

stresses are calculated from strains, which are expressed in terms of derivatives of the deflections. The above discrepancies are not uncommon in analytical solutions using the Fourier series approach.

5.5 Sandwich Panel Failure

Sandwich panel failure may occur in the modes shown in Figures 5.7 (a) and (b). Facesheet failure is primarily due to compressive hoop stresses because of the initial shell curvature. As indicated in Figure 5.7 (a), it is the distal or inner facesheet, with a smaller radius of curvature and higher circumferential strain than the loaded or outer facesheet, that first experiences compressive facesheet failure near the clamped boundary. If the foam is very weak or the facesheet is very strong, the core of the curved sandwich panel can fail in a transverse shear mode, which is also shown in Figure 5.7 (a). Finally, a very strong core and facesheet may prevent the failure modes shown in Figure 5.7 (a) but the curved sandwich panel may still fail due to dynamic pulse buckling [1] as described in Figure 5.7 (b). This failure mode of composite shells subjected to external blast has received some attention in recent years [74], and has been dealt with in Chapter IV. The following section describes simply equations that can be used for facesheet and core failure modes.

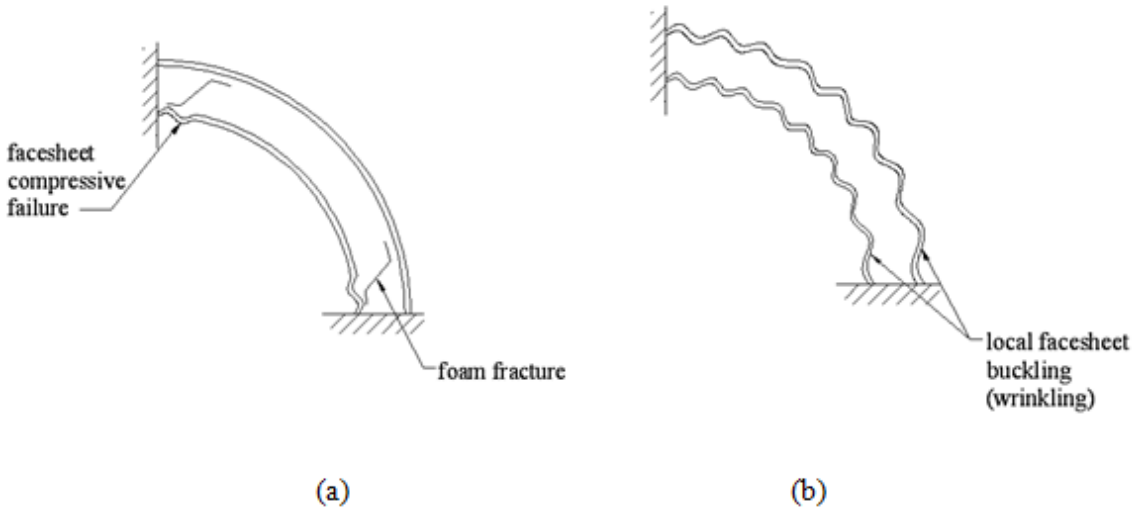

Figure 5.7 Failure modes of sandwich shell: (a) facesheet and foam fracture during stable response and (b) dynamic instability of facesheets.

5.5.1 Facesheet failure

The modified Hashin-Rotem criteria are used to examine lamina failure of the woven roving E-Glass/Vinyl Ester [97]. According to Appendix D, the modified Hashin-Rotem failure criteria can be used by substituting Equation (D.6) into Equation (D.2),

$$\frac{\overline{Q}_{22}\varepsilon_\theta}{Y_T} = 1 \text{ if } \sigma_\theta > 0 \tag{5.51}$$

and

$$\frac{\overline{Q}_{22}\varepsilon_\theta}{Y_C} = 1 \text{ if } \sigma_\theta < 0 \tag{5.52}$$

Thus the value of the hoop strain at which failure occurs is given by

$$\varepsilon_f = \frac{\min\left(Y_T, Y_c\right)}{\overline{Q}_{22}} \tag{5.53}$$

The above expression describes the maximum allowable strain based on a Hashin-Rotem composite failure criterion.

5.5.2 Core shear fracture

Although the core fracture is of a mixed mode type involving transverse shear and hoop, radial and axial compression, a simple criterion for the onset of core shear failure is to set the transverse shear strain in the core equal to the core transverse fracture strain, γ_f. Since the transverse shear strain in the core is given by Equation (5.22), the criterion for core shear fracture becomes

$$\gamma_f = -\frac{\left(\zeta_1' + \mu\zeta_2'\right)}{\left(1+\mu\right)} - a_1 \frac{\left(\mu\psi_2 - \psi_1\right)}{H} + \frac{\left(\psi_1 + \mu\psi_2\right)}{\left(1+\mu\right)} \tag{5.54}$$

5.6 Dissipated Plastic Work

If the foam core crushes and experiences plasticity before sandwich panel failure, the plastic work dissipated in the core may be approximated. In Figure 5.8 (a), plastic regions extend over angular regions with extent $\Delta\theta$. The stress-strain behaviour at the initial yield points, C_1 and C_2, is shown in Figure 5.8 (b), where ε_{ijf} denotes the final strain components at fracture and the onset of elastic unloading. Assuming that these strain components linearly decrease from ε_{ijf} to ε_{ij0} at the elastic and plastic boundaries, one gets the following expression for the energy dissipated by plastic work up to shell failure:

$$E_d = \frac{1}{2}\left[\sigma_{r0}\left(\varepsilon_{rf} - \varepsilon_{r0}\right) + \sigma_{\theta 0}\left(\varepsilon_{\theta f} - \varepsilon_{\theta 0}\right) + \tau_{r\theta 0}\left(\gamma_{r\theta f} - \gamma_{r\theta 0}\right)\right]\left(a_1^2 - a_2^2\right)\Delta\theta \tag{5.55}$$

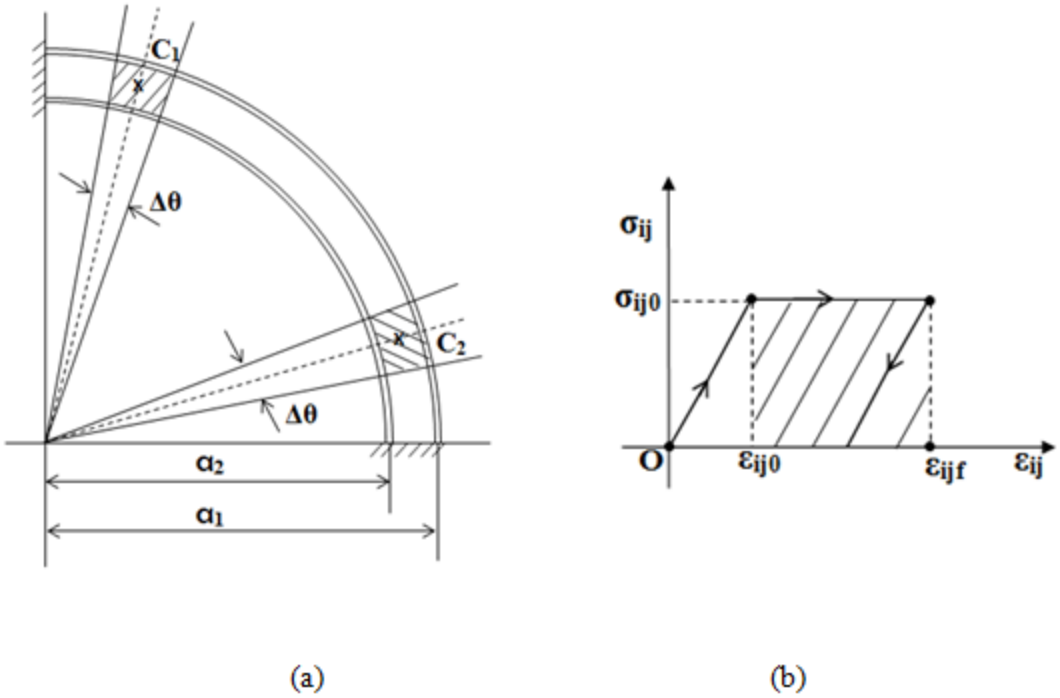

Figure 5.8 Plastic work dissipated in core at failure: (a) plastic regions and (b) stress-strain curve at initial yield points.

5.7 Parametric Study

A parametric study was used to determine the mode of failure and energy dissipation of curved sandwich panels. The effect of three parameters, sandwich radius-to-thickness ratio, angular extent, and foam core, is discussed below. The facesheets are made of 0/90 woven E-Glass/Vinyl Ester, with properties given in Table 5.1, in all the cases discussed below.

5.7.1 Radius-to-thickness ratio

The mean radius-to-thickness ratio of the sandwich shell will determine the global stiffness and strength of the panel. This parametric study was done on a composite

sandwich shell with Divinycell H200 core, $h = 5\text{mm}$, $H = 25\text{mm}$, $\theta_0 = 90^o$ and various facesheet radii. Figure 5.9 shows that the blast resistance decreases as the radius-to-thickness ratio increases, as to be expected since the sandwich panel loses global bending resistance as this ratio increases. What is also shown in Figure 5.9 is that the amount of plastic work dissipated in the core before failure reaches a value of about 20J when the radius-to-thickness ratio is high, over 30. For high radius-to-thickness ratios, the curved sandwich panel is becoming more of a thin shell, in which hoop or membrane stresses dominate over radial stresses in the foam.

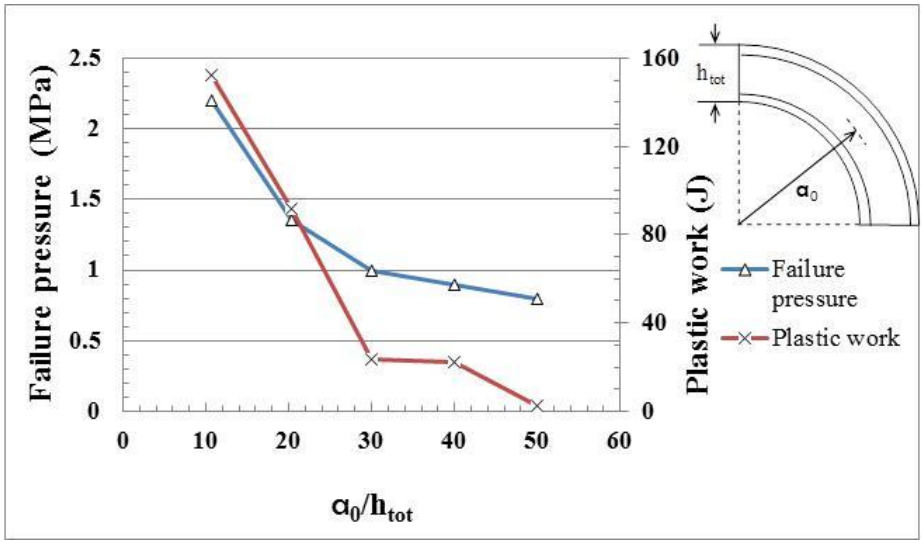

Figure 5.9 Variation of blast resistance and energy absorption with radius-to-thickness ratio.

5.7.2 Angular extent/shallowness

Many analytical models for double curvature sandwich shells are based on so-called shallow shell theory in order to simplify shell kinematics. A shallow shell is defined when the angular extent θ_0 is less than 25 degrees. A parametric study was done to examine what happens when the curved sandwich panel is made into a shallow

sandwich shell. A composite sandwich shell with Divinycell H200 core, $h = 5$ mm, $H = 25$ mm, $a_1 = 1{,}437$ mm, $a_2 = 1{,}407$ mm and various angular extent θ_0 is considered. Figure 5.10 shows that for deep shells, the blast resistance does not vary substantially, but it increases as θ_0 decreases in the case of shallow shells. Also the plastic work dissipation in the core of a shallow shell is substantially higher than in a deep shell.

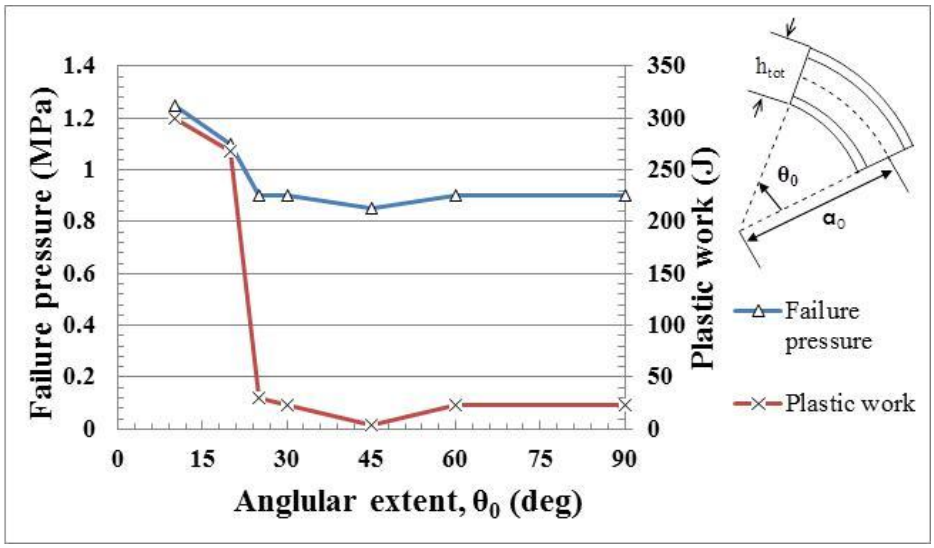

Figure 5.10 Variation of blast resistance and energy absorption with angular extent.

5.7.3 Type of foam core

Both thick and thin composite sandwich shells are considered in this parametric study. Each sandwich shell is composed of facesheets made of 0/90 woven E-Glass/Vinyl Ester and thickness $h = 5$ mm. The cores in them are composed of the various foams listed in Table 5.1 and have thickness $H = 25$ mm. Foam properties listed in Table 5.1 were obtained from References [92, 96, 101-103]. The shear strains at fracture for the foams were specifically taken from Diab [103].

The thick sandwich shell considered has dimensions $a_1 = 396\,\text{mm}, a_2 = 365\,\text{mm}$ and $\theta_0 = 90^o$. This gives a sandwich radius-to-thickness ratio $a_0/(2h+H) = 10.7,$ which means it is fairly thick. Figure 5.11 (a) indicates that the highest load is sustained by the sandwich shell with the Divinycell H200 foam core. This sandwich shell and those with Divinycell H30 and H100 foams underwent plasticity before sandwich panel failure (see Figure 5.11 (b)). The sandwich panel with Divinycell H30 core actually failed by core shear fracture, while all the other sandwich panels failed by facesheet fracture. The sandwich shells with stiffer and stronger foams, Klegecell R300 and Divinycell HCP100, remained fully elastic and absorbed no energy up to the point of facesheet fracture.

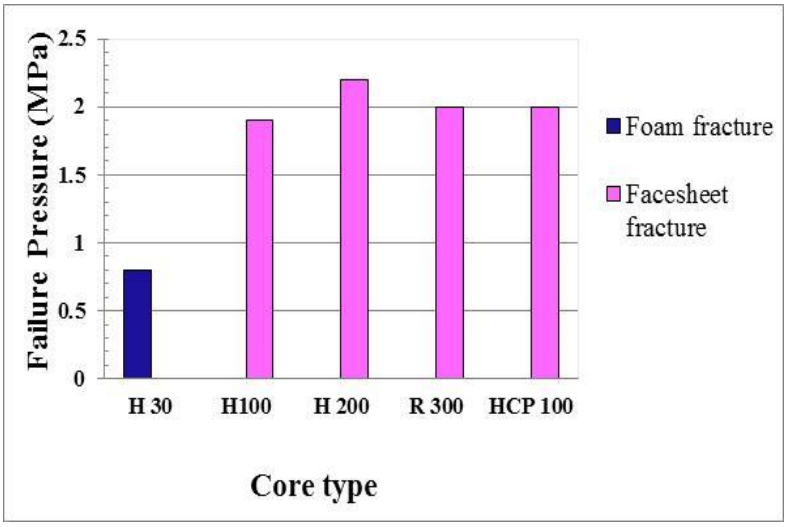

(a)

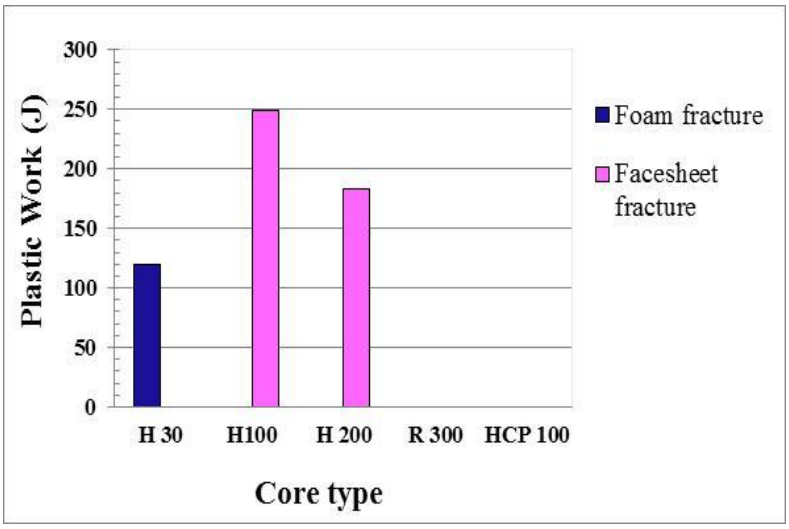

(b)

Figure 5.11 Thick sandwich shell with $a_0/(2h+H)=10.7$ and $\theta_0=90$ deg: (a) blast resistance and (b) energy dissipation.

The thin sandwich shell considered has dimensions $a_1=1{,}437.6$ mm, $a_2=1{,}407.2$ mm and $\theta_0=30^o$. This gives a sandwich radius-to-thickness ratio $a_0/(2h+H)=40,$ which makes it a thin sandwich shell. Figures 5.12 (a) and (b) show the blast resistance and energy absorption associated with failure for the thin sandwich shell. While the failure pressure loads are all lower than the thick sandwich shells, similar conclusions are drawn. The panel that was most blast resistant is still the one with the Divinycell H200 core, and it underwent plastic core crushing although not as much plastic work was absorbed during failure. The panel with Divinycell H30 underwent plasticity and core shear failure, while the panels with strong cores, Klegecell R300 and Divinycell HCP100, experienced no plastic core crushing before facesheet fracture.

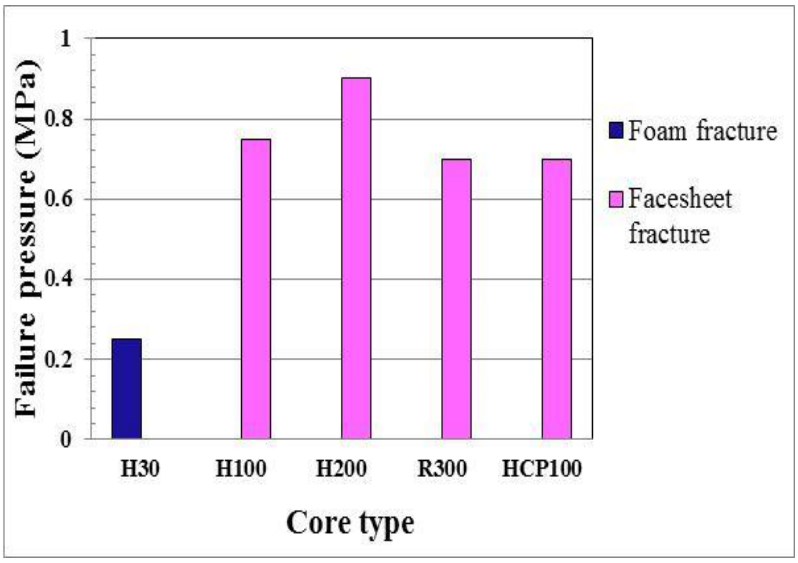

(a)

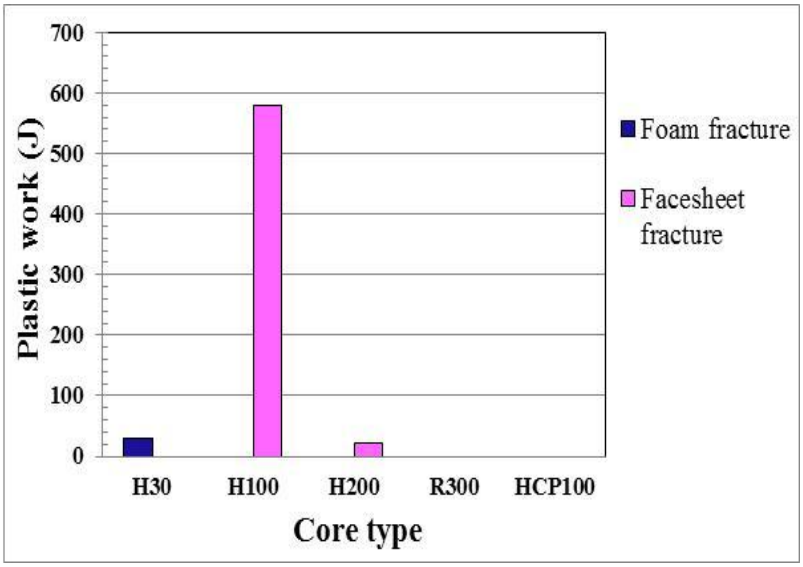

(b)

Figure 5.12 Thin sandwich shell with $a_0/(2h+H)=40$ and $\theta_0=30$ deg: (a) blast resistance and (b) energy dissipation.

This parametric study indicates that contrary to popular belief, stiffer and stronger cores do not increase the blast resistance of a curved, composite sandwich shells. The most blast resistant curved sandwich panel with Divinycell H200 core underwent some,

but not significant, plastic core crushing. In a related study on flat sandwich panels [88], a similar conclusion was made but only on a per unit weight basis for the entire panel.

5.8 Concluding Remarks

An elastic-plastic model was developed for predicting the blast response of a foam-core, curved composite sandwich panel. The curved sandwich panel was described with a single radius of curvature, being clamped along the axis of zero curvature. It was also long enough along the clamped edge to be in a state of plane strain. A multi-layered approach was used to distinguish facesheets and core deformations. Core compressibility and transverse shear through the thickness were accounted for using linear displacement fields through the thickness. The predicted solution from the elastic-plastic model was shown to compare well with FEA from ABAQUS Implicit.

A parametric study showed that blast resistance of the sandwich shell may be increased by allowing cores to undergo plastic crushing. Very thick, i.e. radius-to-thickness aspect ratio less than 10, and shallow shells derive much of their resistance to blast from core crushing. Strong, dense foam cores did not increase the blast resistance of the curved sandwich panel but allowed facesheets to fracture while the core remained elastic. Shells with strong cores and very thin facesheets may be susceptible to local pulse buckling or facesheet wrinkling, and this was addressed in Chapter IV.

CHAPTER VI

CONCLUDING REMARKS AND FUTURE WORK

In this thesis, dynamic pulse buckling of single-curvature composite shells, including sandwich shells, under external pressure pulse loading was examined using Lagrange's equation of motion and the Budiansky-Roth dynamic stability criterion. The predicted transient shell response compared very well with FEA results from ABAQUS Implicit, and the predicted buckling loads also agreed with experiments on steel arches. Load duration determined whether the buckling was impulsive, dynamic or quasi-dynamic. Thicker composite shells were more likely to fail by first-ply failure rather than buckling. It was shown that the composite lay-up could be adjusted to increase the buckling resistance of the shell.

The single-curvature shell study was expanded by considering a curved composite sandwich panel with thin facesheets and an elastic compressible core. Local facesheet buckling of the curved sandwich panel subjected to external pressure pulse loading was investigated. Equations of motion for the facesheet transient deformations in the sandwich shell were derived from Lagrange's equations of motion, and solutions using this approach compared well with FEA results from ABAQUS Implicit. Both facesheet fracture during stable deformation response and local dynamic pulse buckling of facesheets were considered as possible modes of failure in the curved sandwich panel.

Parametric studies indicated that local facesheets buckling is more likely to occur than facesheet fracture in thin and deeply curved sandwich panels. The facesheet laminate lay-up could also be adjusted to improve the local buckling resistance of the curved panel.

A curved composite sandwich panel with thin facesheets and a crushable elastic-plastic foam core was also studied in this thesis. Plastic core damping was introduced into the equations of motion as a damping force. The predicted solutions from the elastic-plastic model were shown to compare well with FEA results from ABAQUS Implicit. A parametric study showed that blast resistance of the sandwich shell may be increased by allowing cores to undergo plastic crushing. Very thick sandwich shells, i.e. radius-to-thickness aspect ratio less than 10, and shallow shells derive much of their resistance to blast from core crushing. Strong, dense foam cores did not increase the blast resistance of the curved sandwich panel but allowed facesheets to fracture while the core remained elastic.

Future work will be to extend this analysis to various shell geometries that are subjected to dynamic research, such as double-curvature composite sandwich shells. The addition of another in-plane degree-of-freedom to the shell will lead to double Fourier series as well as several other strain components and equations of motion. The second aspect will concentrate on dynamic analyses which are typically performed, including transient analysis, impact, shock loading, dynamic stability and other dynamic behaviors.

BIBLIOGRAPHY

[1] Lindberg, H.E. and Florence, A.L., *Dynamic Pulse Buckling*. 1987, Dordrecht: Martinus Nijhoff Publishers.

[2] Budiansky, B. and Roth, R.S., *Axisymmetric dynamic buckling of clamped shallow spherical shells*, in *Collected Papers on Instability of Shell Structures, NASA TN D-1510*. 1962: Washington DC. p. 597-606.

[3] Cauchy, A.L., *The equilibrium and motion of a solid plate.* Mathematical Exercises, 1828. 3: p. 328-355.

[4] Poisson, S.D., *Memory on the equilibrium and motion of elastic corp.* Memories of the Royal Academy of Sciences Institute 1829. 8: p. 357-570.

[5] Kirchhoff, G., *About the equilibrium and motion of an elastic disc.* Journal for the Pure and Applied Mathematics (Crelle's), 1850. 40: p. 51-88.

[6] Love, A.E.H., *A Treatise on the Mathematical Theory of Elasticity, 1st ed, 1892*. 1944, New York: Cambridge University Press, 4th ed. Dover Publications.

[7] Von Karman, T., *Cyclopedia of Mathematical Sciences.* Strength problems in engineering, 1910. 4(4): p. 311-385.

[8] Donnell, L.H., *A new theory for the buckling of thin cylinders under axial compression and bending.* Transactions of the ASME, 1934. 56: p. 795-806.

[9] Mushtari, K.M. and Galimov, K.Z., *Nonlinear theory of thin elastic shells*. 1957, Kazan: Academy of Sciences (Nauka). English version, NASA TT-F62 in 1961.

[10] Sanders, J.L., *Nonlinear theories for thin shells.* Quarterly of Applied Mathematics, 1963. 21: p. 21-36.

[11] Koiter, W.T., *On the nonlinear theory of thin elastic shells I, II, III.* Proceedings Koninklijke Nederlandse Akademie van Wetenschappen, 1966. B 69: p. 1-54.

[12] Ginsberg, J.H., *Large-amplitude forced vibrations of simply supported thin cylindrical shells.* ASME Journal of Applied Mathematics, 1973. 40: p. 471-477.

[13] Flugge, W., *Stresses in Shells*. 1962: Springer-Verlag.

[14] Novozhilov, V.V., *Foundations of the Nonlinear Theory of Elasticity*. 1953, Rochester, NY, USA: Graylock Press.

[15] Reissner, E., *New derivation of the equations of the deformation of elastic shells.* Am. J. Math, 1941. 63: p. 177-184.

[16] Timoshenko, S. and Woinowsky-Krieger, S., *Theory of Plates and Shells, 2nd ed*. 1959: McGraw-Hill.

[17] Vlasov, V.Z., *General Theory of Shells and its Applications in Engineering*. 1949, Moskva-Leningrad: English translation, NASA TTF-99, 1964.

[18] Sanders, J., *An Improved First Approximation Theory of Thin Shells.* NASA TR-R24, 1959.

[19] Rayleigh, L., *Theory of Sound*. Vol. I and II. 1877: Dover Publications 1945.

[20] Timoshenko, S., *On the correction for shear of the differential equation for transverse vibration of prismatic bars.* Phil. Mag., 1921. 6: p. 41, 742.

[21] Reissner, E., *The effect of transverse shear deformation on the bending of elastic plates.* ASME Journal of Applied Mechanics, 1945. 12: p. A68-77.

[22] Mindlin, R.D., *Influence of rotatory inertia and shear on flexural motions of isotropic, elastic plates.* ASME Journal of Applied Mechanics, 1951. 18: p. 31-38.

[23] Reddy, J.N. and Chandrashekhara, K., *Geometrically non-linear transient analysis of laminated, doubly curved shells.* International Journal of Non-Linear Mechanics, 1985. 20: p. 79-90.

[24] Reddy, J.N., *Exact solutions of moderately thick laminated shells.* Journal of Engineering Mechanics, 1984. 110: p. 794-809.

[25] Reddy, J.N. and Liu, C.F., *A higher-order shear deformation theory of laminated elastic shells.* International Journal of Engineering Science, 1985. 23: p. 319-330.

[26] Reddy, J.N., *A general non-linear third-order theory of plates with moderate thickness.* International Journal of Non-Linear Mechanics, 1990. 25: p. 677-686.

[27] Ambartsumian, S.A., *Theory of Anisotropic Shells*. 1961, Fizmatgiz Moskva: English translation, NASA TTF-118, 1964.

[28] Leissa, A.W., *Vibration of Shells*. 1973: NASA SP288, US Government Printing Office, Washington DC, Republished 1993, Acoustical Society of America.

[29] Librescu, L., *Elastostatics and Kinetics of Anisotropic and Heterogeneous Shell-Type Structures*. 1976, Leyden: Noordhoff International.

[30] Librescu, L., *Refined geometrically nonlinear theories of anisotropic laminated shells.* Quarterly of Applied Mathematics, 1987. 45: p. 1-22.

[31] Vinson, J.R. and Sierakowski, R.L., *The behavior of structures composed of composite materials*. 1986, Dordrecht: M. Nijhoff.

[32] Librescu, L., Khdeir, A.A. and Frederick, D., *A shear-deformable theory for laminated composite shallow shell-type panels and their response analysis I: free vibration and buckling.* Acta Mechanica, 1989. 76: p. 1-33.

[33] Librescu, L., Khdeir, A.A. and Frederick, D., *A shear-deformable theory for laminated composite shallow shell-type panels and their response analysis II: static analysis.* Acta Mechanica, 1989. 77: p. 1-12.

[34] Leissa, A.W. and Chang, J., *Elastic deformation of thick, laminated composite shallow shells.* Composite Structures, 1996. 35: p. 153-170.

[35] Mouritz, A.P., Gellert, E., Burchhill, P. and Challis, K., *Review of advanced composite structures for naval ships and submarines.* Composite Structures, 2001. 53: p. 21-41.

[36] Plantema, F.J., *Sandwich Construction*. 1966, New York: Wiley.

[37] Allen, H.G., *Analysis and design of structural sandwich panels*. 1969, Oxford: Pergamon.

[38] Xue, Z. and Hutchinson, J.W., *Preliminary assessment of sandwich plates subject to blast loads.* International Journal of Mechanics Science, 2003. 45: p. 687-705.

[39] Librescu, L., Oh, S.Y. and Hohe, J., *Linear and non-linear dynamic response of sandwich panels to blast loading.* Composites Part B, 2004. 35: p. 673-683.

[40] Deshpande, V.S. and Fleck, N.A., *One-dimensional response of sandwich plates to underwater shock loading.* Journal of Mechanics and Physics of Solids, 2005. 53: p. 2347-2383.

[41] Liang, Y., Spuskanyuk, A.V., Flores, S.E., Hayhurst, D.R., Hutchinson, J.W., McMeeking, R.M. and Evans, A.G., *The response of metallic sandwich panels to water blast.* ASME Journal of Applied Mechanics, 2007. 74(1): p. 81-99.

[42] Nemat-Nasser, S., Kang, W.J., McGee, J.D., Guo, W.G. and Issacs, J.B., *Experimental investigation of energy-absorption characteristics of components of sandwich structures.* International Journal of Impact Engineering, 2007. 34: p. 1119-1146.

[43] Benson, A.S. and Mayers, J., *General instability and face wrinkling of sandwich plates-unified theory and applications.* AIAA Journal, 1967. 5: p. 729-739.

[44] Pearce, T.R.A. and Webber, J.P.H., *Buckling of sandwich panels with laminated face plates.* Aeron Quart, 1972. 23: p. 148-160.

[45] Pearce, T.R.A. and Webber, J.P.H., *Experimental buckling loads of sandwich panels with carbon fiber face plates.* Aeron Quart, 1973. 24: p. 295-312.

[46] Skvortsov, V. and Bozhevolnaya, E., *Two-dimensional analysis of shallow sandwich panels.* Composite Structures, 2001. 53: p. 43-53.

[47] Ferreira, J.M., Barbosa, J.T., Torres Marques, A. and Cesar de Sa, J., *Non-linear analysis of sandwich shells: the effect of core plasticity.* Computers and Structures, 2000. 76: p. 337-346.

[48] Barut, A., Madenci, E., Heinrich, J. and Tessler, A., *Analysis of thick sandwich construction by a {3,2}-order theory.* Int J. Sol. Struct, 2001. 38: p. 6063-6077.

[49] Frostig, Y., Baruch, M., Vilnay, O. and Sheiman, I., *High-order buckling theory for sandwich beam behavior with transversely flexible core.* Journal of Engineering Mechanics, 1992. 118: p. 1026-1043.

[50] Bozhevolnaya, E. and Frostig, Y., *Non-linear closed-form high-order analysis of curved sandwich panels.* Composite Structures, 1997. 38: p. 383-394.

[51] Frostig, Y., *Buckling of sandwich panels with a flexible core-high-order theory.* Int J. Sol. Struct, 1998. 35: p. 183-204.

[52] Dawe, D.J. and Yuan, W.X., *Overall and local buckling of sandwich plates with laminated faceplates. Part I: analysis.* Computer Methods in Applied Mechanics and Engineering, 2001. 190: p. 5197-5213.

[53] Pai, P.F. and Palazotto, A.N., *A higher-order sandwich plate theory accounting for 3-D stresses.* Int J. Sol. Struct, 2001. 38: p. 5045-5062.

[54] Librescu, L. and Hause, T., *Recent developments in the modeling and behavior of advanced sandwich constructions: a survey.* Composite Structures, 2000. 48: p. 1-17.

[55] Ganapathi, M. and Haboussi, M., *Free vibrations of thick laminated anisotropic non-circular cylindrical shells.* Composite Structures, 2003. 60: p. 125-133.

[56] Korhevskaya, E.A. and Mikhasev, G.I., *Free vibrations of a laminated cylindrical shell subjected to nonuniformly distributed axial forces.* Mechanics of Solids, 2006. 41: p. 130-138.

[57] Shang, X.C., *An exact analysis for free vibration of a composite shell structure-hermetic capsule.* Applied Mathematics and Mechanics, 2001. 22: p. 1035-1045.

[58] Krishnamurthy, K.S., Mahajan, P. and Mittal, P.K., *Impact response and damage in laminated composite cylindrical shells.* Composite Structures, 2003. 59: p. 15-36.

[59] Krishnamurthy, K.S., Mahajan, P. and Mittal, P.K., *A parametric study of the impact response and damage of laminated cylindrical composite shells.* Composite Science and Technology, 2001. 61: p. 1655-1669.

[60] Kim, Y.N., Im, K.H., Lee, K.S., Cho, Y.J., Kim, S.H. and Yang, I.Y., *Experimental approach on the behavior of composites laminated shell under transverse impact loading.* Rev Quant Nondestruct Anal, 2005. 24: p. 1100-1106.

[61] Hoo Fatt, M.S. and Sirivolu, D., *A wave propagation model for the high velocity impact response of a composite sandwich panel.* International Journal of Impact Engineering, 2010. 37(2): p. 117-130.

[62] Sahu, S.K. and Datta, P.K., *Research advances in the dynamic stability behavior of plates and shells: 1987-2005-Part I: conservative systems.* Appl Mech Rev, 2007. 60: p. 65.

[63] Zhou, C.T. and Wang, L.D., *Nonlinear theory of dynamic stability for laminated composite cylindrical shells.* Applied Mathematics and Mechanics, 2001. 22: p. 53-62.

[64] Von Karman, T. and Tsien, H.S., *The buckling of thin cylindrical shells under axial compression.* Journal of the Aeronautical Sciences, 1941. 8: p. 303-312.

[65] Pinto Correiaa, I.F., Barbosa, J.I. and Mota Soares, C.A., *A finite element semi-analytical model for laminated axisymmetric shells: statics, dynamics and buckling.* Computers and Structures, 2000. 76: p. 299-317.

[66] Sahu, S.K. and Datta, P.K., *Parametric resonance characteristics of laminated composite doubly curved shells subjected to non-uniform loading.* J. Reinforce Plast Compos, 2001. 20: p. 1556-1576.

[67] Ribeiro, P. and Jansen, E., *Nonlinear vibrations of laminated cylindrical shallow shells under thermomechanical loading.* J Sound Vib, 2008. 315: p. 626-640.

[68] Li, J. and Hua, H., *Transient vibrations of laminated composite cylindrical shells exposed to underwater shock waves.* Engineering Structures, 2009. 31: p. 738-748.

[69] Qatu, M.S., Sullivan, R.W. and Wang, W., *Recent research advances on the dynamic analysis of composite shells: 2000-2009.* Composite Structures, 2010. 93: p. 14-31.

[70] Simitses, G.J., *Dynamic Stability of Suddenly Loaded Structures*. 1990, New York: Springer-Verlag.

[71] Humphreys, J.S., *On dynamic snap buckling of shallow arches.* AIAA Journal, 1965. 4: p. 878-886.

[72] Goodier, J.N. and McIvor, I.K., *The elastic cylindrical shell under nearly uniform radial impulse.* Journal of Applied Mechanics, 1964. 31: p. 259-266.

[73] Mallon, N.J., Fey, R.H.B., Nijmeijer, H. and Zhang, G.Q., *Dynamic buckling of a shallow arch under shock loading considering the effects of arch shape.* International Journal of Non-Linear Mechanics, 2006. 41: p. 1057-1067.

[74] Hoo Fatt, M.S. and Pothula, S.G., *Dynamic pulse buckling of composite shells subjected to external blast.* Composites Structures, 2010. 92: p. 1716-1727.

[75] Tanov, R., Tabiei, A. and Simitses, G.J., *Effect of static preloading on the dynamic buckling of laminated cylinders under sudden pressure.* Mechanics of Composite Materials and Structures, 1999. 6: p. 195-206.

[76] Schokker, A., Sridharran, S. and Kasagi, A., *Dynamic buckling of composite shells.* Computers and Structures, 1996. 59: p. 43-53.

[77] Rahman, T., Jansen, E. and Gurdal, C., *Dynamic buckling analysis of composite cylindrical shells using a finite element perturbation method.* Nonlinear Dynamics, 2011. 66: p. 389-401.

[78] Ovenshire, L.J. and McIvor, I.K., *On the dynamic snap-thorugh of a shallow cylindrical shell subject to nearly symmetric impulsive loading.* Int J. Sol. Struct, 1971. 7: p. 585-601.

[79] Singer, J., Arbocz, J. and Weller, T., *Vol. 2, Shells, built-up structures, composites and additional topics,* in *Buckling Experiments: Experimental methods in buckling of thin-walled structures*. 2002, John Wiley and Sons: New York.

[80] Hsu, C.S., *Equilibrium configurations of a shallow arch of arbitrary shape and their dynamic stability character.* Int. J. Nonlinear Mech, 1968. 3: p. 113-136.

[81] Diab, *Sandwich Technology*. <http://www.diabgroup.com/~/media/Files/Products/Core-material-pdf/HCP%20Oct%202012%20rev10%20SI.ashx>.

[82] Hause, T. and Librescu, L., *Dynamic response of doubly-curved anisotropic sandwich panels impacted by blast loadings.* International Journal of Solids and Structures, 2007. 44: p. 6678-6700.

[83] Hohe, J. and Librescu, L., *A nonlinear theory for doubly curved anisotropic sandwich shells with transversely compressible core.* International Journal of Solids and Structures, 2003. 40: p. 1059-1099.

[84] Hohe, J. and Librescu, L., *Recent results on the effect of the transverse core compressibility on the static and dynamic response of sandwich structures.* Composites Part B, 2008. 38: p. 108-119.

[85] Li, R., Kardomateas, G.A. and Simitses, G.J., *Nonlinear response of a shallow sandwich shell with compressible core to blast loading.* ASME Journal of Applied Mathematics, 2008: p. 75.

[86] Li, R. and Kardomateas, G.A., *A high-order theory for cylindrical sandwich shells with flexible cores.* J Mech Math Struct, 2009. 4: p. 1453-1467.

[87] Hoo Fatt, M.S. and Surabhi, H., *Blast resistance and energy absorption of foam-core cylindrical sandwich shells under external blast.* Composite Structures, 2012. 94: p. 3174-3185.

[88] Hoo Fatt, M.S. and Chapagain, P., *Pressure pulse response of composite sandwich panels with plastic core damping.* J Sandwich Struct Mater, 2012. 14: p. 392-429.

[89] Deshpande, V.S. and Fleck, N.A., *Multi-axial yield behavior of polymer foams.* Acta Mater, 2001. 49: p. 1859-1866.

[90] Chen, W.F. and Han, D.J., *Plasticity for Structural Engineers*. 2007, Ft. Lauderdale: J. Ross Publishing.

[91] Mines, R.A.W. and Alias, A., *Numerical simulation of the progressive collapse of polymer composite sandwich beams under static loading.* Composites: Part A, 2002. 33: p. 11-26.

[92] Rivoz, V. and Mladensky, A., *Static indentation response of H30 foam-An experimental and computational study.* Multidiscipline Model Mater Struct, 2008. 4: p. 255-266.

[93] Boh, J.W., Louca, L.A., Choo, Y.S. and Mouring, S.E., *Damage modeling of SCRIMP woven roving laminated beams subjected to transverse shear.* Composites Part B, 2005. 36: p. 427-438.

[94] *ABAQUS User Manual, Version 6.7*, in *Dassault Systèmes*. 2007, ABAQUS, Inc.

[95] Lapp, C.K., *Design allowables substantiation*, in *Handbook of Composites*, Peters, S.T., Editor. 1998, Chapman and Hall: London. p. 758-777.

[96] Rivoz, V., *Local crushing of HCP100 structural foam due to low-velocity impact.* Mar Struct, 2008. 21(1): p. 47-58.

[97] Daniel, I.M., *Failure of composite materials.* Strain, 2007. 43: p. 4-12.

[98] Reissner, E., *Stresses and displacements of shallow spherical shells.* J Math Phys, 1946. 25: p. 80.

[99] Lee, J.K., Leissa, A.W. and Wang, A.J., *Vibrations of cantilevered circular cylindrical shells: shallow versus deep shell theory.* Int J Mech Sci, 1983. 25(5): p. 361-383.

[100] Ventsel, E. and Krauthammer, T., *Thin plates and shells: theory, analysis, and applications*. 2001, New York: Marcel Dekker, Inc.

[101] Fleck, N.A. and Sridhar, I., *End compression of sandwich columns.* Appl Sci Manufact, 2002. 33: p. 353-359.

[102] Mahfuz, H., Thomas, T. and Rangari, V., *On the dynamic response of the sandwich composites and their core materials.* Composites Sci Technol, 2006. 66: p. 2465-2472.

[103] Group, D., *Core Material*. *http://www.diabgroup.com/en-GB/Products-and-Services*. 2013.

APPENDICES

APPENDIX A

NOMENCLATURE

a	shell radius
a_0	mid-surface radius of foam core
a_1	mid-surface radius of outer facesheet
a_2	mid-surface radius of inner facesheet
A_{ij}	membrane stiffness of facesheet
c	circumferential wave speed in facesheet
C_{ij}	stiffness of foam core
dS	differential shell surface area
dV	differential core volume
D_{ij}	bending stiffness of facesheet
E_d	plastic work dissipated
e_n, f_n, g_n, h_n	mode amplitudes
E_{ij}	Young's modulus
f	yield function
G_{ij}	shear modulus

h facesheet thickness

H foam core thickness

k sequence number of lamina

M_{ij} bending moment resistance

n mode number

N_{ij} force resultant

p pressure pulse loading

p_0 peak pressure

$\bar{p}$ normalized pressure pulse loading

q_n generalized coordinate

Q_n generalized external force

$\overline{Q}_{ij}$ reduced stiffness of facesheet

r radial coordinate

s_{ij} deviatoric stress

S_L, S_T longitudinal and transverse shear strength

t time

T kinetic energy

T_c kinetic energy of foam core

T_f kinetic energy of facesheets

U strain energy

U_{ce} elastic strain energy of foam core

U_{cep} nonlinear elastic strain energy of foam core

U_f strain energy of facesheets

v tangential deformation of foam core

v_0 mid-surface tangential deformation of foam core

v_1 outer facesheet tangential deformation

v_2 inner facesheet tangential deformation

V_e elastic regions volumes of foam core

V_p plastic regions volumes of foam core

w radial deflection of foam core

w_0 mid-surface radial deflection of foam core

w_1 outer facesheet radial deflection

w_2 inner facesheet radial deflection

X_C, X_T compressive and tensile strength along fiber direction

Y_C, Y_T compressive and tensile strength perpendicular to fiber direction

z radial coordinate measured inward from the mid-surface

z_1 radial coordinate measured inward from the mid-surface of outer facesheet

z_2 radial coordinate measured inward from the mid-surface of inner facesheet

α^2 circumferential bending-to-membrane stiffness ratio

α_1^2 outer facesheet circumferential bending-to-membrane stiffness ratio

α_2^2 inner facesheet circumferential bending-to-membrane stiffness ratio

$\beta^2, \gamma^2, \eta, \omega^2$ elastic constants for strain energy of foam core

δ_{ij} Kronecker delta

δq_n virtual mode amplitude

δW virtual work

$\delta \zeta_1$ virtual normalized outer facesheet radial deflection

ΔT load duration

$\Delta \theta$ angular extent of plastic zone

ε_f failure hoop strain of facesheet

ε_{ij} strain

ε_{ijm} mid-surface strain

ε_r radial strain in foam core

ε_{r0} radial component of foam core yield strain

ε_x axial strain

ε_{xm} mid-surface axial strain

ε_θ hoop strain in foam core

$\varepsilon_{\theta 0}$ hoop component of foam core yield strain

$\varepsilon_{\theta 1}$ outer facesheet hoop strain

$\varepsilon_{\theta 2}$ inner facesheet hoop strain

$\varepsilon_{\theta m}$ mid-surface hoop strain

$\varepsilon_{\theta m1}$ outer facesheet mid-surface hoop strain

$\varepsilon_{\theta m2}$ inner facesheet mid-surface hoop strain

ϕ_0 rotation angle of foam core plane sections

$\gamma_0^2, \eta_0, \omega_0^2$ plastic constants for strain energy of foam core

$\gamma_{r\theta}$ transverse shear strain in foam core

$\gamma_{r\theta 0}$ transverse shear component of foam core yield strain

$\gamma_{x\theta}$ in-plane shear strain

$\gamma_{x\theta m}$ mid-surface in-plane shear strain

ζ normalized radial deflection

ζ_0 normalized mid-surface radial deflection of foam core

ζ_1 normalized outer facesheet radial deflection

ζ_2 normalized inner facesheet radial deflection

θ circumferential coordinate

θ_0 shell subtended angle

θ_e angular elastic regions of foam core

θ_p angular plastic regions of foam core

κ_{ij} change in curvature

κ_x change in axial curvature

$\kappa_{x\theta}$ change in in-plane curvature

κ_θ change in hoop curvature

$\kappa_{\theta 1}$ outer facesheet bending curvature in hoop direction

$\kappa_{\theta 2}$ inner facesheet bending curvature in hoop direction

Λ foam core aspect ratio

μ inner-to-outer radius ratio

ν_{ij} Poisson's ratio

ρ_c core density

ρ_f facesheets density

$\bar{\rho}$ constant for kinetic energy of foam core

σ_0 flow stress of foam core

σ_e von Mises stress

σ_{ij} stress

σ_m mean stress

σ_r radial stress in foam core

σ_x axial stress in foam core

σ_θ hoop stress in foam core

$\hat{\sigma}$ effective stress of foam core

τ normalized time

τ_0 normalized load duration

$\tau_{r\theta}$ transverse shear stress in foam core

$\tau_{x\theta}$ in-plane shear stress

ψ normalized tangential deformation

ψ_0 normalized mid-surface tangential deformation of foam core

ψ_1 normalized outer facesheet tangential deformation

ψ_2 normalized inner facesheet tangential deformation

$[\dot{\ }]$ derivative with respect to τ

$[\ ]'$ derivative with respect to θ

APPENDIX B

HOOP STRAINS IN SINGLE CURVATURE THIN SHELL

The strain-displacement relation presented here was first established by Goodier and McIvor [72] for cylindrical shells and has been used for dynamic buckling analysis of cylindrical shells in Reference [1]. The hoop strain ε_θ for the shell is

$$\varepsilon_\theta = \varepsilon_{\theta m} + z\kappa_\theta \tag{B.1}$$

where $\varepsilon_{\theta m}$ is the mid-surface strain, κ_θ is the change in curvature of the shell and z is the radial coordinate measured inward from the mid-surface of the shell. The mid-surface hoop strain of the shell is found by considering the differential arc length before and after deformation shown in Figure B.1. Points on the mid-surface of the shell have polar coordinates a, θ. After the deformation, points have polar coordinates r, ϕ in the deformed configuration.

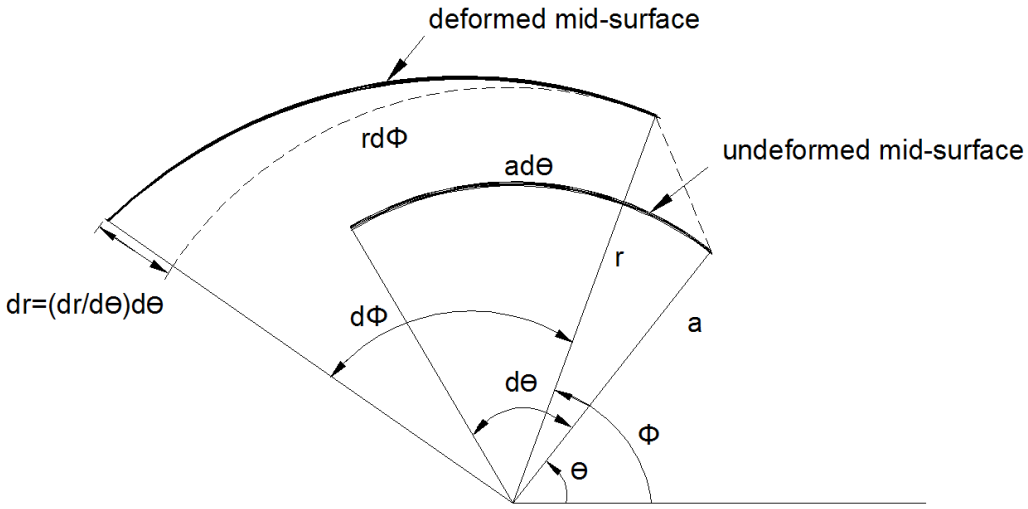

Figure B.1 Deformed and undeformed differential element at the mid-surface of shell.

The shell has radial displacement $w(\theta,t)$ and tangential displacement $v(\theta,t)$ where

$$w = a - r \tag{B.2}$$

and

$$\frac{v}{a} = \phi - \theta \tag{B.3}$$

The mid-surface strain is the change in length of the differential element in Figure B.1 divided by the initial length,

$$\begin{aligned}\varepsilon_{\theta m} &= \frac{1}{ad\theta}\left\{\left[\left(\frac{dr}{d\theta}\cdot d\theta\right)^2 + \left(r\frac{d\phi}{d\theta}\cdot d\theta\right)^2\right]^{\frac{1}{2}} - ad\theta\right\} \\ &= \frac{1}{a}\left(r'^2 + r^2\phi'^2\right)^{\frac{1}{2}} - 1\end{aligned} \tag{B.4}$$

Differentiating Equations (B.2) and (B.3) gives,

$$\frac{dr}{d\theta} = -\frac{dw}{d\theta} \tag{B.5}$$

and

$$\frac{d\phi}{d\theta} = 1 + \frac{1}{a}\frac{dv}{d\theta} \tag{B.6}$$

Substituting Equations (B.2), (B.5) and (B.6) into Equation (B.4) gives

$$\varepsilon_{\theta m} = \frac{1}{a}\left[w'^2 + (a-w)^2\left(1+\frac{v'}{a}\right)^2 \right]^{\frac{1}{2}} - 1 \tag{B.7}$$

By introducing normalized displacements $\zeta = w/a$, $\psi = v/a$, Equation (B.7) becomes

$$\varepsilon_{\theta m} = \left[\zeta'^2 + (1-\zeta)^2(1+\psi')^2\right]^{\frac{1}{2}} - 1 \tag{B.8}$$

Upon expansion to terms of second order, the mid-surface strain is obtained as

$$\varepsilon_{\theta m} = \psi' - \zeta - \zeta\psi' + \frac{1}{2}\zeta'^2 \tag{B.9}$$

Similarly, the change in curvature of the shell is given as

$$\kappa_\theta = \left[\phi'(r^2\phi'^2 - rr'' + 2r'^2) + \phi'' rr'\right](r'^2 + r^2\phi'^2)^{-3/2} \tag{B.10}$$

By simplifying Equation (B.10), the change in shell curvature is

$$\begin{aligned} \kappa_\theta &= -\frac{1}{a^2}\left(\frac{\partial^2 w}{\partial\theta^2} + w\right) \\ &= -\frac{1}{a}(\zeta'' + \zeta) \end{aligned} \tag{B.11}$$

The membrane and bending strains are based on large deflection theory. Here the term "large" refers to the fact that transverse deflections are greater than the shell thickness so that the undeformed and deformed configurations are different.

APPENDIX C

STRAIN ENERGY OF THE LAMINATED COMPOSITE SHELL

Consider a laminated composite shell with n laminae in the cylindrical coordinate as shown in Figure C.1. The generalized shell forces and moments are related to the strains by

$$\begin{Bmatrix} N_x \\ N_\theta \\ N_{x\theta} \\ M_x \\ M_\theta \\ M_{x\theta} \end{Bmatrix} = \begin{bmatrix} A_{11} & A_{12} & A_{16} & B_{11} & B_{12} & B_{16} \\ A_{12} & A_{22} & A_{26} & B_{12} & B_{22} & B_{26} \\ A_{16} & A_{26} & A_{66} & B_{16} & B_{26} & B_{66} \\ B_{11} & B_{12} & B_{16} & D_{11} & D_{12} & D_{16} \\ B_{12} & B_{22} & B_{26} & D_{12} & D_{22} & D_{26} \\ B_{16} & B_{26} & B_{66} & D_{16} & D_{26} & D_{66} \end{bmatrix} \begin{Bmatrix} \varepsilon_{xm} \\ \varepsilon_{\theta m} \\ \gamma_{x\theta m} \\ \kappa_x \\ \kappa_\theta \\ 2\kappa_{x\theta} \end{Bmatrix} \tag{C.1}$$

where $A_{ij} = \sum_{k=1}^{n} (\overline{Q}_{ij})_k (z_k - z_{k-1})$ is the membrane stiffness, $B_{ij} = \frac{1}{2}\sum_{k=1}^{n} (\overline{Q}_{ij})_k (z_k^2 - z_{k-1}^2)$ is the coupling stiffness, $D_{ij} = \frac{1}{3}\sum_{k=1}^{n} (\overline{Q}_{ij})_k (z_k^3 - z_{k-1}^3)$ is the bending stiffness, ε_{ijm} is the mid-surface strain and κ_{ij} is the change in curvature. In the expressions of stiffness, $\overline{Q}_{ij}$ is the reduced stiffness, z is the radial coordinate measured from the mid-surface and the k^{th} lamina is bounded by $z = z_{k-1}$ and $z = z_k$. The single curvature shell is in plane strain so that $\varepsilon_{xm}, \gamma_{x\theta m}, \kappa_x$ and $\kappa_{x\theta}$ are equal to zero. Hence N_θ and M_θ reduce to

$$N_\theta = A_{22}\varepsilon_{\theta m} + B_{22}\kappa_\theta \tag{C.2}$$

$$M_\theta = B_{22}\varepsilon_{\theta m} + D_{22}\kappa_\theta \tag{C.3}$$

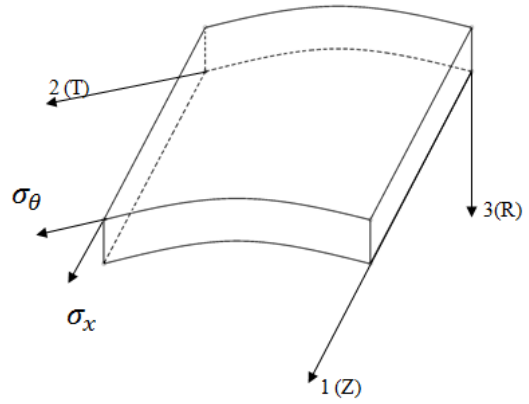

Figure C.1 Laminated composite shell in cylindrical coordinates.

In general, the elastic strain energy of a laminated composite shell is given by

$$U = \frac{1}{2}\int (N_x\varepsilon_{xm} + N_\theta\varepsilon_{\theta m} + N_{x\theta}\gamma_{x\theta m} + M_x\kappa_x + M_\theta\kappa_\theta + 2M_{x\theta}\kappa_{x\theta})dS \tag{C.4}$$

where $dS = ad\theta$ is the differential shell surface area. Following plane strain conditions and substituting Equations (C.2) and (C.3) into Equation (C.4), the elastic strain energy of the long, laminated composite shell reduces to

$$U = \frac{1}{2}\int (A_{22}\varepsilon_{\theta m}^2 + 2B_{22}\varepsilon_{\theta m}\kappa_\theta + D_{22}\kappa_\theta^2)ad\theta \tag{C.5}$$

A special class of laminated composite shells which have $B_{22} = 0$ is considered. This includes shells that are orthotropic, mid-plane symmetric, anti-symmetric and quasi-isotropic. For these types of laminated composite shells, the elastic strain energy becomes

$$U = \frac{1}{2}\int (A_{22}\varepsilon_{\theta m}^2 + D_{22}\kappa_\theta^2)ad\theta \tag{C.6}$$

Substituting Equations (3.6) and (3.7) into Equation (C.6) gives

$$U = \frac{1}{2} A_{22} a \int_0^{\theta_0} [(\psi' - \zeta)^2 + (\psi' - \zeta)(\zeta'^2 - 2\zeta\psi') + \left(\zeta\psi' - \frac{1}{2}\zeta'^2\right)^2 + \alpha^2(\zeta'' + \zeta)^2] d\theta \qquad \text{(C.7)}$$

APPENDIX D

PLY FAILURE CRITERIA FOR ORTHOTROPIC SHELL

A modified Hashin-Rotem failure criterion [97] is used to examine ply failure of the orthotropic shell. The failure occurs when

$$\frac{|\sigma_x|}{X_T} = 1 \quad \text{if } \sigma_x > 0 \quad \text{, or } \frac{|\sigma_x|}{X_C} = 1 \text{ if } \sigma_x < 0 \tag{D.1}$$

$$\frac{|\sigma_\theta|}{Y_T} = 1 \quad \text{if } \sigma_\theta > 0 \quad \text{, or } \frac{|\sigma_\theta|}{Y_C} = 1 \text{ if } \sigma_\theta < 0 \tag{D.2}$$

$$\frac{|\tau_{x\theta}|}{S_L} = 1 \tag{D.3}$$

For the orthotropic shell as shown in Figure C.1, the stress-strain relations $(\sigma_{ij} - \varepsilon_{ij})$ are given by

$$\begin{Bmatrix} \sigma_x \\ \sigma_\theta \\ \tau_{x\theta} \end{Bmatrix} = \begin{bmatrix} \overline{Q}_{11} & \overline{Q}_{12} & \overline{Q}_{16} \\ \overline{Q}_{12} & \overline{Q}_{22} & \overline{Q}_{26} \\ \overline{Q}_{16} & \overline{Q}_{26} & \overline{Q}_{66} \end{bmatrix} \begin{Bmatrix} \varepsilon_x \\ \varepsilon_\theta \\ \gamma_{x\theta} \end{Bmatrix} \tag{D.4}$$

where $\overline{Q}_{11} = E_{11}/(1-\nu_{12}\nu_{21})$, $\overline{Q}_{22} = E_{22}/(1-\nu_{12}\nu_{21})$, $\overline{Q}_{12} = \nu_{12}E_{22}/(1-\nu_{12}\nu_{21})$, $\overline{Q}_{66} = G_{12}$, $\overline{Q}_{16} = 0$ and $\overline{Q}_{26} = 0$. With plane strain conditions, $\varepsilon_x = 0$ and $\gamma_{x\theta} = 0$, the stresses σ_{ij} reduce to

$$\sigma_x = \overline{Q}_{12}\varepsilon_\theta \tag{D.5}$$

$$\sigma_\theta = \overline{Q}_{22}\varepsilon_\theta \tag{D.6}$$

$$\tau_{x\theta} = 0 \tag{D.7}$$

Since $X_T = Y_T, X_C = Y_C$ for the woven roving E-Glass/Vinyl Ester and $\overline{Q}_{22} > \overline{Q}_{12}$, it can be noticed that $\sigma_\theta > \sigma_x$ and ply failure of the shell occurs in tangential direction. By substituting Equation (D.6) into Equation (D.2) the critical value of hoop strain at which failure occurs in tangential direction is thus given by

$$\varepsilon_\theta = \frac{Y_T}{\overline{Q}_{22}} \quad \text{if} \quad \varepsilon_\theta > 0, \quad \text{or} \quad |\varepsilon_\theta| = \frac{Y_C}{\overline{Q}_{22}} \quad \text{if} \quad \varepsilon_\theta < 0 \tag{D.8}$$

The maximum hoop strain would occur at either center or boundary position of the shell, which means

$$\varepsilon_{\theta\max} = \varepsilon_\theta(\tau, 0/\frac{\theta_0}{2}/\theta_0) \tag{D.9}$$

At these three critical positions, the maximum hoop strain occurs at the outer plies where the bending strains are maximum, i.e., at $z = \pm h/2$. Hence the maximum strain can be expressed as

$$\varepsilon_{\theta\max} = \varepsilon_{\theta m} \pm \frac{h}{2}\kappa_\theta \tag{D.10}$$

APPENDIX E

ELASTIC STRAIN ENERGY OF CORE

Under plane strain conditions, the elastic stress-strain constitutive equations in the core are

$$\begin{Bmatrix} \sigma_r \\ \sigma_\theta \\ \tau_{r\theta} \end{Bmatrix} = \begin{bmatrix} C_{11} & C_{12} & 0 \\ C_{12} & C_{11} & 0 \\ 0 & 0 & C_{66} \end{bmatrix} \begin{Bmatrix} \varepsilon_r \\ \varepsilon_\theta \\ \gamma_{r\theta} \end{Bmatrix} \tag{E.1}$$

where $C_{11} = 2G + \lambda,\ C_{12} = \lambda,\ C_{66} = G,\ \lambda = \nu E/((1+\nu)(1-2\nu))$, and G, E and ν are the shear modulus, Young's modulus and Poisson's ratio, respectively. The axial stress is

$$\sigma_x = \nu(\sigma_r + \sigma_\theta) \tag{E.2}$$

The elastic strain energy in the core is given by

$$U_{ce} = \frac{1}{2}\int (\sigma_r \varepsilon_r + \sigma_\theta \varepsilon_\theta + \tau_{r\theta}\gamma_{r\theta}) dV \tag{E.3}$$

where $dV = rdrd\theta$. Substituting Equation (E.1) into Equation (E.3) gives

$$U_{ce} = \frac{1}{2}\int (C_{11}\varepsilon_r^2 + 2C_{12}\varepsilon_\theta \varepsilon_r + C_{11}\varepsilon_\theta^2 + C_{66}\gamma_{r\theta}^2) dV \tag{E.4}$$

The core strains are

$$\varepsilon_r = \frac{a_1}{H}(\mu\zeta_2 - \zeta_1) \tag{E.5}$$

$$\varepsilon_\theta = \frac{(\psi_1' + \mu\psi_2')}{(1+\mu)} - \frac{(\zeta_1 + \mu\zeta_2)}{(1+\mu)} + \frac{z}{a_0}\frac{a_1}{H}(\mu\psi_2' - \psi_1') \tag{E.6}$$

$$\gamma_{r\theta} = -\frac{(\zeta_1' + \mu\zeta_2')}{(1+\mu)} - a_1\frac{(\mu\psi_2 - \psi_1)}{H} + \frac{(\psi_1 + \mu\psi_2)}{(1+\mu)} \tag{E.7}$$

The first term of Equation (E.4) is

$$U_{c1} = \frac{1}{2}C_{11}a_1^2\Lambda\int_0^{\theta_0}(\mu\zeta_2 - \zeta_1)^2\,d\theta \tag{E.8}$$

where $\Lambda = (1+\mu)/(2(1-\mu))$.

The second term of Equation (E.4) is

$$\begin{aligned} U_{c2} &= C_{12}\frac{a_0 a_1}{(1+\mu)}\int_0^{\theta_0}(\mu\zeta_2 - \zeta_1)(\mu\psi_2' + \psi_1' - \mu\zeta_2 - \zeta_1)d\theta \\ &+ C_{12}\frac{a_1^2 H}{12a_0}\int_0^{\theta_0}(\mu\zeta_2 - \zeta_1)(\psi_1' - \mu\psi_2')d\theta \end{aligned} \tag{E.9}$$

The third term of Equation (E.4) is

$$\begin{aligned} U_{c3} &= \frac{1}{2}C_{11}\frac{a_0 H}{(1+\mu)^2}\int_0^{\theta_0}(\psi_1' + \mu\psi_2' - \zeta_1 - \mu\zeta_2)^2\,d\theta \\ &+ C_{11}\frac{a_1 H^2}{12a_0(1+\mu)}\int_0^{\theta_0}(\psi_1' + \mu\psi_2' - \zeta_1 - \mu\zeta_2)(\psi_1' - \mu\psi_2')d\theta \\ &+ C_{11}\frac{a_1^2 H}{24a_0}\int_0^{\theta_0}(\mu\psi_2' - \psi_1')^2\,d\theta \end{aligned} \tag{E.10}$$

The last term of Equation (E.4) is

$$U_{c4} = \frac{1}{2}C_{66}\frac{a_0 H}{(1+\mu)^2}\int_0^{\theta_0}[-\mu\zeta_2' - \zeta_1' - 2\Lambda(\mu\psi_2 - \psi_1) + \mu\psi_2 + \psi_1]^2\,d\theta \tag{E.11}$$

Combining Equations (E.8)-(E.11) gives

$$
\begin{aligned}
U_{ce} = \eta \frac{A_{22} a_1}{2} \int_0^{\theta_0} \Big\{ & (\mu\zeta_2 - \zeta_1)^2 + \omega^2 (\psi_1' + \mu\psi_2' - \zeta_1 - \mu\zeta_2)^2 \\
& + \frac{\omega^2}{3\Lambda} (\mu\psi_2' - \psi_1') \left[(-\psi_1' - \mu\psi_2' + \zeta_1 + \mu\zeta_2) + \Lambda (\mu\psi_2' - \psi_1') \right] \\
& + \frac{\beta^2}{6\Lambda} (\mu\zeta_2 - \zeta_1) \left[6\Lambda (\psi_1' + \mu\psi_2' - \zeta_1 - \mu\zeta_2) - (\mu\psi_2' - \psi_1') \right] \\
& + \gamma^2 \left[-\zeta_1' - \mu\zeta_2' - 2\Lambda (\mu\psi_2 - \psi_1) + \psi_1 + \mu\psi_2 \right]^2 \Big\} d\theta
\end{aligned}
\tag{E.12}
$$

where

$$\eta = \frac{C_{11} a_1 \Lambda}{A_{22}}$$

$$\omega^2 = \frac{1}{4\Lambda^2}$$

$$\beta^2 = \frac{C_{12}}{C_{11}\Lambda}$$

$$\gamma^2 = \frac{C_{66}}{4\Lambda^2 C_{11}}$$

APPENDIX F

NONLINEAR ELASTIC STRAIN ENERGY OF CORE

The following nonlinear strain energy expression can be used to determine the elastic-plastic motion using Lagrange's method:

$$U_{cep} = \frac{1}{2}\int_{R_e}\left(C_{11}\varepsilon_r^2 + 2C_{12}\varepsilon_\theta\varepsilon_r + C_{11}\varepsilon_\theta^2 + C_{66}\gamma_{r\theta}^2\right)dV + \frac{1}{2}\int_{R_p}\Big[C_{11}\varepsilon_r^2 + 2C_{12}\varepsilon_\theta\varepsilon_r + C_{11}\varepsilon_\theta^2 + C_{66}\gamma_{r\theta}^2$$
$$- C_{11}\left(\varepsilon_r - \varepsilon_{r0}\right)^2 - 2C_{12}\left(\varepsilon_\theta - \varepsilon_{\theta 0}\right)\left(\varepsilon_r - \varepsilon_{r0}\right) - C_{11}\left(\varepsilon_\theta - \varepsilon_{\theta 0}\right)^2 - C_{66}\left(\gamma_{r\theta} - \gamma_{r\theta 0}\right)^2\Big]dV \tag{F.1}$$

The first integrand is the same as in purely elastic response. Hence,

$$\frac{1}{2}\int_{R_e}\left(C_{11}\varepsilon_r^2 + 2C_{12}\varepsilon_\theta\varepsilon_r + C_{11}\varepsilon_\theta^2 + C_{66}\gamma_{r\theta}^2\right)dV$$
$$= \eta\frac{A_{22}a_1}{2}\int_{\theta_e}\Big\{\left(\mu\zeta_2 - \zeta_1\right)^2 + \omega^2\left(\psi_1' + \mu\psi_2' - \zeta_1 - \mu\zeta_2\right)^2$$
$$+ \frac{\omega^2}{3\Lambda}\left(\mu\psi_2' - \psi_1'\right)\left[\left(-\psi_1' - \mu\psi_2' + \zeta_1 + \mu\zeta_2\right) + \Lambda\left(\mu\psi_2' - \psi_1'\right)\right] \tag{F.2}$$
$$+ \frac{\beta^2}{6\Lambda}\left(\mu\zeta_2 - \zeta_1\right)\left[6\Lambda\left(\psi_1' + \mu\psi_2' - \zeta_1 - \mu\zeta_2\right) - \left(\mu\psi_2' - \psi_1'\right)\right]$$
$$+ \gamma^2\left[-\zeta_1' - \mu\zeta_2' - 2\Lambda\left(\mu\psi_2 - \psi_1\right) + \psi_1 + \mu\psi_2\right]^2\Big\}d\theta$$

Expansion of the second integrand gives

$$\begin{aligned}
&\frac{1}{2}\int_{R_p}\Big[C_{11}\varepsilon_r^2+2C_{12}\varepsilon_\theta\varepsilon_r+C_{11}\varepsilon_\theta^2+C_{66}\gamma_{r\theta}^2\\
&-C_{11}(\varepsilon_r-\varepsilon_{r0})^2-2C_{12}(\varepsilon_\theta-\varepsilon_{\theta0})(\varepsilon_r-\varepsilon_{r0})-C_{11}(\varepsilon_\theta-\varepsilon_{\theta0})^2-C_{66}(\gamma_{r\theta}-\gamma_{r\theta0})^2\Big]dV\\
&=\frac{1}{2}\int_{R_p}\big[2C_{11}\varepsilon_{r0}\varepsilon_r+2C_{12}\varepsilon_{\theta0}\varepsilon_r+2C_{12}\varepsilon_{r0}\varepsilon_\theta+2C_{11}\varepsilon_{\theta0}\varepsilon_\theta+2G\gamma_{r\theta0}\gamma_{r\theta}\\
&-C_{11}\varepsilon_{r0}^2-2C_{12}\varepsilon_{\theta0}\varepsilon_{r0}-C_{11}\varepsilon_{\theta0}^2-C_{66}\gamma_{r\theta0}^2\big]dV
\end{aligned}\tag{F.3}$$

In this expression, the constant terms $C_{11}\varepsilon_{r0}^2, 2C_{12}\varepsilon_{\theta0}\varepsilon_{r0}, C_{11}\varepsilon_{\theta0}^2, C_{66}\gamma_{r\theta0}^2$ can be neglected because they will vanish when U_{cep} is made derivative in Lagrange's equation of motion. Hence Equation (F.3) can be expressed as

$$\begin{aligned}
&\frac{1}{2}\int_{R_p}\big[2C_{11}\varepsilon_{r0}\varepsilon_r+2C_{12}\varepsilon_{\theta0}\varepsilon_r+2C_{12}\varepsilon_{r0}\varepsilon_\theta+2C_{11}\varepsilon_{\theta0}\varepsilon_\theta+2C_{66}\gamma_{r\theta0}\gamma_{r\theta}\big]dV\\
&=\eta_0\frac{A_{22}a_1}{2}\int_{\theta_p}\Big\{\mu\zeta_2-\zeta_1+\omega_0^2(\psi_1'+\mu\psi_2'-\zeta_1-\mu\zeta_2)+\frac{\omega_0^2}{6\Lambda}(\psi_1'-\mu\psi_2')\\
&+\gamma_0^2\big[-\zeta_1'-\mu\zeta_2'-2\Lambda(\mu\psi_2-\psi_1)+\psi_1+\mu\psi_2\big]\Big\}d\theta
\end{aligned}\tag{F.4}$$

where

$$\eta_0=\frac{2a_0}{A_{22}}(C_{11}\varepsilon_{r0}+C_{12}\varepsilon_{\theta0})$$

$$\omega_0^2=\frac{1}{2\Lambda}\frac{(C_{11}\varepsilon_{\theta0}+C_{12}\varepsilon_{r0})}{(C_{11}\varepsilon_{r0}+C_{12}\varepsilon_{\theta0})}$$

$$\gamma_0^2=\frac{1}{2\Lambda}\frac{C_{66}\gamma_{r\theta0}}{(C_{11}\varepsilon_{r0}+C_{12}\varepsilon_{\theta0})}$$

Substituting Equations (F.2)-(F.4) into Equation (F.1) gives

$$
\begin{aligned}
U_{cep} = \eta \frac{A_{22} a_1}{2} \int_{\theta_e} \Big\{ & (\mu\zeta_2 - \zeta_1)^2 + \omega^2 (\psi_1' + \mu\psi_2' - \zeta_1 - \mu\zeta_2)^2 \\
& + \frac{\omega^2}{3\Lambda} (\mu\psi_2' - \psi_1') \left[(-\psi_1' - \mu\psi_2' + \zeta_1 + \mu\zeta_2) + \Lambda (\mu\psi_2' - \psi_1') \right] \\
& + \frac{\beta^2}{6\Lambda} (\mu\zeta_2 - \zeta_1) \left[6\Lambda (\psi_1' + \mu\psi_2' - \zeta_1 - \mu\zeta_2) - (\mu\psi_2' - \psi_1') \right] \\
& + \gamma^2 \left[-\zeta_1' - \mu\zeta_2' - 2\Lambda (\mu\psi_2 - \psi_1) + \psi_1 + \mu\psi_2 \right]^2 \Big\} d\theta \\
& + \eta_0 \frac{A_{22} a_1}{2} \int_{\theta_p} \Big\{ \mu\zeta_2 - \zeta_1 + \omega_0^2 (\psi_1' + \mu\psi_2' - \zeta_1 - \mu\zeta_2) + \frac{\omega_0^2}{6\Lambda} (\psi_1' - \mu\psi_2') \\
& + \gamma_0^2 \left[-\zeta_1' - \mu\zeta_2' - 2\Lambda (\mu\psi_2 - \psi_1) + \psi_1 + \mu\psi_2 \right] \Big\} d\theta
\end{aligned}
\tag{F.5}
$$